Dynamic Resource Allocation Techniques for Half- and Full-Duplex Systems

Sean Huberman

Department of Electrical & Computer Engineering
McGill University
Montréal, Canada

November 2014

A thesis submitted to McGill University in partial fulfillment of the requirements for the degree of Doctor of Philosophy.

2014/11/07

Abstract

The demand for data-intensive services is on the rise. In order to meet the demands, communication systems must increase their spectral efficiency (i.e., bits/s/Hz/Area). The more resources (e.g., time, frequency) are shared, the more interference will be present, but the higher the potential spectral efficiency gains if the interference can be effectively managed. The focus of this thesis is on the design of scalar and vectored Dynamic Power Allocation (DPA) transmission techniques to manage interference in severely interference-limited environments with applications to both wireline and wireless Half-Duplex (HD) and Full-Duplex (FD) systems. In particular, this thesis focuses on the design of practical, low-complexity scalar DPA- and precoding-based sum-rate maximization algorithms.

For HD multi-link systems, a low-complexity distributed scalar DPA algorithm is proposed, introducing the concept of a virtual network, to achieve a near-ideal balance between performance, complexity, and sensitivity to users entering/leaving the system. As well, a lower-bound on the expected sum-rate is developed to provide better insight into the actual spectral efficiency of the system than existing models, which can be a useful tool for system operators to predict achievable data-rates.

For FD systems, a FD Precoding (FDP) transceiver structure is proposed which applies precoding to jointly control the forward channel precoding and the self-interference cancellation, applicable for both FD MIMO-OFDM (Multiple-Input-Multiple-Output Orthogonal Frequency-Division Multiplexing) point-to-point and point-to-multi-point systems. The FDP structure allows for different algorithms and optimization objectives to be developed. Various separate and joint FDP algorithms are proposed and the results indicate that using the proposed FDP structure can provide between 1.6 to 1.8 times and between 1.2 to 1.3 times the spectral efficiency of optimized HD systems in a wide-range of practical FD MIMO point-to-point and point-to-multi-point scenarios, respectively.

Sommaire

La demande pour les services à hauts débits augmente. Afin de répondre à cette demande, les systèmes de communication doivent accroître leur rendement spectral (c.à.d., bits/s/Hz/m^2). Plus les ressources (par exemple, temps, fréquence) sont partagées, plus il y aura d'interférence présente; cependant, il y aura aussi plus de potentiel de réaliser des gains en rendement spectral si l'interférence peut être gérée efficacement. L'objectif de cette thèse est la conception de techniques de transmission avec allocation scalaire et vectorielle dynamique de puissance (Dynamic Power Allocation ou DPA) pour les environnements sévèrement limités par l'interférence avec des applications que l'on retrouve dans les systèmes filaires et sans-fil semi-duplex (Half-Duplex ou HD) et duplex intégral (Full-Duplex ou FD). En particulier, l'objectif de cette thèse est la conception de DPA scalaire pratique à complexité-réduite et la conception d'algorithmes de précodage dans le but de maximiser le débit total.

Pour les systèmes à liaisons multiples HD, un algorithme distribué scalaire à complexité-réduite est proposé, ce qui introduit la notion de réseau virtuel, qui permet d'obtenir un équilibre quasi-idéal entre la performance, la complexité et la sensibilité aux usagers entrant ou sortant du système. De plus, une borne inférieure sur le débit total espéré est dérivée pour améliorer l'estimation du débit total réel comparativement aux modèles existants, ce qui peut aider les fournisseurs de services à prévoir leur débit réalisable.

Pour les systèmes FD, une structure émetteur-récepteur radio FD avec précodage (FD precoding ou FDP) est proposée qui permet de contrôler conjointement le précodage sur le canal principal et l'annulation de l'auto-brouillage, avec des applications pour les systèmes de communication FD MIMO-OFDM (multiplexage par répartition orthogonale de la fréquence) point-à-point et point-à-multi-point. La structure FDP permet la conception de différents algorithmes ainsi qu'une diversité d'objectifs d'optimisation. Différents algorithmes FDP séparés et conjoints sont proposés et les résultats indiquent que l'utilisation de la structure FDP proposée offre une amélioration entre 1.6 à 1.8 fois et entre 1.2 à 1.3 fois supérieure au rendement spectral du HD optimisé dans une multitude de scénarios FD MIMO pratiques point-à-point et point-à-multi-point, respectivement.

Acknowledgments

I would like express my sincere gratitude to the people who have supported me throughout the process of completing my Ph.D. First, I would like to thank my supervisor, Professor Tho Le-Ngoc. His guidance and support have been invaluable. I particularly appreciated his vast subject knowledge, genuine excitement towards research, and sense of humour. His ability to combine the theoretical, analytical design aspects with the experimental, practical implementation aspects of engineering design has significantly enhanced my knowledge and the calibre of my thesis. I am honoured to have been a member of the Broadband Communications Research Laboratory (BCRL).

I would also like to express my appreciation to the members of my Ph.D. supervisory committee, Professor Harry Leib and Professor Bruce Shepherd. Their feedback and suggestions have significantly contributed to improving the quality of my thesis.

I am also thankful for the financial support that I have received. Specifically, I would like to acknowledge the Hydro Quebec Engineering Doctoral Award, Vadasz Doctoral Fellowship in Engineering, McGill Engineering Doctoral Award (MEDA), and Natural Sciences and Engineering Research Council (NSERC) of Canada. Additionally, I would like to thank Bell Canada and Huawei Technologies for their financial support and feedback throughout the course of our collaboration.

I would also like to thank my colleagues and friends throughout the years in the BCRL at McGill University. In particular, I would like to thank Robert, Chris, Leonardo, Danny, Sanjeewa, Mahsa, Ahmed, Loic, Peng, Beri, Kevin, Jamshid, Suman, Amir, Soham, Prabhat, Pragyan, Ruikai, Saeideh, Seonghwan, Chaitanya, and Ngon. The quality of my thesis was significantly enhanced through our many discussions over the years.

I would like to especially thank my family for all their loving support throughout the years. I would like to thank my mother Adeena, father Ron, sister Jackie, and brother Mitchell for their unconditional support, guidance, assistance, and love. I would also like to thank my extended family for all their support.

Most of all, I would like to thank my fiance and best friend, Jordan, who was a constant source of support and encouragement, while also motivating me to enjoy life and travel the world with her. Thank you also to our dog, Teddy, for always putting a smile on my face. Finally, I would like to thank both Jordan's immediate and extended families for their constant support and for always making me feel like a welcomed member of the family.

Contents

List of Figures

List of Tables

List of Acronyms

ADC	Analog-to-Digital Converter
ANSI	American National Standards Institute
AP	Access Point
ASB	Autonomous Spectrum Balancing
AWG	American Wire Gauge
BS	Base Station
CO	Central Office
CP	Customer Premise
dB	Decibels
dBm	Decibel-milliwatts
DAC	Digital-to-Analog Converter
DC	Difference of Convex functions
DCA	Difference of Convex functions Algorithm
DCP	Disciplined Convex Programming
DMT	Discrete Multi-Tone
DoF	Degree of Freedom
DP	Diagonalizing Precoder
DPA	Dynamic Power Allocation
DRA	Dynamic Resource Allocation
DSB	Distributed Spectrum Balancing
DSL	Digital Subscriber Line
DSLAM	Digital Subscriber Line Access Multiplexer
DSM	Dynamic Spectrum Management
FD	Full-Duplex

FDP	Full-Duplex Precoding
FTTC	Fiber-To-The-Curb
FTTN	Fiber-To-The-Node
FFT	Fast Fourier Transform
HD	Half-Duplex
IA	Interference Alignment
IFFT	Inverse Fast Fourier Transform
INR	Self-Interference-to-Noise Ratio
IP	Interference Pricing
IWF	Iterative Water-Filling
JWI	Junction Wire Interface
KKT	Karush-Kuhn-Tucker
LNA	Low-Noise Amplifier
MIMO	Multiple-Input-Multiple-Output
MMSE	Minimum Mean Squared Error
MRU	Multiple Reference Users
MS	Mobile Station
MU	Multi-User
NE	Nash Equilibrium
OFDM	Orthogonal Frequency-Division Multiplexing
OSB	Optimal Spectrum Balancing
PA	Power Amplifier
PoM	Percentage of the Maximum
RA	Resource Allocation
RT	Remote Terminal
SCALE	Successive Convex Approximation for Low-complExity
SCAMP	Sequential Convex Approximations for Matrix-variable Programming
SCP	Sequential Convex Programming
SINR	Signal-to-Interference-plus-Noise Ratio
SIP	Self-Interference Pricing
SIR	Signal-to-Interference Ratio
SIT	Self-Interference Threshold
SMC	Spectrum Management Center

SNR	Signal-to-Noise Ratio
SRA	Static Resource Allocation
SU	Single-User
UE	User Equipment
VDSL	Very high bit-rate DSL
ZF	Zero-Forcing

List of Symbols

$\mathbf{C}$	Receive covariance matrix
f	Frequency sub-carrier index value
F	Number of frequency sub-carriers
f_s	Symbol rate
$\mathbf{G}$	Self-interference channel matrix
$\mathbf{H}$	Forward channel matrix
k, l	User index values
K	Number of users
$\mathcal{L}$	Lagrange function
M, N	Number of antennas
p	Transmit power
P	Total power constraint
$\mathbf{Q}$	Transmit covariance matrix
R	Sum-rate
$\mathbf{U}$	Postcoding matrix
$\mathbf{V}$	Precoding matrix
$\mathbf{x}$	Transmitted signal vector
$\mathbf{y}$	Received signal vector
$\mathbf{z}$	Noise vector
α	Auxiliary path gain
Γ	SNR gap
Δ_f	Frequency sub-carrier spacing
$\Delta\lambda$	Lagrange multiplier frequency offset
θ	Threshold value

λ	Lagrange multiplier
ν	Iteration number
π, ψ	Pricing functions
σ^2_{err}	Estimation error variance

Mathematical Notation

A, a	Non-bold variables denote scalars
$\mathbf{a}$	Lower-case bold variables denote vectors
$\mathbf{A}$	Upper-case bold variables denote matrices
$[\mathbf{A}]_{(i,j)}$	Refers to the (i,j)-th element of matrix $\mathbf{A}$
$\mathbf{A}^T$	Transpose of matrix $\mathbf{A}$
$\mathbf{A}^\dagger$	Conjugate transpose of matrix $\mathbf{A}$
$\mathbf{A} \succcurlyeq 0$	Refers to $\mathbf{A}$ as a positive semi-definite matrix
$E[\cdot]$	Expected value operation
$\mathbf{I}_d$	Identity matrix of dimensions $d \times d$
$\mathcal{O}(\cdot)$	Big-O notation
$\text{Tr}[\mathbf{A}]$	Trace of matrix $\mathbf{A}$
$\lvert\mathbf{A}\rvert$	Determinant of matrix $\mathbf{A}$
$\mathbf{0}_d$	All-zeros matrix of dimensions $d \times d$
$[x]_b^a$	$\min\{\max\{x, b\}, a\}$

Chapter 1

Introduction

1.1 Frequency Reuse and Interference Issues in Multi-User Systems

This thesis considers multi-user communication systems where users are serviced via an Access Point (AP). For example, an AP can refer to a Base Station (BS) for cellular networks or a Digital Subscriber Line Access Multiplexer (DSLAM) for DSL networks. Each AP services its respective users, referred to as User Equipments (UEs), in the downlink using point-to-multi-point communication and in the uplink using multi-point-to-point communication. For both downlink and uplink, when transmitters send signals over the same frequency, at the same time, within the same geographical area, the receivers experience co-channel interference.

A conventional approach to avoiding such interference involves the use of fractional frequency reuse where nearby groups (e.g., cells or DSLAMs) are allotted different frequency bands to avoid the more dominant co-channel interference. Conversely, groups which are sufficiently far may reuse the same frequency band. However, in order to support the demands for content-rich services, more efficient use of the frequency spectrum is required. In particular, universal frequency reuse, in which each group shares the same frequencies, is employed. Universal frequency reuse increases the amount of inter-group interference; however, if such interference is handled in an efficient manner, the spectral efficiency (i.e., bits/s/Hz/Area) can be significantly increased.

The networks under consideration are assumed to be linear interference-limited sys-

tems, where the main performance degradation is caused by co-channel interference as opposed to background noise. There are two main approaches to managing interference in interference-limited environments. The first approach makes use of the fact that the interference generated is known and can be used to enhance the performance, while the second approach is that of interference avoidance.

More specifically, the first approach makes use of the interference by applying results from Multiple-Input-Multiple-Output (MIMO) systems. Using this approach, each user and Degree of Freedom (DoF, e.g., time, frequency, space) represents one virtual antenna. Hence, a super-node approach can be taken by applying MIMO beamforming across all users and all dimensions to maximize the throughput of the overall network.

Beamforming is a signal processing technique that is used to represent the physical manipulation of the angular direction of transmitted signal energy (i.e., beams), typically referring to wireless networks. Mathematically, beamforming is implemented using precoding at the transmitter. For DSL networks, since there are no physical beams being manipulated, the technique is referred to as vectored DSL and it can be applied at either the transmitter (i.e., downlink) or the receiver (i.e., uplink). Precoding and/or postcoding are signal processing techniques that can be used to modify the transmission channel for linear systems (e.g., to remove or minimize the effect of interference). More specifically, the precoder can be designed at the transmitter to pre-cancel interference, whereas the postcoder can be designed at the receiver to post-cancel interference.

The second approach attempts to avoid interference through orthogonality. A classic form of interference avoidance is partitioning the available resources (e.g., time, frequency) to avoid users sharing the same frequency channel at the same point in time. A more sophisticated approach is known as interference alignment. Interference alignment designates separate signal and interference subspaces at each receiver in order to avoid interference and will be discussed in greater detail in Section 2.2.

1.2 Point-to-Point and Point-to-Multi-Point Channels

This section briefly describes the channels under consideration. A multi-user channel is any channel that is shared between multiple users (i.e., UEs). Each channel consists of nodes which are connected by links. A link can correspond to single or multiple spatial dimensions (i.e., single or multiple antennas).

For example, Fig. 1.1 shows an example of a point-to-point or single-user unidirectional communication channel (i.e., a communication connection between two nodes).

Fig. 1.1 Point-to-point or single-user channel.

Similarly, Fig. 1.2 shows examples of point-to-multi-point (i.e., downlink) and multi-point-to-point (i.e., uplink) unidirectional communication channels.

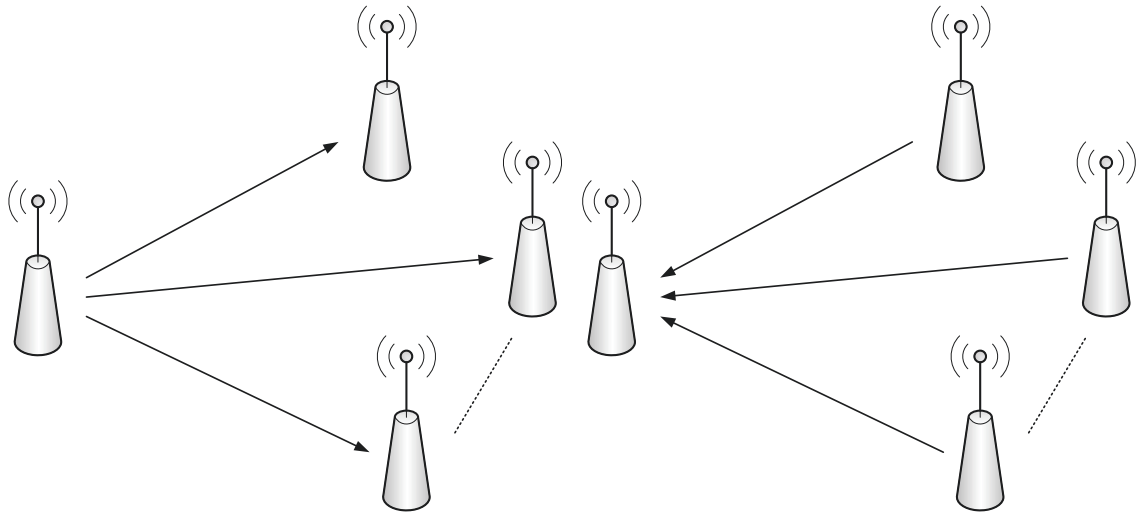

(a) Point-to-multi-point or downlink channel. (b) Multi-point-to-point or uplink channel.

Fig. 1.2 Downlink vs. uplink channel.

Finally, Fig. 1.3 shows an example of a unidirectional multi-link point-to-point[1] or interference channel (i.e., multi-point-to-multi-point, typically with equal numbers of transmitters and receivers), where each solid link refers to an intended signal and the dashed links refer to the resulting interference signals.

[1]Multi-user DSL is an example of a multi-link point-to-point system.

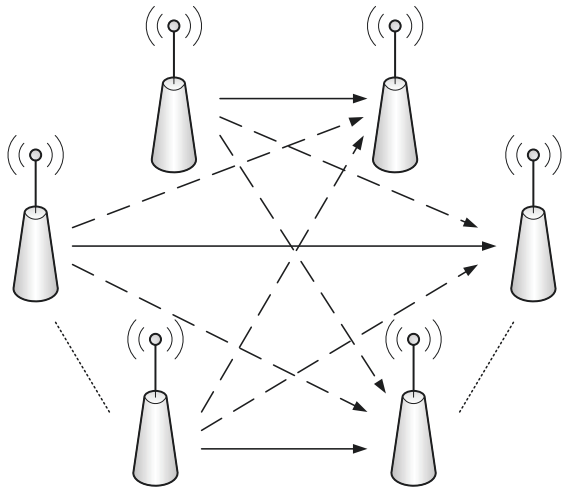

Fig. 1.3 Multi-link point-to-point or interference channel.

1.3 Half-Duplex vs. Full-Duplex Transmission

Conventional systems apply Half-Duplex (HD) transmission, which provides uplink and downlink communication using separate time and/or frequency slots. As discussed in Section 1.1, universal frequency reuse can be employed to increase the spectral efficiency of the system. Full-Duplex (FD) communication systems attempt to further increase the spectral efficiency of the system by increasing the amount of sharing between the uplink and downlink. In particular, for FD systems, nodes transmit and receive signals simultaneously over the same frequency at the same time.

FD systems can potentially have a sum-rate "double" that of their HD counterparts [1, 2]. However, FD transmission incurs additional interference, known as self-interference, from the transmitter to the receiver of the same node, as shown in Fig. 1.4. Typically, the self-interference is significantly larger than the received signal strength, which can prevent the potential "double" sum-rate gains of FD transmission, and hence, calls for effective self-interference management. The FD approach lends itself well to the concept of small cells (e.g., picocells or femtocells), since for shorter distances, the received signal-to-self-interference ratio is larger. The concept of small cells is discussed in Section 1.5.2.

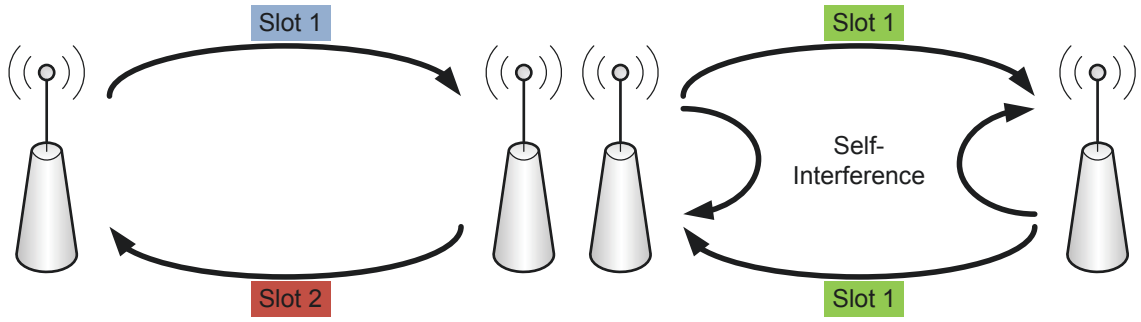

(a) Half-duplex transmission. (b) Full-duplex transmission.

Fig. 1.4 Half-duplex vs. full-duplex transmission.

1.4 Dynamic Resource Allocation Techniques

The demand for data-intensive services is on the rise. In order to support more sophisticated services higher data-rates are required. Hence, more efficient spectral efficiency is required. Resource Allocation (RA) techniques can be employed to achieve this goal. The most basic form of RA is known as Static RA (SRA). SRA implements a pre-determined and fixed RA, typically based on a worst-case scenario assumption for all users in the network. This leads to an inefficient use of resources whenever the scenario is not the worst-case and consequently leads to highly sub-optimal performance.

Dynamic RA (DRA)[2] is a wide field which looks to adaptively apply different RAs for each user with the intent of improving the resource efficiency of the overall system. DRA allows for a far more efficient use of the spectrum than SRA does. DRA can be applied to mitigate interference and/or to apply signal-level coordination to cancel interference.[3] Signal level coordination applies precoding and/or postcoding to effectively manage interference.

1.5 Environments Under Consideration

This thesis provides illustrative results to demonstrate the effectiveness of the derived DRA techniques. More specifically, in this thesis, illustrative results will correspond to either wireline or wireless systems. In particular, DSL systems offer a multi-link environment,

[2] In DSL literature, this is referred to as Dynamic Spectrum Management (DSM).

[3] When these signal-level coordination techniques are applied to DSL networks they are often referred to as vectored DSL and when they are applied to wireless networks they are often referred to as beamforming.

while cellular networks offer point-to-multi-point and multi-point-to-point environments. The following subsections provide a brief introduction to these environments.

1.5.1 Digital Subscriber Line Networks

DSL makes use of twisted-pair copper telephone wires to transmit digital data. The interference between lines is known as crosstalk. Generally, DSL direct channels are smooth, monotonically decreasing functions of frequency, due to the fact that copper-wire attenuation increases with frequency. Conversely, DSL crosstalk frequency responses are typically very curvy, often containing manly local minima and maxima and typically increase with frequency relative to the direct channels. Finally, since DSL lines are typically buried underground, the channel is slow time-varying.

DSL uses Discrete Multi-Tone (DMT) transmission, a scheme which is similar to Orthogonal Frequency-Division Multiplexing (OFDM). The basic idea is to transmit the data in parallel over each frequency sub-carrier. Fig. 1.5 shows a typical DSL network. As

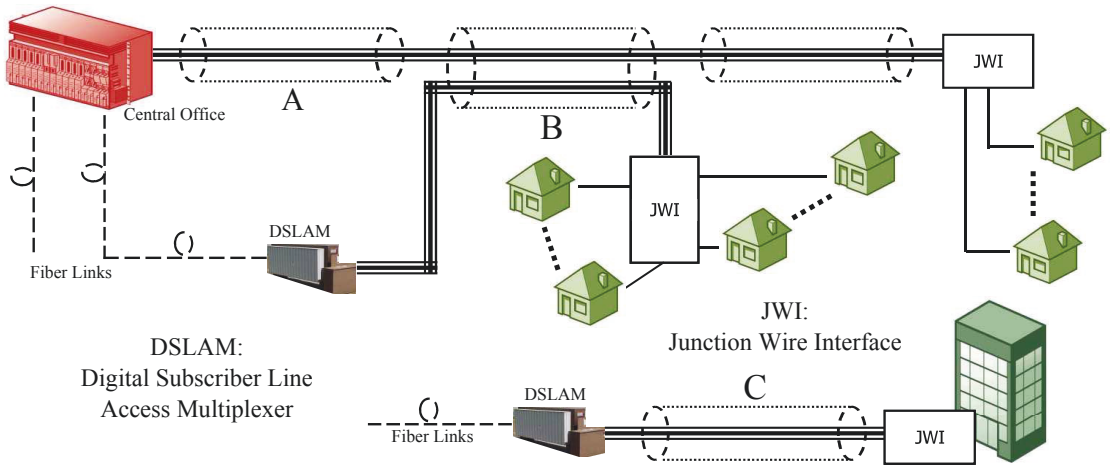

Fig. 1.5 Example of a typical DSL network.

shown in Fig. 1.5, the twisted-pair copper wire is run through binders. Binders can be shared by various groups of lines causing interference to one another. Binder B in Fig. 1.5 is an example of this type of binder configuration. Binder B is shared between the loop from the Central Office (CO) to the Customer Premises (CPs) or UEs at the top right of the diagram and the loop between a DSLAM and the CPs or UEs in the middle of the diagram.

Twisted-pair copper wire attenuation increases with length. As such, when the receivers are in close proximity to the transmitters of another bundle, they receive large amounts of crosstalk. Hence, effectively managing interference in multi-link systems is a key issue for DSL systems.

1.5.2 Cellular Networks

A cellular network is a radio network distributed over a land area referred to as a cell. Each cell is operated by a BS which serves multiple users known as Mobile Stations (MSs) or UEs. Downlink transmission refers to transmission from BSs to MSs, while uplink transmission refers to transmission from MSs to BSs. As discussed in Section 1.1, the concept of universal frequency re-use has emerged. To this end, the concept of small cells has developed. Small cells are low-powered radio access nodes that are located within a larger cellular network while sharing the same frequency spectrum and making use of a wired back-haul. There are two main types of small cells, namely, femtocells and picocells. Fig. 1.6 shows an example of a cellular network with pico- and femto cells, where the picocells correspond to the larger of the two small cells.

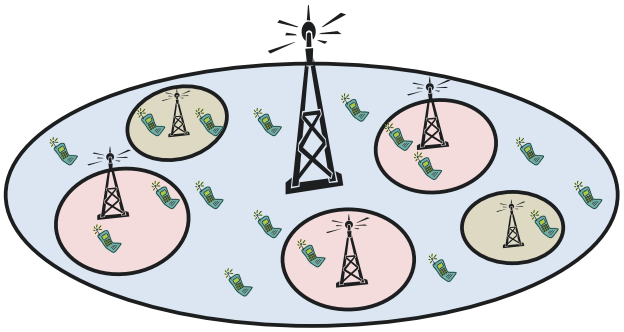

Fig. 1.6 Example of a cellular network with pico- and femtocells.

Cellular networks suffer from frequency-selective fading. Fading can be caused by many factors (e.g., signals traveling along different paths, tunnels, hills, large buildings). Due to the dynamic nature of the wireless channel, the channel coefficients for cellular networks are highly time-varying. Due to the frequency selective nature of the wireless channel, OFDM modulation is typically implemented, where the frequency range is split into sub-channels over which the frequency response is relatively flat.

Small cell networks encourage shorter transmission to and from the UE which increases network capacity but can potentially introduce additional co-channel interference. As such, small cells typically operate with low powers to attempt to reduce additional co-channel interference. Due to the low power operation of small cells, they are a good candidate for applying FD transmission.

1.6 Thesis Contributions and Organization

Increasing the amount of resource sharing (e.g., time, frequency) increases the amount of interference present but also increases the potential spectral efficiency gains provided the interference can be effectively managed. The focus of this thesis is on the design of scalar and vectored DRA transmission techniques to manage interference in severely interference-limited environments with applications to both wireline and wireless systems.

The remainder of this thesis is organized as follows. Chapter 2 reviews the relevant literature on HD multi-link scalar Dynamic Power Allocation (DPA), HD point-to-point MIMO precoding, and FD point-to-point and point-to-multi-point systems.

Chapter 3 applies a distributed HD multi-link scalar DPA approach where each user performs its own resource allocation with some indirect cooperation in mind. This is achieved by introducing the concept of a virtual network of reference users which provides approximate global knowledge by taking advantage of the clustered nature of networks to avoid the super-node structure. The proposed approach is a non-cooperative game theoretic approach where each user's utility function is designed with cooperation in mind. That is, each user operates using a modified water-filling procedure which allows for the algorithm to be implemented with low-complexity and in a distributed nature with no per-iteration message passing requirements. Additionally, a method for estimating the spectral efficiency prior to allocating resources is derived.

Chapter 4 focuses on FD MIMO point-to-point systems. A Full-Duplex Precoding (FDP) structure is proposed which applies joint beamforming and self-interference cancellation using precoding. The FDP structure allows for many different optimization objectives (e.g., sum-rate maximization, energy efficiency, self-interference minimization) and for many different algorithms to be developed. Numerous FDP algorithms are proposed focusing on the objective of sum-rate maximization. In particular, for the FDP structure, separate and joint optimization techniques are proposed and compared.

Chapter 5 considers FD MIMO point-to-multi-point systems. The sum-rate maximization problem leads to a non-convex optimization problem for which finding solutions is difficult. A Sequential Convex Programming (SCP) approach is taken to solve the non-convex optimization problem by constructing and solving a sequence of convex optimization problems. Two SCP algorithms are developed. The first is based on the difference of convex functions structure of the optimization problem and the second is a general algorithm we developed referred to as Sequential Convex Approximations for Matrix-variable Programming (SCAMP). Finally, analytical expressions for the loss in sum-rate incurred due to the effect of residual self-interference are derived.

Chapter 6 provides some concluding remarks and summarizes the key results of this thesis.

Chapter 2

Literature Review

This chapter provides a short literature review of the state-of-the-art approaches in scalar and vectored DPA techniques for HD and FD systems. Section 2.1 provides a literature review of the main HD multi-link scalar DPA approaches. Section 2.2 focuses on the main HD MIMO point-to-point precoding approaches. Finally, Section 2.3 provides a literature review of the main FD MIMO point-to-point and point-to-multi-point approaches.

2.1 Half-Duplex Multi-Link Scalar Dynamic Power Allocation

In order to improve resource efficiency, effective resource management techniques must be employed. In this section, we focus on scenarios where users share a particular frequency band (i.e., multi-carrier or single-carrier). As such, this section focuses on wide- or narrow-band scalar power allocation techniques. In particular, scalar Dynamic Power Allocation (DPA) is a wide field which looks to adaptively apply different power allocations for each user with the intent of maximizing the throughput of the system (or conversely minimize the total power consumption under fixed rate constraints).

DPA treats each line/antenna independently. As such, the interference is not manipulated, instead the power allocation of each line/antenna is dynamically adjusted to maximize the system sum-rate in the presence of interference. Typically, the DPA approach performs worse than the vectored approach (i.e., precoding).

DPA allows for a far more efficient use of resources than static power allocation. As a result, many different DPA algorithms have been proposed. The focus of the literature review in this section will be on HD DPA techniques (i.e., adaptive power control). A

detailed survey of DPA with specific applications to DSL networks is provided in our previous work [3]. The rate adaptive DPA problem can be written as follows:

$$\begin{aligned} \max_{p_f^k, \forall\ f,\ k} \quad & \sum_{k=1}^{K} w_k R_k \\ \text{subject to:} \quad & \sum_{f=1}^{F} p_f^k \leq P_{k,\max} \quad \forall \quad k, \\ & 0 \leq p_f^k \leq p_f^{k,\text{mask}}, \quad \forall \quad f,\ k, \end{aligned} \tag{2.1}$$

where p_f^k is the transmit power of user k on frequency sub-carrier f, $P_{k,\max}$ is the total power constraint for user k, $p_f^{k,\text{mask}}$ is the per-sub-carrier total power constraint for user k on sub-carrier f, w_k is the weighting function for user k, and R_k is the rate of user k.

The main criteria in comparing different DPA algorithms is their performance and their complexity. The performance relates how well an approach succeeds at maximizing the achievable weighted sum-rate as compared to the theoretical optimum. The complexity of the algorithm is related to the amount of time required to derive the power allocation as the number of users and frequency sub-carriers increase.

There are two main types of DPA algorithms: centralized and distributed. Centralized systems require a central hub with full knowledge of the network. In general, this system allows for better performance at a cost of increasing the complexity and computational time. On the other hand, distributed systems allow for every user to self-optimize, fully autonomously, without the need of explicit message passing. In general, distributed systems reduce the complexity and computational time but often sacrifice some optimality in terms of performance. The final type of algorithms are semi-centralized DPA algorithms, where the users self-optimize but require some per-iteration messaging passing with a central hub.

One of the first distributed DPA algorithms was Iterative Water-Filling (IWF) [4]. In IWF, each user selfishly maximizes their own sum-rate. While IWF gives significant sum-rate improvements over static techniques, in many situations, it leads to sub-optimal performance. In an attempt to improve the performance of IWF, many heuristic variations have been proposed (e.g., [5–10]).

A centralized algorithm called Optimal Spectrum Balancing (OSB) [11], which maximizes the weighted sum-rate across the users, was derived to solve for the globally optimal

power allocation. OSB uses dual decomposition to solve for the optimal transmit powers for each user separately on each frequency sub-carrier by exhaustive search. While OSB is not computationally tractable for many users, it serves as an upper-bound on the performance of other DPA algorithms for cases with few users. Due to the complexity limitations of OSB, some lower-complexity near-optimal variations have been proposed (e.g., [12–14]).

Centralized systems are generally harder to implement in practice. It is for this reason that many other algorithms were introduced. One such algorithm is Autonomous Spectrum Balancing (ASB) [15, 16]. ASB uses the same problem formulation as OSB but operates in a distributed fashion without the need for any explicit message passing. ASB uses the concept of a virtual user (referred to as a reference line/user), which represents the typical victim in the network. Each user self-optimizes to protect the reference user, and hence, attempts to better the overall network. Generally ASB cannot find a globally or locally optimal solution; however, its performance has been shown to be strong in some scenarios while maintaining a relatively low complexity.

One issue regarding the ASB algorithm is that the update formula can be relatively time-consuming. It is for this reason that [17] proposed the ASB-2 algorithm. The ASB-2 algorithm works exactly like the ASB algorithm but uses a slightly different update formula. This update formula has a significantly lower complexity. ASB and ASB-2 do not necessarily converge to the same solution; however, the ASB-2 algorithm converges significantly faster than ASB, especially when the number of users and/or frequency sub-carriers are very large.

An algorithm called semi-blind spectrum balancing [18] builds on the concepts introduced in ASB. Semi-blind spectrum balancing operates in the same fashion as ASB but also dynamically updates a unique virtual reference user for each user separately, to more accurately represent the network. The virtual users are updated at a Spectrum Management Center (SMC) based on message passing to and from the users. This requires the algorithm to be run in a semi-centralized manner, but generally leads to an improved sum-rate.

Due to the computational complexity of solving for globally-optimal power allocations, the focus of research has been on semi-centralized locally-optimal power allocations. Distributed Spectrum Balancing (DSB) [17] and Successive Convex Approximation for Low-complExity (SCALE) [19, 20] are semi-centralized algorithms which require full channel knowledge and per-iteration message passing. They can achieve strong performance but cannot operate in a fully distributed manner.

DSB writes the objective function as a Difference of Convex functions (DC) and applies the Karush-Kuhn-Tucker (KKT) conditions directly. With the use of a message passing system, the DSB algorithm solves for a locally optimal solution in an iterative fashion. SCALE is an algorithm that applies a series of concave lower-bounds to the maximization problem. This enables SCALE to make use of the well-researched area of convex optimization to maximize the concave lower-bound. Each successive iteration tightens the lower-bound towards a locally optimal solution.

SCALE is an example of a Sequential Convex Programming (SCP) algorithm (i.e., an iterative algorithm which solve a sequence of convex subproblems to find a locally optimal solution). Another example of a SCP algorithm is the DC Algorithm (DCA) [21]. DCA is a centralized algorithm that begins by re-writing the non-convex objective function in terms of the difference of two convex functions (i.e., $f = g - h$), as in the DSB approach; however, DCA iteratively creates an affine minorization (multivariate first-order approximation) of h, denoted by $\tilde{h}$, which is used to make the objective function, $\tilde{f} = g - \tilde{h}$, convex. Each successive iteration more closely approximates the locally optimal solution. For any function f, many DC decompositions exist (e.g., $g - h = (g + \phi) - (h + \phi)$). The choice of decomposition has a crucial impact on the convergence speed as well as the performance. There are still a lot of heuristics regarding the DCA implementation which have yet to be explored in great detail.

Interested readers are referred to our previous works, [3, 22], for a detailed overview of DPA algorithms. The most significant DPA algorithms as far as this thesis is concerned are: IWF, ASB-2, DSB, and SCALE. Typically, DSB and SCALE perform very similarly as they both search for locally optimal solutions. In particular, the semi-centralized nature of DSB and SCALE allow for them to make use of more channel knowledge, and hence, lead to better performance than other approaches. Most of the above mentioned algorithms have a similar structure. In particular, they are iterative algorithms whereby on each iteration the power spectrum of each user is adjusted. While SCALE uses a slightly different update formula, IWF, ASB-2, and DSB all have identical structural roots. More specifically, their update formulas are of the following form:

$$p_f^k = \left[\frac{w_k}{\lambda_k + \Delta\lambda_f^k} - \frac{\Gamma \mathrm{int}_f^k}{|h_f^{k,k}|^2} \right]_0^{p_f^{k,\mathrm{mask}}}, \tag{2.2}$$

where p_k^f is the transmit power of user k on frequency sub-carrier f, λ_k is the Lagrange multiplier associated with the total power constraint for the k-th user, Γ is the Signal-to-Noise Ratio (SNR) gap, $h_f^{k,k}$ is the direct channel gain of user k on frequency sub-carrier f, int_f^k is the interference seen by user k on frequency sub-carrier f, $p_f^{k,\text{mask}}$ is the power constraint associated with the f-th frequency sub-carrier for the k-th user, and $[x]_b^a = \min\{\max\{x, b\}, a\}$.

The difference between the approaches of IWF, ASB-2, and DSB are in the selection of the parameter $\Delta\lambda_f^k$. For IWF, $\Delta\lambda_f^k = 0$, whereas for ASB-2 and DSB, the value of $\Delta\lambda_f^k$ are adjusted and tuned after each iteration. We refer to this parameter as the Lagrange multiplier frequency offset. Chapter 3 will investigate and discuss the offset in more detail.

2.2 Half-Duplex MIMO Point-to-Point Precoding

Precoding and postcoding are signal processing techniques which exploit the spatial separation between the desired signal and its interference [23]. An extensive survey on precoding and postcoding applied to DSL systems is provided in our previous work [24]. As well, our previous work, [25], discusses various implementation challenges (e.g., computation load, memory storage, line management, partial cancellation, and the effects of imperfect channel knowledge).

For illustrative purposes, consider a single-carrier communication network with a set of users $\mathcal{K} = \{1, \ldots, K\}$. HD transmissions can be modeled as follows:

$$\mathbf{y} = \mathbf{H}\mathbf{x} + \mathbf{z}.$$

The vector $\mathbf{x} \triangleq (x_1, \ldots, x_K)^T$ contains the transmitted signals for all users. Similarly, $\mathbf{y} \triangleq (y_1, \ldots, y_K)^T$ and $\mathbf{z} \triangleq (z_1, \ldots, z_K)^T$ contain the received signals and background noise for all users, respectively. $\mathbf{H}$ is a $K \times K$ matrix such that $[\mathbf{H}]_{(k,l)}$ is the channel gain from transmitter l to receiver k.

The transmitted signals, $\mathbf{x}$, can be pre-processed using a precoding matrix[1], $\mathbf{x} = \mathbf{V}\tilde{\mathbf{x}}$. Similarly, the received signal can be post-processed using a postcoding matrix, $\tilde{\mathbf{y}} = \mathbf{U}^\dagger\mathbf{y}$.

[1]Note that the choice of $\mathbf{V}$ will be subject to transmit power constraints.

Hence, the modified transmission can be written as:

$$\tilde{\mathbf{y}} = \mathbf{U}^{\dagger}\mathbf{H}\mathbf{V}\tilde{\mathbf{x}} + \mathbf{U}^{\dagger}\mathbf{z}.$$

Essentially, the precoding and postcoding matrices "modify" the true channel (i.e., the original channel, $\mathbf{H}$, is effectively replaced by the modified channel, $\mathbf{U}^{\dagger}\mathbf{H}\mathbf{V}$). There are many different techniques for selecting the precoding and decoding matrices. As well, depending on the scenario, it may be more practical to only apply a precoding or a postcoding matrix, but not both.[2]

Precoding approaches can be divided into two sub-categories: linear precoding and non-linear precoding. Non-linear precoding techniques involve operations which affect the linearity of the system (e.g., a modulo operation). Examples of non-linear precoding techniques include the Tomlinson-Harashima precoder [26–28], and the decision-feedback canceller [28]. Non-linear techniques have been shown to be capable of achieving the capacity region in some scenarios (e.g., using a dirty-paper coding approach) [29] but have a high computational complexity.

Conversely, linear precoding techniques maintain the linearity of the system. Linear precoding techniques can often achieve strong performance while operating at a significantly reduced computational complexity. Some examples of linear precoding techniques include Minimum Mean Squared Error (MMSE) filtering [30], the Zero-Forcing (ZF) [30–32] precoder and canceller, and the Diagonalizing Precoder (DP) [33]. The extent of the sub-optimality of linear precoding can vary based on the environment and, more specifically, the channel. For example, it is shown in [32] and [33] that the DSL channel is diagonally dominant, and hence, linear precoding techniques can lead to near-optimal performance.

The focus of this literature review will be on linear techniques such as MMSE and ZF [30], since they are more practically applicable. The ZF approach is designed to zero-out all the interference, whereas the MMSE approach is designed to maximize the received SNR but not necessarily zeroing-out the interference. Hence, the MMSE approach provides optimal performance in terms of bit-error rate with increased complexity while the ZF approach doesn't achieve as strong performance but operates at a reduced computational complexity.

[2]For example, this is the case for DSL systems, where for downstream transmission only precoding is used and for upstream transmission only postcoding is used.

The super-node precoding approach (i.e., jointly processing all users) can be a very effective technique for cancelling the effects of interference between users when the number of users and the number of DoFs are not too large. More specifically, as the number of users and the number of DoFs increase, the super-node precoding complexity increases greatly (e.g., requiring computing the inverse of very large matrices).

In order to tackle this issue, various interference coordination approaches have been developed whereby the interference is manipulated using precoding and/or postcoding techniques. Arguably the most popular interference coordination approach in known as Interference Alignment (IA) [34–43]. IA is a linear precoding technique which aligns the interference signals into a subspace with respect to the number of DoF (i.e., time, frequency or space). IA schemes are designed such that users coordinate their transmissions so that the interference at each receiver lies within a reduced dimensional subspace and can therefore be removed using post-processing by applying an appropriate postcoding matrix at each receiver.

IA was proposed in [34] as a method for removing the effects of interference, where each user makes use of half the available DoF. Distributed iterative algorithms based on minimizing leakage interference and maximizing the Signal-to-Interference-plus-Noise Ratio (SINR, where perfect IA is not guaranteed) were proposed in [36, 44]. The concept of subspace IA for the application of cellular networks was introduced in [40]. The idea is to align interference into a multi-dimensional subspace rather than along a single dimension for simultaneous alignment at multiple BSs. An IA algorithm which selects an alignment that maximizes the sum-rate given the constraint that perfect IA is achieved was proposed in [37]. A set of linear precoding designs (both iterative and non-iterative) by selecting orthonormal basis vectors which maximize the number of DoF at the receiver and maximizes the weighted sum-rate using a gradient descent approach at the transmitter was proposed in [38].

Another interference control approach is known as Interference Pricing (IP) [45–49]. IP was first introduced in [45] as a method for increasing network throughput through user cooperation. Typically, "prices" are Lagrange multipliers for a constrained resource, whereas with the IP approach, the prices represent the interference among users. With the IP approach, users exchange price signals that indicate the "cost" of receiving interference. Based on the exchanged prices, each user self-optimizes their power allocation using a modified objective function which balances its own rate gain and the interference it causes

to others. The interference caused to others is represented by each user's pricing function, which is the marginal decrease in its own utility due to interference.

The modified utility function for each user is written out as follows:

$$\mathcal{U}_k = R_k - \sum_{l \neq k} \pi_l I_{l,k},$$

where R_k is the achievable rate for user k which is a function of the transmit powers of all users, $I_{l,k}$ is the interference generated from user k to user l and π_l is the marginal decrease in the l-th user's rate due to interference and is computed as:

$$\pi_l = -\frac{\partial R_l}{\partial \mathrm{INT}_l},$$

where $\mathrm{INT}_l = \sum_{i \neq l} I_{l,i}$.

IP was applied to wireless Orthogonal Frequency-Division Multiplexing (OFDM) networks in [46] and extended to non-separable utility functions. IP was applied to updating precoding matrices for a two-user MIMO interference channel in [47]. First, MMSE receivers are fixed while the precoding matrices and powers are optimized. The MMSE receivers and interference prices are updated on every iteration. The approach was generalized in [48] to multi-user peer-to-peer wireless networks with MIMO channels using rank one precoding matrices (i.e., beamforming vectors). Finally, a sub-optimal beamforming algorithm for the multiple-input-single-output interference channel was presented in [49].

2.3 Full-Duplex MIMO Point-to-Point and Point-to-Multi-Point Systems

Three main types of FD systems, namely FD relay, FD MIMO point-to-point, and FD MIMO point-to-multi-point, have been considered.[3] Research on precoding design for FD relay networks typically focuses on the suppression of self-interference (e.g., [50–54]).

Antenna selection [50] selects the precoding and postcoding matrices as scaled row and column selection matrices. The approach is to simply select the antenna pairs which lead to

[3]This thesis will not consider FD relay networks; however, most of the existing literature on FD self-interference management has been focused on relay networks. As such, a brief discussion is provided in this section.

a minimal residual self-interference. Beam selection [50, 55] first applies the singular value decomposition to diagonalize the self-interference channel and selects the precoding and postcoding matrices by applying antenna selection on the resulting diagonalized channel. The null-space projection method [50, 56–60] is an IA approach that selects the precoding and postcoding matrices such that the transmitter and receiver operate in different subspaces. More specifically, the transmit signals are projected into the null-space of the self-interference channel via the postcoding matrix. MMSE filtering [50, 54, 61] selects the postcoding matrices to minimize the distortion while reducing the self-interference.

A Signal-to-Interference Ratio (SIR) maximization [51] approach was designed for the FD relay network. The approach designs the postcoder to maximize the ratio of the source-to-relay and self-interference links and designs the precoder to maximize the ratio of the relay-to-destination and self-interference links. One limitation of the SIR maximization approach is that it is unable to give priority to either the forward channel or the self-interference channel, causing issues in the high interference and high SNR regimes. Finally, the algorithm is designed for FD relay systems, and hence, is not directly applicable to other FD models.

For FD MIMO point-to-point systems, [62] proposed a time-domain beamforming method for self-interference cancellation. A precoding design for a partial analog interference cancellation model combined with self-interference and additional transmit power constraints was proposed in [63]. A beamforming design which minimizes the required transmit power subject to total SINR constraints and self-interference constraints was proposed in [64]. While modeling the dynamic-range limitations explicitly, [65] applies pilot-aided channel estimates to perform transmit/receive beamforming using a gradient projection method. A low-complexity distributed version of [65] was proposed in [66] using a null-space projection method.

FD MIMO point-to-multi-point systems where APs operate in FD-mode while UEs operate in HD-mode are studied in [67] and [68]. In order to simplify the derivations, the interference caused by uplink transmission to downlink UEs was ignored in [67] and [68]. Two precoding schemes were presented in [67] to approximate the solution of the non-convex optimization problem. More specifically, [67] presented a sequential precoding scheme which first selected a downlink precoding scheme and then optimized the uplink precoding scheme assuming the fixed downlink precoding. As well, [67] presented a joint precoding scheme by applying a first-order approximation to the DC objective function. The work in [67] was

extended in [68] to incorporate both spectral and energy efficient designs. On the other hand, the interference caused by uplink transmission to downlink UEs is considered in [69], where the effect of large-scale MIMO systems on FD is investigated by selecting the ratio between the number of transmit and receive antennas at the AP.

While recent research has focused on precoding design techniques, more typical FD transceiver design approaches focus on either passive (e.g., [70–73]) or active (e.g., [74,75]) cancellation techniques. Passive cancellation is typically done at the antenna level (e.g., using a circulator [70,76]).

The active cancellation approach involves subtracting an estimate of the self-interference at the receiver. Active cancellation can be performed in either the analog domain, digital domain, or both (e.g., [77], [78], and [79], respectively).

The passive and active cancellation approaches focus solely on the cancellation of self-interference. The approaches are additive in the sense that the passive cancellation suppresses some of the self-interference at transmission, while the active cancellation attempts to further suppress the self-interference at the receiver.

Applying active cancellation in the MIMO-case requires the self-interference from each transmit antenna be replicated and subtracted at each receiver. As well, in the MIMO case, the active cancellation approach requires a separate beamformer for forward transmission, as shown in Fig. 2.1.

Fig. 2.1 shows an example of a MIMO FD active analog cancellation structure. Fig. 2.1 shows that the active cancellation approach makes use of auxiliary paths from the transmitter to the receiver controlled by a self-interference replica generator.

2.4 Concluding Remarks

In this chapter, we have provided a survey of the state-of-the-art techniques for scalar and vectored HD and FD DRA. For HD multi-link systems, it was seen that many of the proposed scalar DPA algorithms have a similar structure. In particular, it was discussed that the per-iteration Lagrange multiplier tuning process increases the performance but, typically, requires many iterations to converge.

For HD MIMO point-to-point systems, the concepts of precoding, postcoding, IA, and IP were discussed. The concepts are relevant for both HD and FD precoding design. Effective precoding-based interference control is essential in realizing the potential performance

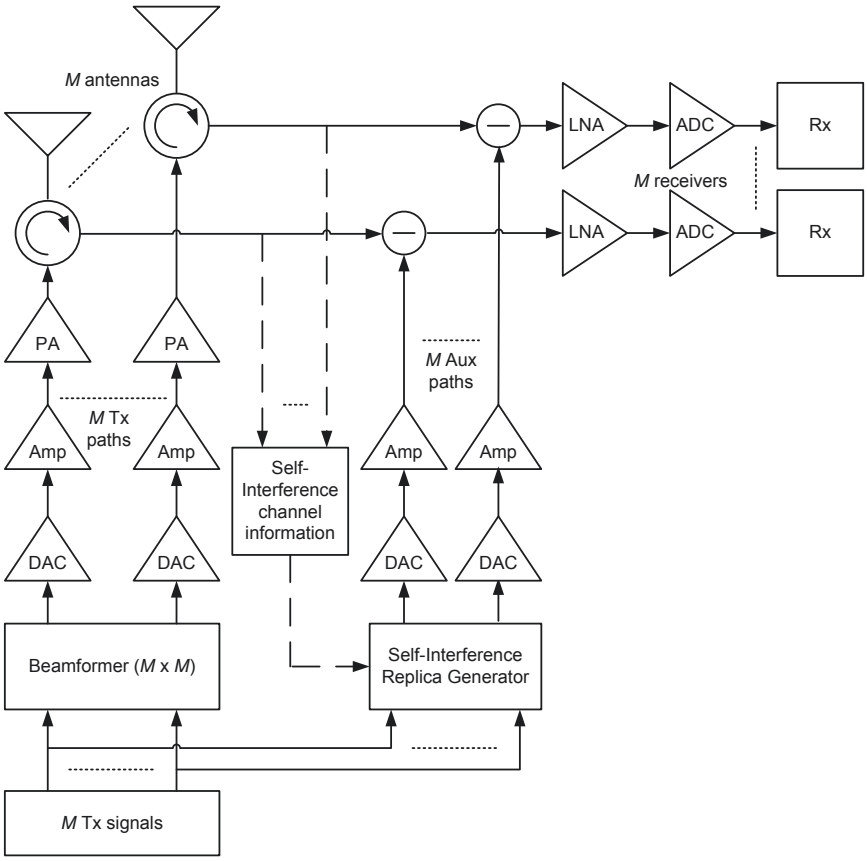

Fig. 2.1 A example of a MIMO FD active cancellation structure.

benefits of the interference-limited communication systems under consideration in this thesis.

Finally, for FD point-to-point and point-to-multi-point systems, many of the proposed approaches focus solely on the suppression of self-interference and algorithms which allow for an effective trade-off between maximizing the forward channel and suppressing the self-interference are necessary.

The above literature review provides some motivation for the research topics presented in this thesis. More specifically, Chapter 3 develops a low-complexity HD multi-link scalar DPA algorithm, while Chapters 4 and 5 develop effective sum-rate maximization-based algorithms for FD MIMO point-to-point and point-to-multi-point systems, respectively.

Chapter 3

Interference Coordination in a Multi-Link Environment[1]

3.1 Introduction

As discussed in Chapter 2, the performance benefits of DRA over SRA techniques are well known. In IWF [4], each user selfishly maximizes their own sum-rate until a, typically, sub-optimal point is reached. Due to the computational complexity of solving for globally-optimal power allocations, the focus of research has been on locally-optimal power allocations (e.g., DSB [17] and SCALE [19, 20]). DSB and SCALE are semi-centralized algorithms which require full channel knowledge and per-iteration message passing. They can achieve strong performance but cannot operate in a fully distributed manner.

On the other hand, ASB [16] and ASB-2 [17] are fully distributed algorithms where each user self-optimizes while attempting to minimize the damage done to a virtual reference user (representative of a typical victim). The authors of [16] and [17] discuss the use of a single reference user and only allude to the fact that Multiple Reference Users (MRU) could also be used. Moreover, a systematic approach for the reference user selection is still an open question.

ASB-2, DSB, and SCALE use water-filling-like transmit power update formulas, where the Lagrange multiplier is modified by frequency-selective offsets. The offsets represent

[1]Parts of Chapter 3 have been presented at the 2010 IEEE Global Communications Conference (GLOBECOM) [80], the 2011 IEEE GLOBECOM [81, 82], published in the IEEE Transactions on Signal Processing [83], and accepted to be published in an IGI Global book chapter [22].

per-frequency sub-carrier penalties and are updated on a per-iteration basis using message passing and central computations. By iteratively updating the offset values, the algorithms improve their performance on a per-iteration basis; however, many iterations are typically required to properly *tune* the offsets until they converge. Between each iteration, the users must take new interference measurements, which can be time-consuming.

The first part of this chapter focuses on the use of MRU and introduces a systematic method for selecting the reference users and their respective parameters that can be blindly applied to practical networks. In the MRU case, the set of reference users can be viewed as a *virtual network*, representative of the true network. Intuitively, in the proposed approach, users self-optimize with approximate global knowledge introduced by the virtual network, representative of both the disturbers and the victims. This chapter also introduces the constant offset ASB-MRU algorithm, where the Lagrange multiplier frequency offsets are calculated based on the virtual network and are *fixed*, and hence, do not need to be tuned on a per-iteration basis. The offsets act as per-sub-carrier quotas for each user and are computed during an initialization phase prior to the optimization phase. The proposed algorithm runs at a near-IWF complexity and avoids the need for per-iteration message passing (as is required for DSB and SCALE); hence, the algorithm is able to converge in significantly fewer iterations by avoiding the Lagrange multiplier frequency offset tuning process. Finally, the proposed constant offset ASB-MRU algorithm can be implemented using locally available information.

The constant offset ASB-MRU algorithm is a hybrid distributed and semi-centralized approach, which takes advantage of the strengths of both approaches. In particular, when optimizing, the algorithm runs in a fully distributed manner; however, it makes use of a semi-centralized initialization phase to guide the distributed optimization. By making use of this one-time semi-centralized initialization phase, substantial performance increases can be made while avoiding the costly per-iteration semi-centralized computations and signaling overhead.

The illustrative results in this chapter consider DSL systems. In particular, DSL systems provide a multi-link point-to-point environment resulting in an interference channel, where multiple users are served by multi-links. As such, DSL systems are more practically suitable for the work presented in this chapter than wireless systems. Typically, current practical wireless systems are point-to-point, point-to-multi-point, or multi-point-to-point systems. Hence, while the work could still be applied to wireless systems, it is not applicable to

current practical wireless environments.

The second part of this chapter deals with the issue of estimating the spectral efficiency of the system. System operators require estimates of their expected spectral efficiency in order to predict service levels. Previous efforts made use of various analytical worst-case channel models in order to calculate or estimate the spectral efficiency of systems. While some worst-case models are based on experimental measurements, they are also based on worst-case scenarios, and as such can lead to overly pessimistic results.

As such, we estimate the spectral efficiency of a DSL binder channel under Gaussian interference and thermal noise by lower-bounding the expected sum-rate. The derived lower-bound is evaluated and compared using two sets of measurement data. The first consists of twenty-five 500-m (1640-ft) co-located users and the second consists of six 183-m (600-ft) co-located users. The 500-m and 183-m test cases are very significant from a Very high bit-rate DSL (VDSL) practical implementation standpoint. In particular, the 500-m measured data corresponds to a typical Fiber-To-The-Node (FTTN) deployment and the 183-m network corresponds to a Fiber-To-The-Curb (FTTC) deployment.

3.2 System Model

Consider a system with a set of users $\mathcal{K} \triangleq \{1, \ldots, K\}$ and a set of frequency sub-carriers $\mathcal{F} \triangleq \{1, \ldots, F\}$. Using DMT/OFDM modulation, transmission can be modeled independently on each sub-carrier, f, as follows:

$$\mathbf{y}_f = \mathbf{H}_f \mathbf{x}_f + \mathbf{z}_f,$$

where the vector $\mathbf{x}_f \triangleq \{x_f^k, k \in \mathcal{K}\}$ contains the transmitted signals for all users on frequency sub-carrier f where x_f^k is the signal transmitted by user k on frequency sub-carrier f. Similarly, $\mathbf{y}_f \triangleq \{y_f^k, k \in \mathcal{K}\}$ where y_f^k is the received signal for user k on frequency sub-carrier f. Likewise, $\mathbf{z}_f \triangleq \{z_f^k, k \in \mathcal{K}\}$ where z_f^k is the additive noise seen by user k on frequency sub-carrier f which contains thermal noise, alien interference, and radio frequency interference. $\mathbf{H}_f$ is a $K \times K$ matrix such that $[\mathbf{H}_f]_{(k,l)}$ is the channel gain from transmitter l to receiver k on frequency sub-carrier f, and is defined as $h_f^{k,l}$. The transmit power of user k on frequency sub-carrier f is defined as $p_f^k \triangleq E[|x_f^k|^2]$. The vector containing the transmit power of user k on all frequency sub-carriers is defined as $\mathbf{p}^k \triangleq \{p_f^k, f \in \mathcal{F}\}$.

When the number of users is large enough, the interference is well approximated by a Gaussian distributed random variable, and hence, the achievable bit rate of user k on sub-carrier f is defined as:

$$b_f^k \triangleq \log_2\left(1+\frac{1}{\Gamma}\frac{|h_f^{k,k}|^2 p_f^k}{\sum_{l\neq k}|h_f^{k,l}|^2 p_f^k+\sigma_f^k}\right), \tag{3.1}$$

where Γ is the SNR gap which is a function of the desired bit error rate, coding gain, and noise margin [84], and σ_f^k is the noise power seen by user k on sub-carrier f. The achievable data-rate for user k is therefore $R_k = f_s \sum_f b_f^k$, where f_s is the DMT/OFDM symbol rate.

This chapter will focus on the rate adaptive optimization problem for some $\mathbf{w} \triangleq \{w_k, k \in \mathcal{K}\}$. w_k is a weighting factor which represents the importance of user k. The rate adaptive optimization problem is outlined in (3.2):

$$\begin{aligned} \max_{\mathbf{p}^k,\, k\in\mathcal{K}} \quad & \sum_{k\in\mathcal{K}} w_k R_k \\ \text{subject to:} \quad & \sum_{f\in\mathcal{F}} p_f^k \leq P_k, \quad \forall \quad k \\ & 0 \leq p_f^k \leq p_f^{k,\text{mask}}, \quad \forall \quad f,k. \end{aligned} \tag{3.2}$$

The first constraint limits user k's total transmit power to P_k and the second constraint provides a per-frequency sub-carrier total transmit power of $p_f^{k,\text{mask}}$.

3.3 Varying Offset ASB-MRU

This section briefly describes a semi-centralized MRU implementation which requires a pre-defined virtual network and per-iteration message passing. With multiple reference users, each user solves a $(1+K_R)$-user sum-rate optimization problem where K_R is the number of reference users used. Let $\mathcal{R}$ be the set of K_R reference users in the virtual network (i.e., $|\mathcal{R}| = K_R$). Any algorithm which solves a general K-user and F-sub-carrier sum-rate maximization problem can be used to derive an ASB-like algorithm with MRU; however, the transmit power and channel characteristics of the K_R reference users are unknown. In this sub-section, it is assumed that the virtual network of reference users and their respective parameters are already provided (e.g., previously heuristically determined). A

systematic approach for the selection of these parameters will be provided in Section 3.4.

ASB-DSB is a MRU version of ASB that uses DSB as its root algorithm. The adaption process transforms the semi-centralized DSB algorithm into a fully-distributed algorithm that each user runs using locally-available information. Such information includes the measured interference and the reference users' channel and transmit power. The following maximization problem is constructed for each user k:

$$\begin{aligned} \max_{\mathbf{p}^k} \quad & w_k R_k + \sum_{r\in\mathcal{R}} \tilde{w}_r \tilde{R}_r \\ \text{subject to:} \quad & \sum_{f\in\mathcal{F}} p_f^k \leq P_k \\ & 0 \leq p_f^k \leq p_f^{k,\text{mask}}, \quad \forall \quad f, \end{aligned} \tag{3.3}$$

where $\tilde{w}_r$ and $\tilde{R}_r$ are the weighting factor and data-rate of the r-th reference user, respectively.

Each user, k, solves (3.3) with their own respective virtual network of reference users. Following the same derivation as DSB in [17], the transmit power update formula for the k-th user is given by:

$$p_f^k = \left[\frac{w_k}{\lambda_k + \sum_{r\in\mathcal{R}} \left(\tilde{w}_r |h_f^{r,k}|^2 \left(\frac{1}{\text{int}_f^{\text{ref},r}} - \frac{1}{\text{rec}_f^{\text{ref},r}} \right) \right)} - \frac{\Gamma \text{int}_f^k}{|h_f^{k,k}|^2} \right]_0^{p_f^{k,\text{mask}}} \tag{3.4}$$

where

$$\begin{aligned} \text{int}_f^{\text{ref},r} &= |h_f^{r,k}|^2 p_f^k + \sum_{q\in\mathcal{R}\setminus r} |h_f^{r,q}|^2 p_f^q + \sigma_f^r, \\ \text{rec}_k^{\text{ref},r} &= \text{int}_f^{\text{ref},r} + \frac{|h_f^{r,r}|^2}{\Gamma} p_f^r, \end{aligned}$$

and int_f^k is the interference user k sees on sub-carrier f. Note that the p_f^r terms do not need to be updated because they are the transmit power of reference users and are assumed to be fixed. Hence, in both int_f^r and rec_f^r, only p_f^k varies after each iteration. When no reference users are used (i.e., $\mathcal{R} = \emptyset$), the update formula in (3.4) reduces to the water-filling update formula. Thus, ASB-DSB adds $7FK_R$ floating point operations per user, per

iteration, to the number of computations required by water-filling.[2] This brings the overall computational complexity[3] of ASB-DSB to $K \times \mathcal{O}(FK_R) = \mathcal{O}(FKK_R)$, which is similar to DSB's overall computational complexity of $\mathcal{O}(FK^2)$, but smaller since $K_R < K$.

3.4 Constant Offset ASB-MRU

This section builds on the ASB-DSB algorithm by presenting the constant offset ASB-MRU algorithm. The transmit power update formula using a Lagrange multiplier offset, $\Delta\lambda_f^k$, for user k on frequency sub-carrier f is given by (2.2). The transmit power update formula, (2.2), generalizes the transmit power update formulas of IWF, DSB, ASB-2, and ASB-DSB. The IWF transmit power update formula can be recovered as a special case when $\Delta\lambda_f^k = 0$ for all f and k. In the update formulas for DSB, ASB-2, and ASB-DSB, the offsets are updated at every iteration, requiring per-iteration message passing. SCALE uses a different transmit power update formula, but it also contains offsets that must be *tuned* on a per-iteration basis. The *tuning* process is responsible for the slow convergence of DSB and SCALE relative to IWF.

Fast Lagrange multiplier offset convergence is typical with the ASB-DSB algorithm (i.e., when using non-constant offsets). This is due to the fact that the virtual network parameters are constant. As such, the interference and received transmit powers of the virtual users are only lightly modified by the real user's transmit power. Hence, the non-constant offsets can be considered almost constant. This observation motivated the constant offset ASB-MRU algorithm.

Assuming that the virtual network of reference users is representative of the overall network, the Lagrange multiplier offsets can be approximately pre-computed before the optimization is run. As such, the Lagrange multiplier offsets become constant. By applying constant offsets, the offset *tuning* process is removed and IWF-like convergence is obtained. The virtual network of reference users is used to obtain offsets that well-approximate the converged offsets generated by other algorithms (e.g., DSB).

[2]The inversion and subtraction of rec_f^r and int_f^r requires 5 operations, multiplication by the weighted channel gains requires an additional operation. The 6 operations are computed K_R times and added together with λ_k. This is repeated for all F sub-carriers resulting in $F[6K_R + (K_R - 1) + 1] = 7FK_R$ operations in addition to what IWF requires.

[3]A brief overview of computational complexity analysis and big-O notation is provided in Appendix A.1.

The constant offset ASB-MRU algorithm can be broken up into several steps:

1. Setup virtual reference user network.
2. Select parameters for each virtual reference user.
3. Determine the Lagrange multiplier offset for each user.
4. Each user iteratively updates their transmit power using (2.2) until convergence.

Once the virtual network of reference users is constructed, the transmit power of each reference user is estimated and then used to compute the per-sub-carrier offsets for each user. The power allocation of each user is computed based on their respective per-sub-carrier offsets in a distributed fashion. The above steps are discussed in the subsections that follow.

3.4.1 Setup Virtual Reference User Network

Clustering is used to determine how many and which reference users should be selected using a systematic approach that can be applied to any arbitrary network topology. Once the clusters are computed, each cluster is replaced by the mean representative reference user. The weight of the reference user, $\tilde{w}_r$, is selected as the mean of the user weights within its cluster.

Note that for a few selected test cases, the clustering algorithm results in only one cluster. Such networks can be accurately represented by only a single reference user; however, due to the construction of the ASB-MRU algorithm, each reference user requires other representative reference users to accurately estimate the Lagrange multiplier offset (this coincides with guideline three for selecting reference users, as outlined in [80]). As such, when the clustering algorithm returns only one reference user, that reference user is doubled (i.e., the result becomes two identical reference users).

The above techniques specify how to select the reference users based on the clusters. In order to cluster the users, an appropriate payoff function (metric) must be determined. By design, this payoff function should produce a numerical value to represent how *weak* the user is. That is, the larger the payoff function value, the weaker the user.

Typically, weaker users can be characterized as having a larger received interference-plus-noise with respect to their direct signal power. As such, the payoff function should

be proportional to the interference-plus-noise that a user experiences, and inversely proportional to the user's direct signal power. In other words, the payoff function should be proportional to the ratio $\left(\sigma_f^k + \sum_{l\neq k} |h_f^{k,l}|^2 p_f^l\right) / \left(|h_f^{k,k}|^2 p_f^k\right)$ for a given frequency sub-carrier f. Hence, the payoff function for user k, $f_{\text{pay}}(k)$, should be a summation over all the sub-carriers, implying equal (unit) weights for all frequency sub-carriers,

$$f_{\text{pay}}(k) = \sum_{f=1}^{F} f\left(\frac{\sigma_f^k + \sum_{l\neq k} |h_f^{k,l}|^2 p_f^{\text{fixed}}}{|h_f^{k,k}|^2 p_f^{\text{fixed}}}\right),$$

where $f(\cdot)$ is a monotonically increasing function and $p_f^{\text{fixed}} = \min\{P_k\}/F$ is a fixed value representing an equal transmit power for all users on all frequency sub-carriers.

The goal of the payoff function is to classify users based on their relative strengths and weaknesses. It is far more important to identify differences between strong users than it is between weak users, since there is no significant benefit to differentiating between one victim and another. Hence, the objective of the payoff function is to easily differentiate between strong users to penalize them accordingly while not overly penalizing weaker users that may be slightly stronger than other weak users. Therefore, the function, $f(\cdot)$, must act as a compression function and should be selected such that it is very effective at differentiating between slight changes for small values and is relatively insensitive to slight changes for large values. This naturally led to the selection of the logarithmic function. In order to ensure that each term in the summation remains positive it is necessary to add a bias term, $b \geq 1$. $b = 1$ is a natural choice to ensure that when the ratio is equal to zero, the compression function value is also zero, resulting in:

$$f_{\text{pay}}(k) \triangleq \sum_{f=1}^{F} \log\left(1 + \frac{\sigma_f^k + \sum_{l\neq k} |h_f^{k,l}|^2 p_f^{\text{fixed}}}{|h_f^{k,k}|^2 p_f^{\text{fixed}}}\right) = \sum_{f=1}^{F} \log\left(\frac{(\text{rec}_{\text{pay}})_f^k}{|h_f^{k,k}|^2 p_f^{\text{fixed}}}\right), \tag{3.5}$$

where $(\text{rec}_{\text{pay}})_f^k \triangleq |h_f^{k,k}|^2 p_f^{\text{fixed}} + \sigma_f^k + \sum_{l\neq k} |h_f^{k,l}|^2 p_f^{\text{fixed}}$. $(\text{rec}_{\text{pay}})_f^k$ represents the full received signal for user k on sub-carrier f when p_f^{fixed} is transmitted by each user. Therefore, $f_{\text{pay}}(k)$ represents the relative strengths and weaknesses of users based solely on the channel conditions. A summary of the algorithm for selecting the virtual network is shown in Algorithm 3.1.

The payoff function can be computed with local channel knowledge by making use

Algorithm 3.1: Setup virtual reference user network.

$f_{\text{pay}}(k) = \sum_f \log\left(\frac{(\text{rec}_{\text{pay}})_f^k}{|h_f^{k,k}|^2 p_f^{\text{fixed}}}\right), \quad \forall\, n;$

Cluster users into groups. Let $f_{\text{pay,cluster}(i)}$ and $E[f_{\text{pay,cluster}(i)}]$ represent the vector of f_{pay} values for the i-th cluster and its mean, respectively ;

foreach *cluster* i **do**

Add one reference user as the user corresponding to:
$\arg\min_{k\in\text{cluster}(i)} \left\{\left|\left[f_{\text{pay,cluster}(i)}\right]_k - E\left[f_{\text{pay,cluster}(i)}\right]\right|\right\}$;
$\tilde{w}_i = E\left[w_k\right], k \in \text{cluster}(i)$;

end

of already available standard channel measurements, and hence, does not add any extra complexity. In particular, only the power-sum of the interference channel gains are needed, not the individual interference channel gains.[4] During an initialization phase, every user transmits an identical pilot signal (with known transmit power) and measures the received sum of interference plus noise, $(\text{int})_f^k \triangleq \sigma_f^k + \sum_{l\neq k} |h_f^{k,l}|^2 p_f^l$.

During the initialization phase, the payoff function for the k-th user can be computed using $(\text{rec}_{\text{pay}})_f^k = |h_f^{k,k}|^2 p_f^k + (\text{int})_f^k$, where $(\text{int})_f^k$ is the measured interference power-sum value for user k on frequency sub-carrier f. As such, $f_{\text{pay}}(k)$ can be computed using only locally available information.

Once the payoff functions are computed, an effective clustering algorithm is required. Two clustering algorithms are presented. For each clustering algorithm, the payoff function values of each user were normalized, as follows:

$$\tilde{f}_{\text{pay}}(k) = \frac{f_{\text{pay}}(k)}{\max_k \{f_{\text{pay}}(k)\}},$$

where $\tilde{f}_{\text{pay}}(k) \in [0, 1]$.

Clustering by Percentage

This clustering technique breaks up the normalized payoff function values into groupings by percentage. More specifically, since $\tilde{f}_{\text{pay}}(k) \in [0, 1]$, each user's normalized payoff function can be thought of as a percentage of the maximum payoff function value. For a fixed

[4] For DSL and LTE systems, interference measurements can be collected using dual-ended line testing [85] and received interference power measurements [86], respectively.

clustering percentage, clusters are formed by grouping users whose normalized payoff functions lie in one of the predefined uniformly distributed ranges. For example, clustering by 10% can form *up to* 10 clusters (i.e., corresponding to normalized payoff function values of: 0–0.1, 0.1–0.2, ..., 0.9–1.0), whereas clustering by 5% can form *up to* 20 clusters (i.e., corresponding to normalized payoff function values of: 0–0.05, 0.05–0.10, ..., 0.95–1.0). After assigning the payoff functions to each grouping, all the empty groupings are discarded.

Agglomerative Hierarchical Clustering

The agglomerative hierarchical clustering algorithm constructs an agglomerative (bottom-up) cluster using the normalized payoff function values. The first step is to calculate the pairwise Euclidean distance between all the pairs of normalized payoff function values. More specifically, since there are K normalized payoff function values, there will be $\binom{K}{2}$ one-dimensional Euclidean distances calculated.

An agglomerative hierarchical cluster tree is constructed using the Euclidean distances calculated. The hierarchical cluster tree begins with each element in a separate cluster and then successively groups them into larger clusters based on the single linkage (nearest neighbour) algorithm using the Euclidean distances calculated. Once the hierarchical cluster tree is constructed, clusters are formed when a node and all of its sub-nodes have an inconsistent value less than one. The inconsistent value characterizes every link in the cluster tree by comparing its height with the average height of other links at the same level in the hierarchy. The higher the inconsistent value, the less similar the objects connected by the link.

3.4.2 Select Parameters for Each Virtual Reference User

Once the virtual network of reference users is generated, standard channel models can be used to generate the channel gains for each reference user. The only remaining parameters to be computed are the transmit powers of each reference user.

For the original ASB algorithm [16], only one reference user was used and, as such, its transmit power was estimated using single-user water-filling, assuming no inter-user interference. This inherently sets the transmit power of the reference user considerably higher than what a typical user would actually use. In the MRU case, this would cause some reference users to use significantly more power than they should and lead to poor

performance. In order to solve this problem, the resulting transmit powers generated by single-user water-filling can be manually scaled back to more accurately represent the transmit power that a real user would use. In this subsection, we present a systematic approach to effectively scale back the single-user water-filling levels.

Algorithm 3.2 systematically estimates an appropriate reference user transmit power by making use of the payoff function discussed in Section 3.4.1. In particular, $f_{\text{pay}}(r)$ is evaluated for each *reference user*, r. $f_{\text{pay}}(r)$ is defined exactly as in Section 3.4.1 except it *only uses the virtual network of reference users*. The resulting transmit power for each reference user, r, is given by single-user water-filling (ignoring inter-user interference) and scaled down by the ratio $f_{\text{pay}}(r)/\max_{r\in\mathcal{R}}\{f_{\text{pay}}(r)\}$. During the single-user water-filling

Algorithm 3.2: Select parameters for each reference user.

Generate channel gains using standard models for each reference user $r \in \mathcal{R}$;
$f_{\text{pay}}(r) = \sum_{f=1}^{F} \log\left(\frac{(\text{rec}_{\text{pay}})_f^r}{|h_f^{r,r}|^2 p_f^{\text{fixed}}}\right), \quad \forall\, r \in \mathcal{R}$;
foreach *reference user* r **do**
  $p_f^r =$ Apply single-user water-filling algorithm (no inter-user interference) ;
  $p_f^r = p_f^r \times \frac{f_{\text{pay}}(r)}{\max_{r\in\mathcal{R}}\{f_{\text{pay}}(r)\}}$;
end

step of Algorithm 3.2, each reference user uses their maximum transmit power. The post-water-filling scaling allows for weaker reference users to use a higher total power than stronger reference users, resulting in transmit powers that are more representative of what actual users might transmit. It is important to note that the exact values of the reference user transmit powers do not need to be accurate; they just need to be "proportional enough" so that when the offsets are computed, they can more accurately estimate what the per-sub-carrier quota should be for each user. This allows for a more accurate approximation of the Lagrange multiplier offsets, and therefore, leads to better overall performance.

3.4.3 Determine the Lagrange Multiplier Offset for Each User

After selecting the reference user parameters, the computation of the Lagrange multiplier offset is fairly straightforward. In particular, the Lagrange multiplier offset formula corresponds to the ASB-DSB Lagrange multiplier offset formula given by (3.4). The method is outlined in Algorithm 3.3.

Algorithm 3.3: Solve for the Lagrange multiplier offset for user k and sub-carrier f

foreach *reference user* r **do**
  $\text{int}_f^r = \sigma_f^k + \sum_{u \in \mathcal{R} \setminus r} |h_f^{r,u}|^2 p_f^u$;
  $\text{rec}_f^r = \text{int}_f^r + |h_f^{r,r}|^2 p_f^r / \Gamma$;
end
$\Delta\lambda_k^n = \sum_{r \in \mathcal{R}} \tilde{w}_r |h_f^{r,k}|^2 (1/\text{int}_f^r - 1/\text{rec}_f^r)$;

3.4.4 Run the Constant Lagrange Multiplier Offset Algorithm

Once the Lagrange multiplier offsets are generated for each user, they are fixed for the duration of the optimization. As such, in each iteration, each user simply performs frequency-selective water-filling, as shown in Algorithm 3.4. The constant Lagrange multiplier offset

Algorithm 3.4: Run the constant offset algorithm.

repeat
  foreach *user* k *and frequency tone* f **do**
    Apply (2.2) using $\Delta\lambda_k^n$ from Algorithm 3.3 ;
  end
until *Transmit powers converge*;

algorithm adds one operation per iteration to the number of computations required by water-filling. As such, after an initialization phase, the constant offset ASB-MRU algorithm has the same computational complexity per iteration as IWF.

3.4.5 Sufficient Conditions for the Convergence, Existence, and Efficiency of the Constant Offset ASB-MRU Algorithm

Theorem 3.1. *If* $\max_{f,k,l \neq k} \left(\frac{\Gamma |h_f^{k,l}|^2}{|h_f^{k,k}|^2} \right) < \frac{1}{(K-1)}$, *the constant offset algorithm using fixed weights will converge to a fixed point.*

Proof. The proof is provided in Appendix A.2. □

Theorem 3.1 provides sufficient conditions for the convergence and existence of a solution to the constant offset ASB-MRU algorithm. While these conditions are not met for every system, convergence issues have not been encountered over a wide-range of network topology simulations.

Theorem 3.2. *If* $\max_{f,k,l\neq k}\left(\frac{\Gamma|h_f^{k,l}|^2}{|h_f^{k,k}|^2}\right) < \frac{1}{(K-1)}$ *and there exists a point satisfying the KKT conditions of the rate adaptive optimization problem outlined in (3.2), then there exists a set of constant offsets,* $\{\Delta\lambda_k^n\}$*, such that the constant offset algorithm will converge to that point.*

Proof. The proof is provided in Appendix A.3. □

Theorem 3.2 shows that with an appropriate choice of constant offsets, convergence to a KKT-point can be achieved. The constant offset ASB-MRU algorithm provides an approximation to this KKT point. If the virtual network of reference users accurately approximates the true network, the constant offset ASB-MRU algorithm will provide a solution very close to the true KKT point. With the assumption that the virtual network is representative of the overall network, Algorithm 3.3 approximates the modified version used for Theorem 3.2. This can be verified by the illustrative results presented in Section 3.4.7.

3.4.6 Practical Implementation

The key practical implementation aspects for DRA algorithms include the computational complexity and amount of signaling (message passing) required. An overview of big-O notation and derivations of the computational complexity and message passing requirements of IWF, SCALE, and DSB are provided in Appendix A.1. The IWF, DSB, SCALE, and constant offset ASB-MRU algorithms are compared in Table 3.1 in terms of computational complexity and message passing during the initialization phase and the optimization phase. The initialization phase performs computations required to setup the variables for the optimization phase. The optimization phase consists of computations performed by the users and computations performed by the SMC. Note that the initialization complexity and signaling are *one-time* costs, whereas the optimization complexity and signaling are *per-iteration* costs.

For the constant offset ASB-MRU algorithm, computing the payoff function requires $\mathcal{O}(F)$ computations per user. The clustering algorithm complexity is dominated by the computation of the pair-wise Euclidean distances of the payoff functions which requires $\mathcal{O}(K^2)$ computations. Generating the virtual network requires a total complexity of $\mathcal{O}(FKK_R)$.

Table 3.1 Comparison of DRA algorithm practical implementation.

DRA Algorithms	Complexity			Messages/User	
	Initial	SMC / Iter	User	Initial	Per Iter
IWF	–	–	$\mathcal{O}(F)$	–	–
SCALE	–	$\mathcal{O}(FK^2)$	$\mathcal{O}(F)$	–	$2F$
DSB	–	$\mathcal{O}(FK^2)$	$\mathcal{O}(F)$	–	$2F$
Constant Offset ASB-MRU	$\mathcal{O}(FKK_R)$	–	$\mathcal{O}(F)$	$2F$	–

Computing the pair-wise interference for the virtual network requires $\mathcal{O}(FK_R^2)$ computations. Finally, computing the offsets requires $\mathcal{O}(FKK_R)$ computations. Hence, the initialization phase requires a total complexity of $\mathcal{O}(FK + K^2 + FKK_R + FK_R^2 + FKK_R) = \mathcal{O}(FKK_R)$, since $K > K_R$ and typically, $F > K$.

During the initialization phase, each user sends their F-dimensional payoff function to the SMC and the SMC sends the F-dimensional offsets to each user. Hence, the initialization phase requires a total of $2F$ messages be sent. The optimization phase is implemented in a fully distributed manner with the same computational complexity as IWF, $\mathcal{O}(F)$ per user. The constant offset ASB-MRU algorithm provides a strong balance between complexity and signaling. Due to the fact that the offsets are constant, the optimization process can be run without the need for message passing. This is a significant practical advantage over DSB and SCALE, which both require message passing, full channel knowledge and recomputing the offsets after every iteration.

Furthermore, as will be shown using illustrative results in Section 3.4.7, the constant offset ASB-MRU re-initialization phase does not need to be run every time a user becomes active or inactive. Once the virtual network of reference users is constructed, the initialization phase only consists of computing the offset for the new users.

In particular, the constant offset of each user is computed using only knowledge of the virtual network of reference users. As such, the constant offsets for current users do not need to be recomputed whenever a new user becomes active or a current user becomes inactive.

Assuming that after the actual network changes, the virtual network is still somewhat representative of the overall network, the algorithm will still achieve strong performance. Thus, once the virtual network of reference users is initially constructed, if existing users leave the system, no initialization is required, since the current users already have their Lagrange multiplier offsets. Similarly, if new users enter the system, the initialization phase only consists of computing the offset for the new users. Hence, the initialization phase for the practical constant offset ASB-MRU algorithm only requires computing the offset of the new users entering the system, which has a computational complexity of $\mathcal{O}(FK_RK_N)$, where K_N is the number of users entering the system. Therefore, from a practical implementation point-of-view, the initialization phase of the constant offset ASB-MRU algorithm may not be a significant source of algorithmic complexity. Note that the virtual network of reference users should still be updated periodically.

Section 3.4.7 provides illustrative results demonstrating the ability of the constant offset ASB-MRU algorithm to adapt to users entering and leaving the system when the virtual network of reference users remains constant. In particular, the illustrative results support the claim that the virtual network of reference users only needs to be updated periodically.

3.4.7 Constant Offset ASB-MRU Illustrative Results

This section provides some simulation results to illustrate the performance of the constant offset ASB-MRU algorithm with respect to the existing state-of-the-art in a DSL environment. More specifically, first, this section discusses two 48-user Monte-Carlo test cases. The test cases assume that the distribution of each user's line lengths are uniform unless otherwise stated. The first test case represents a typical FTTC deployment, and the second test case represents a typical FTTN deployment.

Each random test case consists of 1000 uplink and 1000 downlink network realizations. The FTTC and FTTN test cases are summarized in Table 3.2. The notation "X users from A – [B, C] m" specifies that the X users are offset by A m and their line length is distributed between $[B - A, C - A]$ meters.

This section also compares the performance of different clustering algorithms for the cases of uniformly and exponentially distributed line length. In particular, four 25-user Monte-Carlo test cases consisting of 100 uplink and 100 downlink network realizations are presented.

Table 3.2 Summary of FTTC and FTTN test cases.

FTTC	24 users from 0 – [100, 500] m 24 users from 250 – [350, 750] m
FTTN	48 users from 0 – [100, 1000] m

All test cases use the American National Standards Institute (ANSI) model [87] and assume that 26-gauge (0.4 mm) lines are used. The target symbol error probability, coding gain, and noise margin are 10^{-7}, 3 dB, and 6 dB, respectively. The frequency sub-carrier spacing is $\Delta_f = 4.3125$ kHz, and the DMT symbol rate is $f_s = 4$ kHz. The weight of each line is set to one. Transmit power masks are applied using VDSL Profile 17a band plan [88]. A maximum transmit power of 11.5 dBm is applied to each user.

For each random network realization, DSB, SCALE, IWF, and the constant offset ASB-MRL algorithms are compared. The clustering algorithm for the constant offset ASB-MRU algorithm in the FTTC and FTTN test cases is Matlab's "clusterdata" agglomerative hierarchical clustering function.

The performance of the algorithms is compared based on the Percentage of the Maximum (PoM) weighted sum-rate each algorithm achieves, on a per-realization basis. For comparison purposes, the maximum and minimum values of the PoM are also provided, on a per-realization basis. These quantities represent the possible variation in results from one network realization to another.

The results also provide the number of iterations required. The limiting factor in terms of practical runtime is the number of iterations, since each user must take new interference measurements after each iteration. As well, the semi-centralized algorithms (i.e., DSB and SCALE) require per-iteration message passing and central computations. The number of iterations required for each algorithm to achieve 98% of their final converged rate is also given. This value is relevant for practical dynamic systems where the spectrum is updated on a per-iteration basis. The value of 98% is selected since it was observed that using 99% or 100% required a prohibitively large number of iterations for DSB and SCALE (hundreds).

FTTC Test Case

The FTTC test case represents a typical FTTC deployment scenario where two small DSLAMs, each servicing 24 customers, share a cable binder. Table 3.3 summarizes the

results of the FTTC test case. Table 3.3 shows that the constant offset ASB-MRU algo-

Table 3.3 Summary of FTTC test case results.

FTTC Uplink				
	DSB	SCALE	IWF	Constant Offset ASB-MRU
Avg PoM	99.2	100.0	79.4	97.9
Avg # iters	303.3	351.6	6.7	8.8
Avg # iters (98%)	36.4	37.8	1.9	1.0
Max PoM	100.0	100.0	86.0	100.0
Min PoM	93.2	97.8	72.1	91.1
Avg # Refs	–	–	–	15.8
FTTC Downlink				
	DSB	SCALE	IWF	Constant Offset ASB-MRU
Avg PoM	99.5	99.8	94.0	99.7
Avg # iters	323.4	490.6	74.3	46.8
Avg # iters (98%)	6.9	47.5	1.7	1.0
Max PoM	100.0	100.0	96.8	100.0
Min PoM	97.1	98.6	90.8	98.4
Avg # Refs	–	–	–	15.1

rithm achieves near-DSB and -SCALE performance for both uplink and downlink FTTC transmissions, while requiring significantly fewer iterations to converge. More specifically, the constant offset ASB-MRU outperforms DSB in 17.1% and 63.3% of the realizations for uplink and downlink transmissions, respectively. Note that it is possible for the constant offset ASB-MRU algorithm to outperform DSB and SCALE since many locally optimal points exist and due to the initialization phase of the constant offset ASB-MRU algorithm, the starting point of the algorithms are typically not the same. Fig. 3.1 shows the convergence of the algorithms for both uplink and downlink transmission for a typical realization.

Beyond what is shown in Table 3.3 for uplink transmission, the minimum percentage difference between the constant offset ASB-MRU and IWF is 11.4%, the maximum percentage difference is 26.0%, and the average percentage difference is 18.5%. Beyond what is shown in Table 3.3 for downlink transmission, the minimum percentage difference between the constant offset ASB-MRU and IWF is 2.1%, the maximum percentage difference is 9.0%, and the average percentage difference is 5.7%.

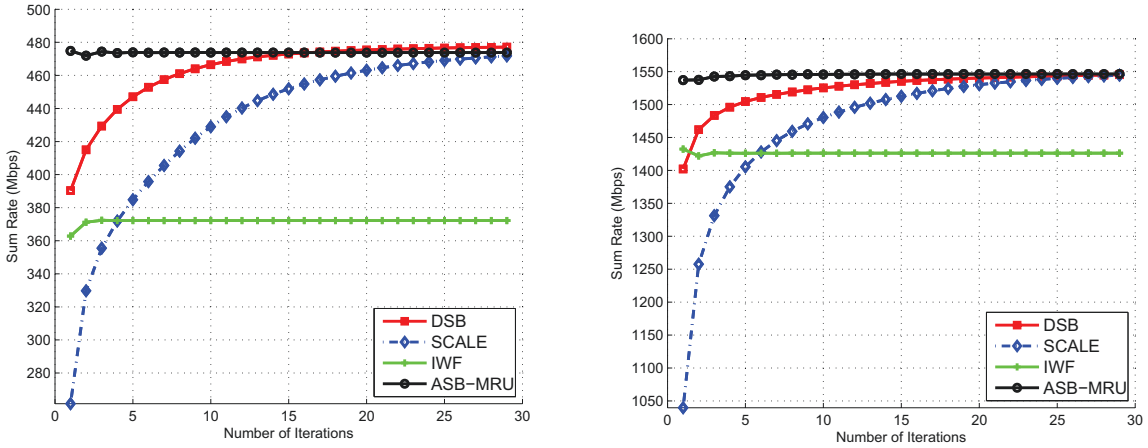

(a) Uplink (b) Downlink

Fig. 3.1 Convergence rate comparison.

The constant offset ASB-MRU simulation results shown in Table 3.3 and the convergence plots shown in Fig. 3.1 suggest that only one iteration of the constant offset ASB-MRU algorithm is required to obtain strong performance. In order to validate this claim, Table 3.4 shows the simulation results after only one iteration of the constant offset ASB-MRU algorithm relative to the *final* converged results of the other algorithms.

Table 3.4 FTTC: Constant offset ASB-MRU algorithm after one iteration.

	Uplink	Downlink
Avg PoM	98.1	99.7
Max PoM	100.0	100.0
Min PoM	92.4	98.7
Avg # Refs	15.8	15.1

When comparing the results of Tables 3.3 and 3.4, one iteration of the constant offset ASB-MRU provides a higher average PoM than the final converged constant offset ASB-MRU result for uplink transmission and provides an identical average PoM for downlink transmission. This result is extremely relevant from a practical implementation point-of-view since there is a significant reduction in the number of interference measurements required (i.e., number of iterations). Hence, the constant offset ASB-MRU algorithm achieves near-DSB and -SCALE performance after only one iteration. The ability of the constant offset ASB-MRU algorithm to achieve such strong performance after just one iteration allows

for the algorithm to very quickly adapt to changes in the network (i.e., active lines going inactive or inactive lines becoming active), provided that the virtual network of reference users is still somewhat representative of the overall network.

In order to demonstrate, simulations were run to test the sensitivity of the constant offset ASB-MRU algorithm to changes in the number of users. In particular, a single realization of the FTTC test case with K users is constructed, DSB and the constant offset ASB-MRU are used to evaluate the transmit power of each user in the system. The virtual network of reference users for the constant offset ASB-MRU is constructed based on the K user system. A new network is then constructed with $K' = K + \Delta K$ users (e.g., $\Delta K = \pm 6, \pm 12, \pm 24, \pm 36$), and the offsets for the "new" ΔK users are generated using the virtual network of reference users based on the K user system. The offsets for the existing users remains unchanged.

Two sets of simulations are provided, one where $\Delta K > 0$ and one where $\Delta K < 0$, corresponding to lines becoming active and lines becoming inactive, respectfully. The value of K is selected as 48 for the lines becoming inactive case, and is selected as 24 for the lines becoming active case. For both sets of simulations, the users entering and leaving the system are randomly selected. The results from one hundred trials for each set of simulations are averaged. Table 3.5 shows the results of the simulations relative to the $\Delta K = 0$ DSB sum-rates.

Table 3.5 shows that the constant offset ASB-MRU algorithm leads to near-DSB performance for both uplink and downlink transmission, even when the number of active lines fluctuates greatly (i.e., $\Delta K = -0.75K$, ..., $1.5K$). The results of this section show that the constant offset ASB-MRU algorithm achieves near-DSB and -SCALE performance after just one iteration and is capable of adapting to various different number of users entering/leaving the network, using the original virtual network of reference users. This demonstrates the robustness of the algorithm from a practical implementation standpoint.

FTTN Test Case

The FTTN test case represents a typical FTTN network where a medium-sized DSLAM is deployed. Table 3.6 summarizes the results of the FTTN test case.

Similar to the FTTC test case, Table 3.6 shows that the constant offset ASB-MRU algorithm achieves near-DSB and -SCALE performance for both uplink and downlink transmis-

Table 3.5 Summary of FTTC results for $K' = K + \Delta K$ users.

$K' = 48 + \Delta K$				
K'	ΔK	$\Delta K/K$	Average Uplink PoM	Average Downlink PoM
48	0	0.00 %	99.8	99.6
42	-6	-12.5 %	99.8	99.7
36	-12	-25.0 %	99.8	99.7
24	-24	-50.0 %	99.8	99.5
12	-36	-75.0 %	99.5	99.0
$K' = 24 + \Delta K$				
K'	ΔK	$\Delta K/K$	Average Uplink PoM	Average Downlink PoM
24	0	0.00 %	97.8	98.6
30	6	25.0 %	97.1	98.9
36	12	50.0 %	96.9	99.1
42	24	100 %	96.7	99.2
48	36	150 %	96.6	99.3

sion. Beyond what is shown in Table 3.6, for uplink transmission, the minimum percentage difference between constant offset ASB-MRU and IWF is 23.8%, the maximum percentage difference is 42.3%, and the average percentage difference is 32.5%. Furthermore, the constant offset ASB-MRU algorithm provides performance increases over IWF for each realization, while operating at a comparable complexity.

Similar to Section 3.4.7, the constant offset ASB-MRU simulation results shown in Table 3.6 suggest that only one iteration of the constant offset ASB-MRU algorithm is required to obtain strong performance. Table 3.7 shows the simulations results after only one iteration of the constant offset ASB-MRU algorithm relative to the *final* converged results of the other algorithms.

When comparing the results of Tables 3.6 and 3.7, it is seen that for both uplink and downlink transmission, one iteration of the constant offset ASB-MRU algorithm provides an average PoM greater than the final converged constant offset ASB-MRU result. Similarly to the results of Section 3.4.7, the one-iteration results demonstrate a large benefit from a practical implementation standpoint. Hence, the proposed algorithm achieves near-DSB and -SCALE performance after only one iteration.

Table 3.6 Summary of FTTN test case results.

FTTN Uplink				
	DSB	SCALE	IWF	Constant Offset ASB-MRU
Avg PoM	100.0	100.0	66.0	98.4
Avg # iters	267.7	225.5	5.1	10.8
Avg iters (98%)	35.9	10.9	2.0	1.0
Max PoM	100.0	100.0	75.9	99.8
Min PoM	100.0	100.0	56.1	93.8
Avg # Refs	–	–	–	15.9
FTTN Downlink				
	DSB	SCALE	IWF	Constant Offset ASB-MRU
Avg PoM	100.0	99.9	96.0	99.2
Avg # iters	158.3	500.0	12.6	12.0
Avg # iters (98%)	2.0	74.4	1.0	1.0
Max PoM	100.0	100.0	97.6	99.7
Min PoM	100.0	99.7	95.0	97.5
Avg # Refs	–	–	–	14.6

Table 3.7 FTTN: Constant offset ASB-MRU algorithm after one iteration.

	Uplink	Downlink
Avg PoM	98.5	98.7
Max PoM	99.5	99.6
Min PoM	95.8	96.9
Avg # Refs	15.9	14.6

In order to demonstrate the ability of the algorithm to adapt to changes in the network, simulations are provided to test the sensitivity of the constant offset ASB-MRU algorithm to changes in the number of users, as in Section 3.4.7. Two sets of simulations are provided, one where $\Delta K > 0$, and one where $\Delta K < 0$. As in Section 3.4.7, the value of K is selected as 48 for the lines becoming inactive case, and is selected as 24 for the lines becoming active case. For both sets of simulations, the users entering and leaving the system are randomly selected. The results of one hundred trials for each set of simulations are averaged. Table 3.8 shows the results of the simulations relative to the $\Delta K = 0$ DSB sum-rates.

Table 3.8 shows that the constant offset ASB-MRU algorithm leads to near-DSB performance for both uplink and downlink transmission, even when the number of active lines

Table 3.8 Summary of FTTN results for $K' = K + \Delta K$ users.

$K' = 48 + \Delta K$				
K'	ΔK	$\Delta K/K$	Average Uplink PoM	Average Downlink PoM
48	0	0.00 %	99.6	99.3
42	-6	-12.5 %	99.6	99.3
36	-12	-25.0 %	99.5	99.3
24	-24	-50.0 %	99.3	99.3
12	-36	-75.0 %	98.7	98.9
$K' = 24 + \Delta K$				
K'	ΔK	$\Delta K/K$	Average Uplink PoM	Average Downlink PoM
24	0	0.00 %	98.1	99.2
30	6	25.0 %	98.4	99.3
36	12	50.0 %	98.6	99.3
42	24	100 %	98.6	99.3
48	36	150 %	98.7	99.3

fluctuates greatly (i.e., $\Delta K = -0.75K, \ldots, 1.5K$). Similarly to Section 3.4.7, the results of this section show that the constant offset ASB-MRU algorithm achieves near-DSB and -SCALE performance after only one iteration and is capable of adapting to various different number of users entering/leaving the network, using the original virtual network of reference users. Along with Section 3.4.7, this further demonstrates the robustness of the algorithm from a practical implementation standpoint.

Clustering Algorithm Comparison

This subsection compares the performance of three clustering algorithms, namely clustering by 5%, 10%, and agglomerative hierarchical clustering. Three different types of simulations are provided where the difference lies in the distribution of user line lengths. In particular, the first simulation assumes the line lengths to be uniformly distributed (i.e., the number of users that have longer line lengths is similar to the number of users that have short line lengths), while the two other simulations assume it to be exponentially distributed (i.e., more users have longer line lengths than short line lengths or vice-versa).

For each type of simulation, four 25-user Monte-Carlo test cases are simulated. The scenarios are described in Table 3.9. The notation "X users from A – [B, C] m" specifies that the X users are offset by A m and their line lengths are distributed (either uniformly or exponentially) between [$B - A$, $C - A$] m. The results of the four test cases scenario, in terms of PoM, are averaged.

Table 3.9 Summary of uniformly vs. exponentially distributed simulation test cases.

Uniformly Distributed	Exponentially Distributed
25 users from 0 – [457, 914] m	25 users from 0 – [457, 1219] m
25 users from 0 – [152, 914] m	25 users from 0 – [152, 1219] m
13 users from 0 – [304, 609] m 12 users from 152 – [457, 762] m	13 users from 0 – [304, 1219] m 12 users from 152 – [457,1341] m
9 users from 0 – [304, 609] m 8 users from 152 – [457, 762] m 8 users from 304 – [457, 762] m	9 users from 0 – [304, 1219] m 8 users from 152 – [457, 1341] m 8 users from 304 – [457, 1341] m

Table 3.10 summarizes the average results for the uniformly distributed simulations. The results show that for uniformly distributed line length, clustering by percentage provides the best performance. For these scenarios, clustering by 5% and 10% provide nearly identical performance. Intuitively, selecting the clustering percentage trades-off between complexity and performance where, typically, for smaller cluster percentages a better performance can be achieved at a higher complexity due to additional reference users in the virtual network. As well, the performance of the agglomerative hierarchical clustering algorithm was very close to that of the clustering by percentage algorithms.

For each exponentially distributed test case, the rate parameter are varied so that the majority of the lines are short (respectively, long), but that at least a few lines were long (respectively, short). Any line lengths generated larger than the maximum allowable length were automatically reduced to the maximum allowable value. Tables 3.11 and 3.12 summarize the average results for the exponentially distributed simulations with more shorter line lengths and more longer line lengths, respectively.

Tables 3.11 and 3.12 show that the agglomerative hierarchical clustering algorithm provides performance benefits over the clustering by percentage algorithms when the line length distributions are exponential. This is due to the fact that the user distributions are skewed, and hence, clustering by percentage will result in some groupings having many

Table 3.10 Summary of uniformly distributed results.

Uniformly Distributed Uplink						
	DSB	SCALE	IWF	Constant Offset ASB-MRU		
				Hierarchical	Cluster by 10%	Cluster by 5%
Avg PoM	100.0	100.0	69.4	98.6	98.9	99.0
Avg # Refs	–	–	–	8.6	7.5	10.4
Uniformly Distributed Downlink						
	DSB	SCALE	IWF	Constant Offset ASB-MRU		
				Hierarchical	Cluster by 10%	Cluster by 5%
Avg PoM	99.9	99.3	91.6	99.1	99.4	99.3
Avg # Refs	–	–	–	7.9	6.4	9.6

Table 3.11 Summary of exponentially distributed results (more short line lengths).

Exponentially Distributed Uplink (more short lines)						
	DSB	SCALE	IWF	Constant Offset ASB-MRU		
				Hierarchical	Cluster by 10%	Cluster by 5%
Avg PoM	100.0	100.0	70.1	97.6	95.6	96.3
Avg # Refs	–	–	–	8.6	6.4	8.2
Exponentially Distributed Downlink (more short lines)						
	DSB	SCALE	IWF	Constant Offset ASB-MRU		
				Hierarchical	Cluster by 10%	Cluster by 5%
Avg PoM	99.7	100.0	90.7	98.3	99.4	99.1
Avg # Refs	–	–	–	7.3	7.0	10.7

users while most others have very few or none. This is observed by comparing the average number of reference users in Tables 3.10, 3.11, and 3.12. In particular, on average, the number of reference users for the agglomerative hierarchical clustering algorithm remains relatively constant, while the clustering by percentage algorithms result in significantly fewer reference users for the exponentially distributed scenarios.

Therefore, while the clustering by percentage algorithms provide slight performance improvements when the line length distributions are uniform, they are unable to effectively capture the network architecture when the line length distributions are exponential. Conversely, the agglomerative hierarchical clustering algorithm is capable of effectively adapting its clustering algorithm based on the network architecture.

Table 3.12 Summary of exponentially distributed results (more long line lengths).

Exponentially Distributed Uplink (more long lines)						
	DSB	SCALE	IWF	Constant Offset ASB-MRU		
				Hierarchical	Cluster by 10%	Cluster by 5%
Avg PoM	93.5	99.3	66.0	91.8	83.7	84.1
Avg # Refs	–	–	–	7.4	5.7	7.6
Exponentially Distributed Downlink (more long lines)						
	DSB	SCALE	IWF	Constant Offset ASB-MRU		
				Hierarchical	Cluster by 10%	Cluster by 5%
Avg PoM	99.8	98.2	89.6	91.2	94.3	94.2
Avg # Refs	–	–	–	5.2	6.1	9.5

3.5 Spectral Efficiency Estimation

System operators that make use of twisted-pair copper wire to transmit digital data require spectral efficiency estimates in order to predict service levels. Previous efforts make use of various analytical worst-case channel models in order to calculate or estimate the spectral efficiency of the system. While some worst-case models are based on experimental measurements, they are also based on worst-case scenarios, and as such can lead to overly pessimistic results. In this section, we estimate the spectral efficiency of a DSL binder channel under Gaussian interference and thermal noise by applying a lower-bound on the expected value of the sum-rate based on measured data.

3.5.1 Expected Spectral Efficiency Lower-Bound

For a DSL binder scenario with identical lines based on the ANSI [87, 88] model, each line has identical channel gains (both direct and crosstalk); however, in practical systems, this is not the case. As such, two sets of channel measurements will be used to justify the assumptions governing the lower-bound. In particular, a 6×183-m 24-AWG system and a 25×500-m 26-AWG system are discussed.

Signals were applied on a line one at a time, and the corresponding direct and crosstalk transfer functions were measured on the receiver side. The 183-m channel measurements consisted of $524,288$ measurements (from approximately -8.5 to 69.5 MHz). The 500-m channel measurements were taken from 0 to 30 MHz with a spacing of 8×4.3125 kHz, the

intermediate values were interpolated.

Fig. 3.2 shows that the direct channel gains are much stronger than the crosstalk generated by the lines. As such, it is assumed that the optimal solution is obtained by frequency-sharing, as opposed to frequency-partitioning.

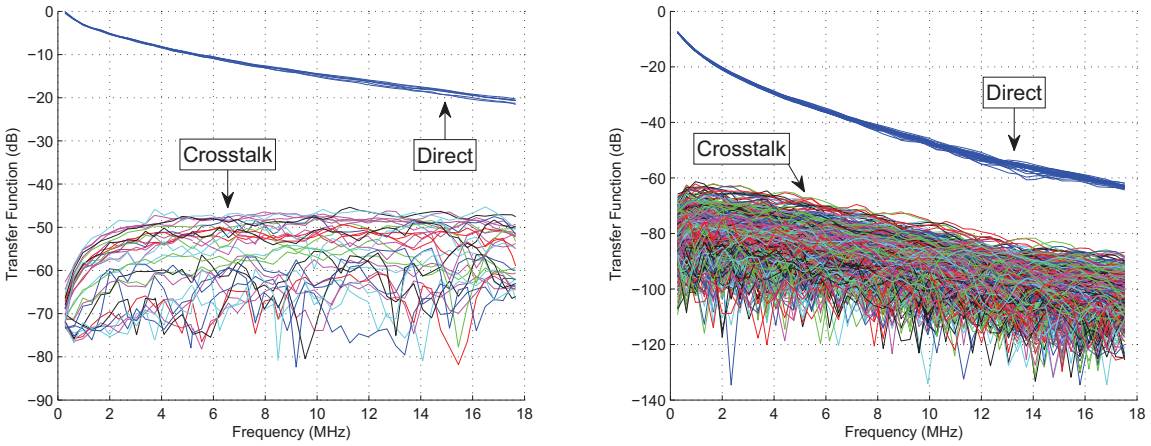

(a) 6×183-m 24-AWG. (b) 25×500-m 26-AWG.

Fig. 3.2 Full channel measurements.

Fig. 3.3 shows the similarity between the direct power gains of the lines. Hence, the direct channel power gains of each line can be well-approximated by the mean of the direct channel power gains of all the lines on a per-sub-carrier basis. Based on this assumption and the fact that all lines are of equal length, the transmit powers for all users will be similar (i.e., $p_f^k \approx p_f^l$ for all l and k).

Using the above assumptions, the bit-loading for line k on frequency sub-carrier f, given by (3.1), can be approximated by:

$$b_f^k(H_f^{k,\mathrm{xt}}) \approx \log_2\left(1 + \frac{1}{\Gamma}\frac{H_f^{\mathrm{dir}}}{H_f^{k,\mathrm{xt}} + \sigma_f^k/p_f^k}\right),$$

where $H_f^{\mathrm{dir}} \triangleq \frac{1}{K}\sum_{k=1}^{K}|h_f^{k,k}|^2$, is the mean of the direct channel power gains of each line on frequency sub-carrier f, and $H_f^{k,\mathrm{xt}} \triangleq \sum_{l\neq k}|h_f^{k,l}|^2$ is a random variable representing the sum of the interference seen by line k on sub-carrier f. Therefore, $b_f^k(H_f^{k,\mathrm{xt}})$ is a different function for each k and f, that takes a random variable as an input. As such, the approximate data-rate for each line, k, is $R_k \approx f_s \sum_f b_f^k(H_f^{k,\mathrm{xt}})$, where f_s is the symbol rate of 4 kHz.

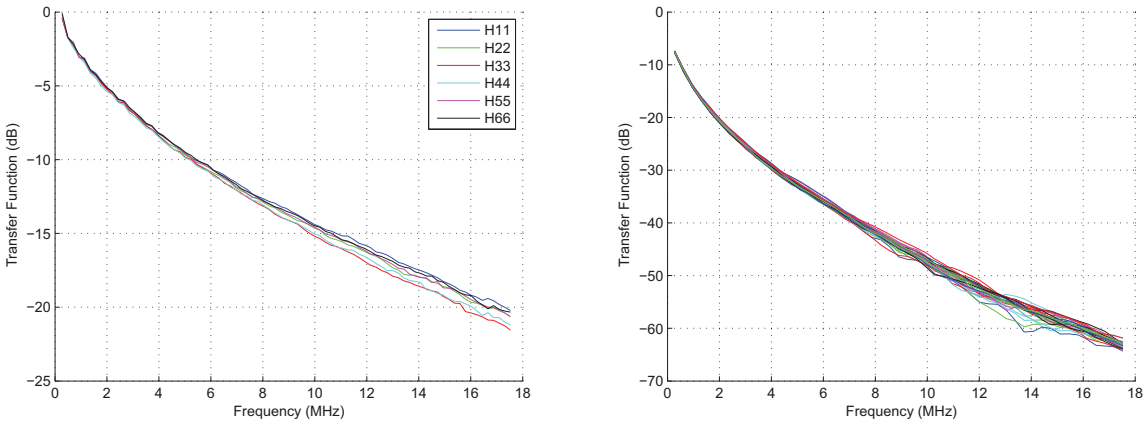

(a) 6×183-m 24-AWG. (b) 25×500-m 26-AWG.

Fig. 3.3 Direct channel measurements.

The expected sum-rate can then be written as:

$$E\left[\sum_{k} R_k\right] \approx f_s E\left[\sum_{f,k} b_f^k(H_f^{k,\mathrm{xt}})\right]. \tag{3.6}$$

It can be shown that the second derivative of $b_f^k(H_f^{k,\mathrm{xt}})$ with respect to $H_f^{k,\mathrm{xt}}$ is:

$$\frac{\mathrm{d}^2\left(b_f^k(H_f^{k,\mathrm{xt}})\right)}{\mathrm{d}\left(H_f^{k,\mathrm{xt}}\right)^2} = \frac{H_f^{\mathrm{dir}}(p_f^k)^3\left(2\Gamma H_f^{k,\mathrm{xt}}p_f^k + 2\Gamma\sigma_f^k + H_f^{\mathrm{dir}}p_f^k\right)}{\left(H_f^{k,\mathrm{xt}}p_f^k + \sigma_f^k\right)^2\left(\Gamma H_f^{k,\mathrm{xt}}p_f^k + \Gamma\sigma_f^k + H_f^{\mathrm{dir}}p_f^k\right)^2\ln(2)}. \tag{3.7}$$

Since all the variables in (3.7) must be greater than or equal to zero for all k and f, the second derivative of $b_f^k(H_f^{k,\mathrm{xt}})$ with respect to $H_f^{k,\mathrm{xt}}$ is always greater than or equal to zero. Therefore, $b_f^k(H_f^{k,\mathrm{xt}})$ is convex over the region of interest.

As such, Jensen's inequality (i.e., for a convex function $f(\cdot)$, and a random variable X, $E[f(X)] \geq f(E[X])$) can be applied to (3.6) to derive a lower-bound on the expected sum-rate, as follows:

$$f_s E\left[\sum_{f,k} b_f^k(H_f^{k,\mathrm{xt}})\right] \geq f_s \sum_{f,k} b_f^k\left(E\left[H_f^{k,\mathrm{xt}}\right]\right).$$

The lower-bound on the expected sum-rate can be maximized using a water-filling approach to solve for the optimal p_f^k, resulting in the following optimization problem:

$$\begin{aligned} \max_{\mathbf{p}^k, k\in\mathcal{K}} \quad & f_s \sum_{f,k} b_f^k \left(E\left[H_f^{k,\mathrm{xt}} \right] \right) \\ \text{subject to:} \quad & \sum_{f\in\mathcal{F}} p_f^k \leq P_k, \quad \forall\, k \\ & 0 \leq p_f^k \leq p_f^{k,\mathrm{mask}}, \quad \forall\, f,k \end{aligned}$$

The lower-bound was maximized by writing out the Lagrange function and incorporating the total power constraint, as follows:

$$\mathcal{L} = f_s \sum_{f,k} \log_2 \left(1 + \frac{1}{\Gamma} \frac{H_f^{\mathrm{dir}}}{E\left[H_f^{k,\mathrm{xt}} \right] + \sigma_f^k / p_f^k} \right) - \sum_{f,k} \lambda_k \left(p_f^k - P_k \right),$$

where λ_k is the Lagrange multiplier for line k. The per-sub-carrier power constraints are dealt with by evaluating and enforcing the boundary conditions after solving for the optimal p_f^k. λ_k is chosen such that the KKT conditions are satisfied. Since $\lambda_k \geq 0$, this reduces to:

$$\lambda_k \left(\sum_f p_f^k - P_k \right) = 0, \quad \forall\, k.$$

The KKT point can be found by taking the derivative of the Lagrange function independently for each line k and sub-carrier f and setting it equal to zero, since transmission is assumed to be synchronized (i.e., all sub-carriers are independent). This results in a quadratic equation (for each f and k) of the form:

$$A(p_f^k)^2 + B(p_f^k) + C = 0, \tag{3.8}$$

where the final value of p_f^k, denoted here as $(p_f^k)^*$, is given by: $(p_f^k)^* = [p_f^k]_0^{p_f^{k,\mathrm{mask}}}$, and where

A, B, and C are defined as follows:

$$A \triangleq \lambda_k \ln(2) \left[\Gamma \left(E\left[H_f^{k,\mathrm{xt}} \right] \right)^2 + \left(E\left[H_f^{k,\mathrm{xt}} \right] \right) H_f^{\mathrm{dir}} \right],$$
$$B \triangleq \lambda_k \ln(2) \sigma_f^k \left[2\Gamma \left(E\left[H_f^{k,\mathrm{xt}} \right] \right) + H_f^{\mathrm{dir}} \right],$$
$$C \triangleq \lambda_k \ln(2) \left(\sigma_f^k \right)^2 \Gamma - f_s H_f^{\mathrm{dir}} \sigma_f^k.$$

A procedure to solve for the optimal Lagrange multiplier, λ_k, and the corresponding optimal transmit powers, $\mathbf{p}^k \; \forall \; k$, is outlined in Algorithm 3.5.

Algorithm 3.5: Algorithm to find the optimal λ_k and $\mathbf{p}^k$ for line k.

```
Initialize λ_min = 0,  λ_max = 2^20 ;
Update p_f^k ∀ f using (3.8) with λ_k = λ_max ;
while Σ_f p_f^k > P_k do
    λ_min = λ_max ;
    λ_max = 2λ_max ;
    Update p_f^k ∀ f using (3.8) with λ_k = λ_max ;
end
while 1 do
    λ_k = (λ_max + λ_min)/2 ;
    Update p_f^k ∀ f using (3.8) with λ_k ;
    if Σ_f p_f^k > P_k then
        λ_min = λ_k ;
    else if P_k − Σ_f p_f^k ≤ 10^−10 then
        Break ;
    else
        λ_max = λ_k ;
    end
end
```

The bisection algorithm, shown in Algorithm 3.5, is performed independently for each k until the total power constraint is met with equality. Once the final value of λ_k is found, the corresponding $\mathbf{p}^k$, is selected as the transmit powers for line k.

The technique presented in this section evaluates a lower-bound on the expected sum-rate that can provide an analytical framework from system operators to help evaluate the performance of their systems. In particular, this technique allows for system operators to

take limited measurements and gain knowledge of the channel statistics (expected values) in order to gain better estimates for their expected spectral efficiency.

3.5.2 Expected Spectral Efficiency Illustrative Results

In this section, channel measurements are used to evaluate the lower-bound on the expected sum-rate of the 6×183-m DSL system using 24-AWG cables and the 25×500-m DSL system using 26-AWG cables. The 183-m channel measurements were taken using a signal generator on the transmitter side and a network analyzer on the receiver side. Signals were applied on a line one at a time, and the corresponding direct and crosstalk transfer functions were measured by the network analyzer on the receiver side. The 183-m channel measurements consisted of $524,288$ measurements (from approximately -8.5 to 69.5 MHz). The 500-m channel measurements were taken using a signal generator and network analyzer, as in the 183-m case; however, the 500-m measurements were taken from 0 to 30 MHz with a spacing of 8×4.3125 kHz, the intermediate values were interpolated.

In VDSL, 1147 uplink and 2285 downlink frequency sub-carriers are used (varying from 276 kHz to 17.6 MHz with a sub-carrier-spacing of 4.3125 kHz) [88]. The measured data was interpolated in order to more accurately represent the frequency sub-carriers used in practical DSL systems.

Two separate types of simulations are compared. The first is based on the measured data taken from actual channel measurements and the second is based on a standard DSL channel model (i.e., the ANSI model which operates on a worst-case scenario assumption). The simulations for both the measured data and the ANSI model used transmit power masks according to VDSL Profile 17a [88]. As well, the background noise for the 183-m and 500-m test cases were measured, while the ANSI model assumes a noise floor of -140 dBm/Hz.

One SRA (i.e., flat power) and two DRA (i.e., IWF and DSB) algorithms are applied to both the measured data and the ANSI models. As well, the derived lower-bound was evaluated for the measured data.

500-m Simulation Results (25 lines)

A typical DSL bundle contains 25 lines. As such, the 25×500-m scenario provides a very accurate representation of a typical FTTN cable bundle. A summary of the simulation

results is shown in Table 3.13 for the 25×500-m case. It is interesting to note that flat power outperforms IWF. This is due to the fact that for this specific scenario, the ratio between the crosstalk and the direct channel gains (see Fig. 3.2(b)) remains relatively constant, thus marginally favoring the flat power approach. Conversely, for the 183-m scenario (see Fig. 3.2(a)), the ratio between the crosstalk and the direct channel gains changes slightly, which is more common in practice. As such, in Section 3.5.2, IWF outperforms flat power.

Table 3.13 Sum-rates (Mbps) for the 25×500-m scenario with the measured data and ANSI models.

	Measured Data	ANSI Model
Flat Power	2152.1	986.5
IWF	2145.7	943.8
DSB	2196.8	986.8
Derived Lower-Bound	2186.9	N/A

The results of Table 3.13 show that each algorithm achieves similar sum-rates for both the measured data and the ANSI models; however, there is a very large discrepancy between the ANSI model and the measured data sum-rates (i.e., more than double the final sum-rate). By using the lower-bound in this scenario, system operators could predict over double the throughput than if the ANSI model was used. This supports the claim that using the 99% worst-case models to evaluate the expected spectral efficiency of a system can lead to overly pessimistic results.

The simulations show that the derived lower-bound could provide a useful analytical framework to evaluate the performance of the system due to the fact that the lower-bound's sum-rate is significantly larger than the maximum achievable value using the ANSI model. Therefore, while the lower-bound is too loose to provide a significant bound for the measured data system, it provides an indication of the type of performance which is achievable using state-of-the-art DRA algorithms. Hence, the lower-bound could be used by system operators in scenarios where the actual channel measured data is not available, but the statistics of the channel are.

183-m Simulation Results (6 lines)

The 183-m scenario provides an indication of the performance of a typical FTTC system cable bundle when 6 lines are active. A summary of the simulation results is shown in Table 3.14 for the 6×183-m case.

Table 3.14 Sum-rates (Mbps) for the 6×183-m scenario with the measured data and ANSI models.

	Measured Data	ANSI Model
Flat Power	670.8	543.6
IWF	670.9	543.6
DSB	710.8	543.6
Derived Lower-Bound	672.9	N/A

Based on the results of Table 3.14, it can be seen that DSB achieves a larger sum-rate than the other techniques for the measured data scenario. This is due to the fact that in a practical scenario, some lines are stronger than others and by adjusting the transmit power of the stronger users to help protect the weaker users, DSB improves the sum-rate.

In an ideal case (i.e., equal channel gains), IWF, DSB, and flat power achieve similar results, as seen by comparing the ANSI model sum-rates. It is also important to note the increase in sum-rate for the measured data scenario over the ANSI model scenario. In this case, the ANSI model would predict only an overall throughput of 543.6 Mbps, whereas the derived lower-bound would indicate that an overall throughput of at least 672.9 Mbps was achievable.

As discussed for the 500-m case, the simulation results show that the derived lower-bound can provide a reasonable analytical framework for system operators to evaluate the performance of their system when only the channel statistics are known. This could be the case in a wide-variety of practical DSL systems.

3.6 Concluding Remarks

There is an important relationship between the achievable sum-rate (performance) and the complexity of an algorithm. This chapter presented the constant offset ASB-MRU algorithm in an attempt to achieve a more favourable trade-off between performance and

complexity. The constant offset ASB-MRU algorithm relies heavily on the use of a payoff function to represent the relative strengths and weaknesses of each user in the system. The construction and development of the payoff function was discussed. By clustering the payoff function values, the constant offset ASB-MRU algorithm systematically constructs a virtual network of reference users. The virtual network represents approximate global channel knowledge that can be obtained during an initialization phase using local channel knowledge. The payoff function is also applied to the virtual network of reference users to more accurately approximate the transmit power of each reference user. Sufficient conditions for convergence, existence, and efficiency of the constant offset algorithm are also provided.

Extensive simulation results show that the constant offset ASB-MRU algorithm achieves near-DSB and -SCALE sum-rates after only one iteration (i.e., requiring only one set of interference measurements). As well, the constant offset ASB-MRU algorithm using a *fixed* virtual network of reference users also provides near-DSB and -SCALE performance with large fluctuations in the number of users entering or exiting the system. Therefore, the constant offset ASB-MRU algorithm results in a near-ideal balance between performance, complexity, and sensitivity to users entering or leaving the system.

This chapter also derives a lower-bound on the expected sum-rate of a DSL binder channel using Jensen's inequality. The lower-bound is maximized using a water-filling approach to optimize the transmit power. Using two measured-data based scenarios, it was shown that the analytic worst-case model leads to overly pessimistic results when compared to full measured data. In particular, for the 25×183-m case, the lower-bound predicts over double the sum-rate than the ANSI model predicts. Hence, while the derived lower-bound is conservative, it provides better insight into the actual spectral efficiency of the system than the ANSI model.

The lower-bound could be a useful tool for system operators to predict achievable data-rates based on limited measurements in order to determine estimates for the channel statistics (i.e., expected values). Providing system operators with better estimates for the spectral efficiency of the network could allow for more accurate service level predictions, and therefore, lead to better overall services.

Chapter 4

Full-Duplex MIMO Point-to-Point Precoding[1]

4.1 Introduction

Chapter 3 considers HD multi-link transmission. This chapter focuses on FD systems, where signals are transmitted and received simultaneously over the same frequency at the same time, as discussed in Chapter 1. In particular, this chapter focuses on the case of sum-rate maximization for FD MIMO point-to-point systems which can also be viewed as a FD SU-MIMO system.

The FD MIMO point-to-point sum-rate maximization problem formulation leads to a non-convex optimization problem for which finding solutions is difficult. SCP [97] is a well-known practical approach to solving non-convex optimization problems by constructing and solving a sequence of convex optimization problems.

In Chapter 5, two SCP-based algorithms are derived for solving the non-convex FD MIMO point-to-multi-point sum-rate maximization problem directly. In this chapter, we present the corresponding FD MIMO point-to-point SCP-based algorithms, which can be recovered as special cases of the algorithms derived in Chapter 5. As such, a detailed derivation of the DC-based and SCAMP algorithms is provided in Chapter 5.

[1]Parts of Chapter 4 have been presented at the 2013 IEEE Global Communications Conference (GLOBECOM) [89], the 2014 IEEE International Conference on Communications (ICC) [90], accepted to be published in the IEEE Wireless Communications Letters [91] and the IEEE Transactions on Vehicular Technology [92], and have been submitted for publication to the IEEE Transactions on Wireless Communications [93]. Finally, parts of Chapter 4 have been disclosed in the following U.S. patent applications [94–96].

This chapter also proposes a FD Precoding (FDP) structure which makes use of MIMO precoding to *jointly* precode the forward transmission and cancel the self-interference [94]. As such, the self-interference cancellation is done by matrix precoding at the transmitter. The FDP Structure makes use of auxiliary paths to increase the dimensionality at the transmitter. The precoding design takes advantage of the increased dimensionality by *jointly* preprocessing the transmit signals for a more effective trade-off between the forward channel precoding and the self-interference suppression.

The proposed FDP structure provides a more generalized framework for the optimization of both FD MIMO point-to-point and point-to-multi-point transceivers, allowing for different optimization objectives rather than solely minimizing the self-interference (e.g., sum-rate maximization, energy efficiency). Specifically, in this thesis, we focus on the objective of sum-rate maximization. As such, this chapter proposes separate and joint FDP algorithms for the sum-rate maximization objective. A comparison between the separate and joint design approaches from both an analytical and a simulation perspective are provided.

This chapter also develops a Self-Interference Pricing (SIP)-based algorithm which replaces the direct non-convex sum-rate maximization problem by creating four pricing-based sub-problems to more consistently provide a favorable trade-off between forward channel maximization and self-interference cancellation using both precoding and postcoding. Therefore, the SIP algorithm must assume some active and/or passive cancellation to ensure the linearity of the Low-Noise Amplifier (LNA) and Analog-to-Digital Converter (ADC) at the receiver. As such, this chapter also proposes a SIP-based FDP (FDP-SIP) algorithm using only precoding at the transmitter. Hence, since the self-interference cancellation effectively takes place prior to the LNA and ADC, the linearity of the system can be ensured. Finally, this chapter also presents the Self-Interference Threshold (SIT) algorithm which can be applied with or without making use of the FDP transceiver structure.

Extensive simulations using both channel models and experimentally measured data demonstrate that the proposed FDP structure offers significant performance improvements and compares the performance of the proposed algorithms.

The illustrative results in this chapter consider wireless systems. The FD design algorithms presented in this chapter could be applied to both wireless and wireline systems (e.g., cable systems). Moreover, the designs are applicable to both multi-link or point-to-

point systems[2]; however, for telephony systems, FD communication already exists in the form of echo cancellation. Echo cancellation was developed in the 1950s to economize the use of the wire for both transmitting and receiving, which was practical but could only provide 20-30 dB of isolation. Wireless environments require more cancellation to manage the strong self-interference which occurs due to transmission over greater distances. In order to effectively manage the strong self-interference, sophisticated FD designs are required (e.g., precoding). As such, the requirements are more stringent, and hence, this chapter focuses on wireless systems.

4.2 System Model

4.2.1 Full-Duplex MIMO Point-to-Point System

The FD SU-MIMO system model, shown in Fig. 4.1, represents a point-to-point link between two nodes where each node operates in FD mode. Since both nodes communicate in FD-mode, each node suffers from the effects of self-interference. The matrix of channel gains from node i to node j is denoted by $\mathbf{H}_i \in \mathbb{C}^{N_R \times N_T}$ and the self-interference at node i is denoted by $\mathbf{G}_i \in \mathbb{C}^{N_R \times N_T}$, where both nodes have N_T transmit and N_R receive antennas, respectively.

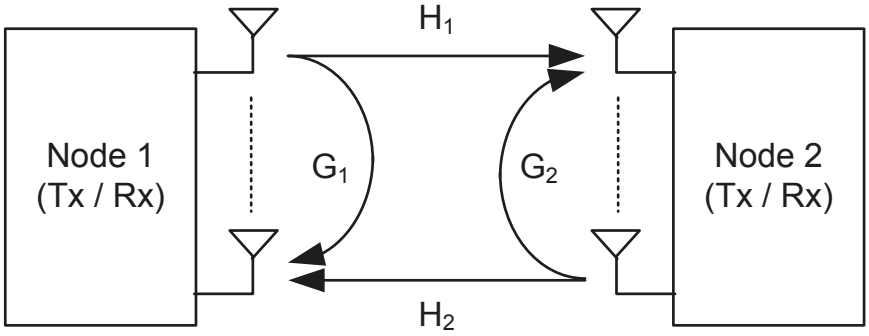

Fig. 4.1 FD MIMO point-to-point system model.

Let $\mathbf{V}_i \in \mathbb{C}^{N_T \times d_i}$ be the precoding matrix for the i-th node, where $d_i \leq N_T$ is the dimensionality of the transmit signal (i.e., $\mathbf{x}_i \in \mathbb{C}^{d_i \times 1}$). Typically, in this chapter, it is

[2]Note that the point-to-point MIMO system discussed in this chapter can be considered a FD version of the HD multi-link system discussed in Chapter 3. Furthermore, Chapter 5 focuses on wireless point-to-multi-point systems where UEs can be either FD or HD.

assumed that $d_i = N_T$. The received signal at the i-th node is:

$$\mathbf{y}_i = \mathbf{H}_j \mathbf{V}_j \mathbf{x}_j + \mathbf{G}_i \mathbf{V}_i \mathbf{x}_i + \mathbf{z}_i,$$

where $\mathbf{z}_i \in \mathbb{C}^{N_R \times 1}$ is the noise at the i-th node. The first term represents the intended signals, while the second term represents the self-interference incurred by operating in FD mode. Let the covariance matrices of the direct and self-interference signals at the i-th receiver be given by:

$$\mathbf{C}_{i,j} = \mathbf{H}_j \mathbf{Q}_j \mathbf{H}_j^\dagger,$$
$$\mathbf{C}_{i,i} = \mathbf{G}_i \mathbf{Q}_i \mathbf{G}_i^\dagger,$$

where $\mathbf{Q}_i = \mathbf{V}_i \mathbf{S}_i \mathbf{V}_i^\dagger$ and $\mathbf{S}_i = E[\mathbf{x}_i \mathbf{x}_i^\dagger]$. The achievable rate at the i-th node is given by:

$$R_i = \log_2 \left| \mathbf{I}_{N_R} + \left(\mathbf{\Sigma}_i + \mathbf{C}_{i,i} \right)^{-1} \mathbf{C}_{i,j} \right|,$$

where $\mathbf{\Sigma}_i = E[\mathbf{z}_i \mathbf{z}_i^\dagger]$.

The self-interference channels, $\mathbf{G}_i$ (i = 1,2), are assumed to be estimated, while the forward channels, $\mathbf{H}_i$ (i = 1,2), are assumed to be known perfectly, in order to more easily compare with the HD case. As well, by assuming imperfect self-interference channel knowledge, we can study the effects of residual self-interference on the achievable sum-rate. More specifically, it is assumed that:

$$\mathbf{G}_i = \hat{\mathbf{G}}_i + \Delta \mathbf{G}_i,$$

where $\mathbf{G}_i$ is the true channel matrix, $\hat{\mathbf{G}}_i$ is the estimated channel matrix, and $\Delta \mathbf{G}_i$ is the estimation error channel matrix, with zero mean and covariance matrix $\sigma_{\text{err}}^2 \mathbf{I}_{N_R}$. As such, we model the imperfect self-interference channel knowledge as $\Delta \mathbf{G}_i$ for analysis (i.e., we model the performance of the estimator).

Let the estimated achievable rate at the i-th node be given by:

$$\hat{R}_i = \log_2 \left| \mathbf{I}_{N_R} + \left(\mathbf{\Sigma}_i + \hat{\mathbf{C}}_{i,i} \right)^{-1} \mathbf{C}_{i,j} \right|,$$

where $\hat{\mathbf{C}}_{i,i} = \hat{\mathbf{G}}_i \mathbf{Q}_i \hat{\mathbf{G}}_i^\dagger$.

The FD MIMO point-to-point sum-rate maximization problem can be written as:

$$\begin{aligned} \max_{\mathbf{Q}_1,\mathbf{Q}_2} \quad & \hat{R}_1 + \hat{R}_2 \\ \text{subject to:} \quad & \mathrm{Tr}[\mathbf{Q}_i] \leq P_{\max,i},\ i = 1, 2, \\ & \mathbf{Q}_i \succcurlyeq 0,\ i = 1, 2, \end{aligned} \tag{4.1}$$

where the constraints on the transmit covariance matrices to be positive semi-definite ensure the feasibility of the solution. Optimization problem (4.1) is non-convex, and hence, difficult to solve directly.

Once the covariance matrices are solved for, the corresponding precoding matrices can be recovered using the Cholesky decomposition. In particular, $\mathbf{Q}_i = \mathbf{L}_i\mathbf{L}_i^\dagger$, and hence, the precoding matrices can be computed as:

$$\mathbf{V}_i = \mathbf{L}_i\mathbf{S}_i^{-1/2}. \tag{4.2}$$

4.2.2 Full-Duplex Precoding (FDP)

The FDP block diagram [94] is shown in Fig. 4.2. The FDP structure (Fig. 4.2) differs from the active cancellation structure (Fig. 2.1) in that precoding is applied to *jointly* perform the forward transmission precoding and the self-interference cancellation. This joint approach allows for additional transmit dimensions and is capable of being optimized with respect to many different objectives as opposed to solely suppressing the self-interference. The FDP structure can also be optimized with the objective of suppressing the self-interference, and hence, it allows for a more general optimization framework for which various objectives and algorithms can be developed. In particular, in this chapter, we focus on the objective of sum-rate maximization.

The FDP structure is designed such that all antennas simultaneously transmit and receive signals, and hence, the number of antennas are assumed to be $N_T = N_R = M$. As shown in Fig. 4.2, M transmit signals are precoded into $2M$ paths, each path includes a Digital-to-Analog Converter (DAC). M of them, used for forward transmission paths (one per antenna), also include a Power Amplifier (PA) and a circulator, while the other M are auxiliary paths. In the transmit direction, the circulator feeds to a single-port antenna and in the receive direction, the circulator of each antenna combines with its respective

auxiliary path.[3] The combined signals are passed through a LNA and an ADC. The self-interference channel is slow time-varying, and hence, *estimated* channel information can be obtained during periodic HD transmission training phases.[4]

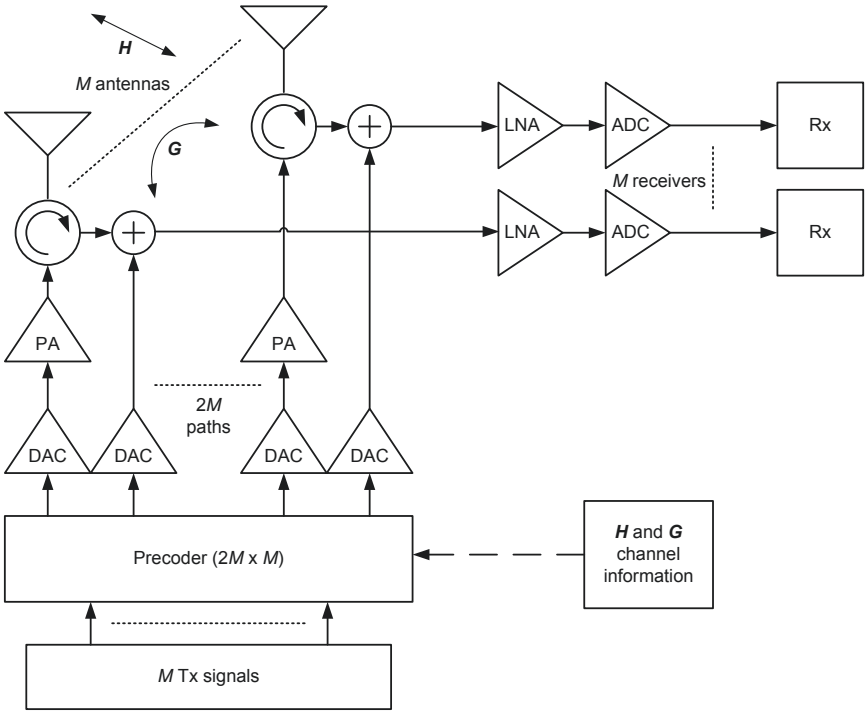

Fig. 4.2 MIMO full-duplex precoding structure.

For comparison, a typical HD transmission structure consists of M separate transmit and receive paths. M transmit signals are passed through an $M \times M$ precoder where each of the M output paths consists of a DAC and PA. Each of the M receive paths consist of a LNA, ADC, and a forward transmit/receive channel estimator.

As shown in Fig. 4.2, M paths are used for forward transmission, while $2M$ paths affect the self-interference. In fact, the group of M paths to the combiners[5] actually form an

[3] In the remainder of this thesis, the paths are numbered so that the first M paths correspond to the forward transmission paths and the last M paths correspond to the auxiliary paths, for notational convenience.

[4] Since the self-interference channel is slow time-varying, it can be estimated using the following training procedure. Start by operating in HD-transmission mode and while transmitting, measure the resulting self-interference channel gain. Then, the system can switch into FD-transmission mode with self-interference channel knowledge (which was measured during the HD-transmission phase). This procedure can be repeated periodically to re-update the self-interference channel knowledge.

[5] A *coupling* combiner is used to avoid degradation in the receiver noise figure.

equivalent active canceller although the objective of the precoding is not necessarily to focus on minimizing the self-interference. As such, the $2M \times M$ precoder is a *joint* forward transmission precoder and self-interference canceller. Additionally, a separate approach can be taken where one $M \times M$ precoder is applied to the forward channel and another $M \times M$ precoder is applied to the self-interference channels. Note that the separate approach, discussed in Section 4.4, is similar to a matrix-version of the active cancellation approach where the cancellations are computed via precoding.

4.2.3 Full-Duplex Precoding Applied to OFDM Systems

Fig. 4.3 illustrates the functional block diagram of a MIMO-OFDM transceiver using the proposed FDP structure. After the Series-to-Parallel (S/P) converter, the signals are modulated on a per-frequency basis. The output of the modulators is passed to the $2M \times M$ per-frequency precoding matrices. Each of the $2M$ output paths from the precoding block is passed to a unique Inverse Fast Fourier Transform (IFFT) block. In particular, each of the M antennas has a corresponding transmission IFFT and auxiliary IFFT. After the IFFT, a cyclic prefix is added and all paths then pass through a DAC, as in Fig. 4.2. The auxiliary paths are then fed to the receiver, as shown in Fig. 4.3. The transmission paths are transmitted as in Fig. 4.2 using a PA and a circulator. The output of the circulator, corresponding to the received signal and the residual self-interference after the circulator's isolation, is passed to the receiver.

On the receiver side, the received and auxiliary paths are combined and then passed through a LNA and ADC. After the ADC, the cyclic prefix is removed and a FFT is applied. Finally, the signals are sent to the decoder.

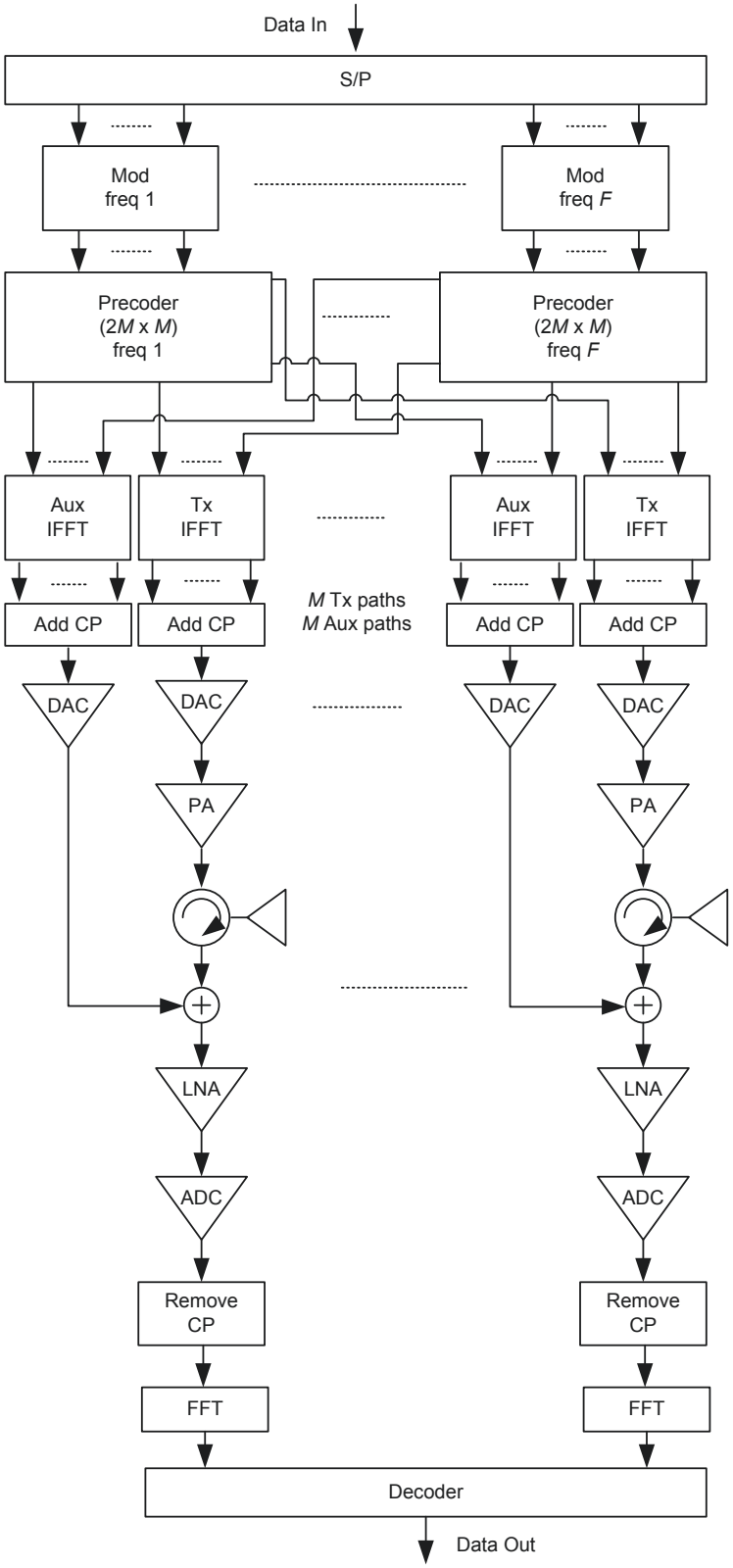

Fig. 4.3 Block diagram of a MIMO-OFDM transceiver using the proposed full-duplex precoder.

4.2.4 Full-Duplex Precoding for FD MIMO Point-to-Point Systems

The FD SU-MIMO system model, shown in Fig. 4.1, represents a point-to-point link between two nodes where each node operates in FD mode with M physical antennas. Let $\mathbf{H}_j \in \mathbb{C}^{M\times 2M}$ be the matrix of channel gains from the $2M$ antenna paths of the j-th node to the M antennas of the i-th node ($i \neq j$). Hence, $\mathbf{H}_j$ has the following structure[6]:

$$\mathbf{H}_j = \begin{bmatrix} \tilde{\mathbf{H}}_j & \mathbf{0}_M \end{bmatrix},$$

where $\tilde{\mathbf{H}}_j \in \mathbb{C}^{M\times M}$ and it is assumed that the paths are numbered such that the first M paths correspond to forward transmission, while the second M paths correspond to the auxiliary paths (i.e., the paths which are not transmitted).

Similarly, let $\mathbf{G}_i \in \mathbb{C}^{M\times 2M}$ be the self-interference matrix of channel gains for the i-th node. Hence, $\mathbf{G}_i$ has the following structure[7]:

$$\mathbf{G}_i = \begin{bmatrix} \tilde{\mathbf{G}}_{i,a} & \alpha\mathbf{I}_M \end{bmatrix},$$

where $\tilde{\mathbf{G}}_{i,a} \in \mathbb{C}^{M\times M}$ and α is a scalar representing the gain of each cancellation path.

The transmission equations and sum-rate expressions are identical to those in Section 4.2.1 with these new definitions of $\mathbf{H}_i$ and $\mathbf{G}_i$ (with the corresponding appropriately sized matrices and vectors). As in Section 4.2.1, $\tilde{\mathbf{G}}_{i,a}$ is assumed to be estimated while α is assumed to be known perfectly since it would be specified by the service provider based on the allowable power consumption, and hence, its exact effects can be measured off-line.

4.3 Sequential Convex Programming

In this section, SCP is applied to approximate the solution to the non-convex optimization problem (4.1). The derivation of the two SCP algorithms for FD MIMO point-to-multi-point systems is given in Chapter 5, where the FD MIMO point-to-point equations presented in this section can be recovered as special cases. As such, in this section, the derivations of the DC-based and SCAMP algorithms are omitted, and instead, only the

[6]The $\mathbf{0}_M$ component of $\mathbf{H}_j$ is due to the fact that the auxiliary paths do not correspond to forward transmission.

[7]Since the interaction between auxiliary paths is negligible, $\alpha\mathbf{I}_M$ represents the gain of the auxiliary paths. Additionally, the gain of each path, α, can be measured off-line.

final equations are provided.

4.3.1 FD MIMO Point-to-Point: DC-Based Algorithm

The DC-based algorithm avoids the original non-convex optimization problem, (4.1), by instead solving a sequence of the following convex optimization problems:

$$\begin{aligned} \min_{\mathbf{Q}_1,\mathbf{Q}_2} \quad & \tilde{f}_{\text{SU-DC}}(\nu) \\ \text{subject to:} \quad & \text{Tr}[\mathbf{Q}_i] \leq P_{\max,i},\ i=1,2, \\ & \mathbf{Q}_i \succcurlyeq 0,\ i=1,2, \end{aligned} \tag{4.3}$$

where $\tilde{f}_{\text{SU-DC}}(\nu)$ is given by:

$$\tilde{f}_{\text{SU-DC}}(\nu) = g_1 + g_2 - \tilde{h}_1(\nu) - \tilde{h}_2(\nu), \tag{4.4}$$

where g_i and $\tilde{h}_i(\nu)$ $(i=1,2)$ are given by:

$$\begin{aligned} g_i &= -\log_2 \left| \mathbf{\Sigma}_i + \hat{\mathbf{G}}_i \mathbf{Q}_i \hat{\mathbf{G}}_i^\dagger + \mathbf{H}_j \mathbf{Q}_j \mathbf{H}_j^\dagger \right|, \\ \tilde{h}_i(\nu) &= \frac{-1}{\ln(2)} \text{Tr}\left[\left(\mathbf{\Sigma}_i + \hat{\mathbf{G}}_i \mathbf{Q}_i^{(\nu)} \hat{\mathbf{G}}_i^\dagger \right)^{-1} \hat{\mathbf{G}}_i \left(\mathbf{Q}_i - \mathbf{Q}_i^{(\nu)} \right) \hat{\mathbf{G}}_i^\dagger \right] - \log_2 \left| \mathbf{\Sigma}_i + \hat{\mathbf{G}}_i \mathbf{Q}_i^{(\nu)} \hat{\mathbf{G}}_i^\dagger \right|, \end{aligned} \tag{4.5}$$

where $\mathbf{Q}_i^{(\nu)}$ refers to the transmit covariance matrix of the i-th node associated with the ν-th iteration. $\tilde{f}_{\text{SU-DC}}(\nu)$ is a convex approximation to the original objective function $f = -\hat{R}_1 - \hat{R}_2$ around the point $\mathbf{Q}_i^{(\nu)}$ $(i=1,2)$. As such, the non-convex optimization problem (4.1) can be locally approximated, around the point $\mathbf{Q}_i^{(\nu)}$ $(i=1,2)$, by the convex optimization problem (4.3).

The resulting Algorithm 4.1 iteratively updates the objective function approximation, $\tilde{f}_{\text{SU-DC}}(\nu)$, and solves the convex approximation until convergence. Note that the convex optimization problem can be solved using cvx, a package for solving disciplined convex programs in Matlab [98, 99].

Algorithm 4.1: FD MIMO point-to-point: DC-based algorithm.

Randomly initialize $\mathbf{Q}_1^{(0)}, \mathbf{Q}_2^{(0)}$;
Initialize $\nu = 0$;
repeat
  Update $\tilde{h}_1(\nu)$, $\tilde{h}_2(\nu)$ using (4.5), using $\mathbf{Q}_1^{(\nu)}, \mathbf{Q}_2^{(\nu)}$;
  Update $\tilde{f}_{\text{SU-DC}}(\nu)$ using (4.4) ;
  Solve (4.3) for $\mathbf{Q}_1^{\star}, \mathbf{Q}_2^{\star}$;
  $\nu = \nu + 1$;
  Update $\mathbf{Q}_i^{(\nu)} = \mathbf{Q}_i^{\star}$, $i = 1, 2$;
until $\tilde{f}_{\text{SU-DC}}(\nu)$ *converges*;
Apply Cholesky decomposition: $\mathbf{Q}_i^{\star} = \mathbf{L}_i \mathbf{L}_i^{\dagger}$, $i = 1, 2$;
Solve for $\mathbf{V}_i$ using (4.2), $i = 1, 2$

4.3.2 FD MIMO Point-to-Point: SCAMP Algorithm

The SCAMP algorithm avoids the original non-convex optimization problem, (4.1), by instead solving a sequence of the following convex optimization problems:

$$\begin{aligned} \min_{\mathbf{Q}_1, \mathbf{Q}_2} \quad & \tilde{f}_{\text{SU-SCAMP}}(\nu) \\ \text{subject to:} \quad & \text{Tr}[\mathbf{Q}_i] \leq P_{\max,i}, \ i = 1, 2, \\ & \mathbf{Q}_i \succcurlyeq 0, \ i = 1, 2, \end{aligned} \tag{4.6}$$

where $\tilde{f}_{\text{SU-SCAMP}}(\nu)$ is given by:

$$\tilde{f}_{\text{SU-SCAMP}}(\nu) = \sum_{i=1}^{2} \left\{ \eta_i + \tilde{\varphi}_i(\nu) + \tfrac{1}{\ln(2)} \tilde{t}_i(\nu) - \beta_i \right\}, \tag{4.7}$$

where η_i, $\tilde{\varphi}_i(\nu)$, $\tilde{t}_i(\nu)$, and β_i are given by:

$$\begin{aligned}
\eta_i &= -\log_2\left|\mathbf{H}_j\mathbf{Q}_j\mathbf{H}_j^\dagger\right|, \\
\tilde{\varphi}_i(\nu) &= \log_2\left|\boldsymbol{\Upsilon}_i^{(\nu)}\right| + \frac{1}{\ln(2)}\mathrm{Tr}\left[\left(\boldsymbol{\Upsilon}_i^{(\nu)}\right)^{-1}\hat{\mathbf{G}}_i\left(\mathbf{Q}_i - \mathbf{Q}_i^{(\nu)}\right)\hat{\mathbf{G}}_i^\dagger\right] \qquad (4.8) \\
\tilde{t}_i(\nu) &= -\mathrm{Tr}\left[\left(\left(\boldsymbol{\Upsilon}_i^{(\nu)}\right)^{-1}\mathbf{H}_j\mathbf{Q}_j^{(\nu)}\mathbf{H}_j^\dagger\boldsymbol{\Phi}_i\left(\boldsymbol{\Upsilon}_i^{(\nu)}\right)^{-1}\right)^\dagger\left(\hat{\mathbf{G}}_i\left(\mathbf{Q}_i - \mathbf{Q}_i^{(\nu)}\right)\hat{\mathbf{G}}_i^\dagger\right)\right] \\
&\quad + \mathrm{Tr}\left[\left(\boldsymbol{\Phi}_i\left(\boldsymbol{\Upsilon}_i^{(\nu)}\right)^{-1}\right)^\dagger\mathbf{H}_j\left(\mathbf{Q}_j - \mathbf{Q}_j^{(\nu)}\right)\mathbf{H}_j^\dagger\right] \qquad (4.9) \\
&\quad + \mathrm{Tr}\left[\boldsymbol{\Phi}_i\left(\boldsymbol{\Upsilon}_i^{(\nu)}\right)^{-1}\mathbf{H}_j\mathbf{Q}_j^{(\nu)}\mathbf{H}_j^\dagger\right], \\
\beta_i &= \log_2\left|\mathbf{I}_{N_R} + \mathbf{X}_{(\nu)}\right| + \tfrac{1}{\ln(2)}\mathrm{Tr}\left[\mathbf{X}_{(\nu)}^{-1}\left(\mathbf{I}_{N_R} + \mathbf{X}_{(\nu)}^{-1}\right)^{-1}\right] - \log_2\left|\mathbf{X}_{(\nu)}\right|,
\end{aligned}$$

where $\boldsymbol{\Upsilon}_i^{(\nu)}$, $\boldsymbol{\Phi}_i$, and $\mathbf{X}_{(\nu)}$ are given by:

$$\begin{aligned}
\boldsymbol{\Upsilon}_i^{(\nu)} &= \boldsymbol{\Sigma}_i + \hat{\mathbf{G}}_i\mathbf{Q}_i^{(\nu)}\hat{\mathbf{G}}_i^\dagger, \\
\boldsymbol{\Phi}_i &= \mathbf{X}_{(\nu)}^{-1}\left(\mathbf{I} + \mathbf{X}_{(\nu)}^{-1}\right)^{-1}\mathbf{X}_{(\nu)}^{-1}, \\
\mathbf{X}_{(\nu)} &= \left(\boldsymbol{\Upsilon}_i^{(\nu)}\right)^{-1}\mathbf{H}_j\mathbf{Q}_j^{(\nu)}\mathbf{H}_j^\dagger.
\end{aligned}$$

By construction, the objective function $\tilde{f}_{\mathrm{SU-SCAMP}}(\nu)$ is a convex function. Note that optimization problems (4.3) and (4.6) differ only in the selection of the convex objective function approximation (i.e., $\tilde{f}_{\mathrm{SU-DC}}(\nu)$ and $\tilde{f}_{\mathrm{SU-SCAMP}}(\nu)$).

The SCAMP algorithm, described in Algorithm 4.2, iteratively updates the objective function approximation, $\tilde{f}_{\mathrm{SU-SCAMP}}(\nu)$, and solves the convex approximation until convergence. As in Section 4.3.1, the convex optimization problem can also be solved using cvx [98, 99].

4.4 Separate Full-Duplex Precoding

In this section, the FDP structure is applied, where the forward precoding and self-interference cancellation are designed separately. More specifically, $\mathbf{V}_i \in \mathbb{C}^{2M\times M}$ is re-

Algorithm 4.2: FD MIMO point-to-point: SCAMP algorithm.

Randomly initialize $\mathbf{Q}_1^{(0)}, \mathbf{Q}_2^{(0)}$;
Initialize $\nu = 0$;
repeat
  Update $\tilde{\varphi}_i(\nu)$, $\tilde{t}_i(\nu)$ $(i = 1, 2)$ using (4.8) and (4.9), using $\mathbf{Q}_1^{(\nu)}, \mathbf{Q}_2^{(\nu)}$;
  Update $\tilde{f}_{\text{SU-SCAMP}}(\nu)$ using (4.7) ;
  Solve (4.6) for $\mathbf{Q}_1^{\star}, \mathbf{Q}_2^{\star}$;
  $\nu = \nu + 1$;
  Update $\mathbf{Q}_i^{(\nu)} = \mathbf{Q}_i^{\star}$, $i = 1, 2$;
until $\tilde{f}_{\text{SU-SCAMP}}(\nu)$ *converges*;
Apply Cholesky decomposition: $\mathbf{Q}_i^{\star} = \mathbf{L}_i \mathbf{L}_i^{\dagger}$, $i = 1, 2$;
Solve for $\mathbf{V}_i$ using (4.2), $i = 1, 2$

written as:

$$\mathbf{V}_i = \begin{bmatrix} \mathbf{V}_{i,\text{F}} \\ \mathbf{V}_{i,\text{S}} \end{bmatrix}.$$

Hence, in this section, $\mathbf{V}_i$ is optimized using a two-step procedure. First, $\mathbf{V}_{i,\text{F}} \in \mathbb{C}^{M \times M}$ is optimized to maximize the sum-rate assuming zero self-interference. Next, $\mathbf{V}_{i,\text{S}} \in \mathbb{C}^{M \times M}$ is optimized in order to suppress the self-interference as much as possible.

The self-interference-free rate formula for the i-th node, $\tilde{R}_i$, can be written as:

$$\tilde{R}_i = \log_2 \left| \mathbf{I}_M + \mathbf{\Sigma}_i^{-1} \mathbf{C}_{i,j} \right|,$$

where the covariance matrix $\mathbf{C}_{i,j}$ can be re-written as: $\mathbf{C}_{i,j} = \mathbf{H}_j \tilde{\mathbf{Q}}_j \mathbf{H}_j^{\dagger}$, where $\tilde{\mathbf{Q}}_j = \mathbf{V}_{i,\text{F}} \mathbf{S}_i \mathbf{V}_{i,\text{F}}^{\dagger}$.

The precoding matrix $\mathbf{V}_{i,\text{F}}$ $(i = 1, 2)$ can be optimized by first optimizing $\tilde{\mathbf{Q}}_i$ and using the Cholesky decomposition to recover the corresponding optimal $\mathbf{V}_{i,\text{F}}$. In particular, let $\tilde{\mathbf{Q}}_i = \mathbf{L}_i \mathbf{L}_i^{\dagger}$, and hence, the precoding matrix can be computed as:

$$\mathbf{V}_{i,\text{F}} = \mathbf{L}_i \mathbf{S}_i^{-1/2}. \tag{4.10}$$

The following optimization problem can be formulated to solve for each $\tilde{\mathbf{Q}}_i$ $(i = 1, 2)$.

$$\begin{aligned} \max_{\tilde{\mathbf{Q}}_1, \tilde{\mathbf{Q}}_2} \quad & \tilde{R}_1 + \tilde{R}_2 \\ \text{subject to:} \quad & \mathrm{Tr}[\tilde{\mathbf{Q}}_i] \leq P_{\max,i},\ i = 1, 2 \\ & \tilde{\mathbf{Q}}_i \succcurlyeq 0,\ i = 1, 2 \end{aligned} \tag{4.11}$$

Optimization problem (4.11) is convex, and hence, can be solved using cvx. Next, $\mathbf{V}_{i,\mathrm{S}}$ is optimized so that $\hat{\mathbf{G}}_i \mathbf{V}_i \approx \mathbf{0}_M$. By re-writing $\hat{\mathbf{G}}_i$ as follows:

$$\hat{\mathbf{G}}_i = \begin{bmatrix} \hat{\mathbf{G}}_{i,a} & \hat{\mathbf{G}}_{i,b} \end{bmatrix},$$

the corresponding $\mathbf{V}_{i,\mathrm{S}}$ can be derived by solving optimization problem (4.12) for the i-th node. Note that for the FDP structure presented in Section 4.2.4, $\hat{\mathbf{G}}_{i,b} = \alpha \mathbf{I}_M$ but here the separate approach is presented in its most general form.

$$\begin{aligned} \min_{\mathbf{V}_{i,\mathrm{S}}} \quad & \left|\left| \hat{\mathbf{G}}_i \mathbf{V}_i \right|\right|_F^2 \\ \text{subject to:} \quad & \mathrm{Tr}[\mathbf{V}_{i,\mathrm{S}} \mathbf{V}_{i,\mathrm{S}}^\dagger] \leq P_{\max,i}. \end{aligned} \tag{4.12}$$

Optimization problem (4.12) can be solved by writing out the Lagrangian as follows:

$$\mathcal{L}_i = \mathrm{Tr}\left[\left(\hat{\mathbf{G}}_{i,a} \mathbf{V}_{i,\mathrm{F}} + \hat{\mathbf{G}}_{i,b} \mathbf{V}_{i,\mathrm{S}} \right) \left(\hat{\mathbf{G}}_{i,a} \mathbf{V}_{i,\mathrm{F}} + \hat{\mathbf{G}}_{i,b} \mathbf{V}_{i,\mathrm{S}} \right)^\dagger \right] + \lambda_i \left(\mathrm{Tr}\left[\mathbf{V}_{i,\mathrm{S}} \mathbf{V}_{i,\mathrm{S}}^\dagger \right] - P_{\max,i} \right).$$

The gradient of the Lagrangian can be derived using the concept of matrix differentials [100, 101] to be:

$$\nabla \mathcal{L}_i = 2 \mathbf{V}_{i,\mathrm{F}}^\dagger \hat{\mathbf{G}}_{i,a}^\dagger \hat{\mathbf{G}}_{i,b} + 2 \hat{\mathbf{G}}_{i,b}^\dagger \hat{\mathbf{G}}_{i,b} \mathbf{V}_{i,\mathrm{S}} + 2 \lambda_i \mathbf{V}_{i,\mathrm{S}}.$$

By setting $\nabla \mathcal{L}_i = \mathbf{0}_M$, the optimal $\mathbf{V}_{i,\mathrm{S}}$ is given by:

$$\mathbf{V}_{i,\mathrm{S}} = -\left(\hat{\mathbf{G}}_{i,b}^\dagger \hat{\mathbf{G}}_{i,b} + \lambda_i \mathbf{I}_M \right)^{-1} \hat{\mathbf{G}}_{i,b}^\dagger \hat{\mathbf{G}}_{i,a} \mathbf{V}_{i,\mathrm{F}},$$

where λ_i is the water-filling level and can be optimized using a bisection search. Note that when $\lambda_i = 0$, corresponding to the case of infinite cancellation power, $\mathbf{V}_{i,\mathrm{S}} = -\hat{\mathbf{G}}_{i,b}^{-1} \hat{\mathbf{G}}_{i,a} \mathbf{V}_{i,\mathrm{F}}$.

4.5 Joint Full-Duplex Precoding

In this section, the FDP structure is applied, where the forward precoding and self-interference cancellation are jointly designed using precoding. In particular, the $\mathbf{V}_i$ ($i = 1, 2$) are optimized jointly. The joint FDP optimization problem is identical to optimization problem (4.1), where the difference lies in the dimensionality of the matrices involved. More specifically, where $\mathbf{H}_i$ and $\mathbf{G}_i$ are given by the equations presented in Section 4.2.4, and $\mathbf{Q}_i = \mathbf{V}_i \mathbf{S}_i \mathbf{V}_i^\dagger$.

Since we directly optimize the $2M \times 2M$ covariance matrices, it becomes difficult to recover the optimal $2M \times M$ precoding matrices. In order to avoid this issue, the vector of transmitted signals for the i-th node, $\mathbf{x}$, can be re-written as:

$$\tilde{\mathbf{x}}_i = \begin{bmatrix} \mathbf{x}_i \\ \mathbf{0}_M \end{bmatrix},$$

and hence, the precoding matrices, $\mathbf{V}_i$, become $2M \times 2M$ matrices which can be easily recovered once optimization problem (4.1) is solved using the Cholesky decomposition. Note that since the last M elements of $\tilde{\mathbf{x}}_i$ are zero, the $2M \times M$ precoding matrices can be recovered by applying the Cholesky decomposition to the $2M \times 2M$ precoding matrices.

As discussed in Section 4.3, SCP can be used to efficiently solve optimization problem (4.1). Hence, two joint FDP algorithms, FDP-DC and FDP-SCAMP are proposed, corresponding to the DC-based and SCAMP algorithms, respectively. The resulting derivation of the FDP-DC and FDP-SCAMP algorithms are identical to those of Sections 4.3.1 and 4.3.2, respectively, where the only difference lies in the dimensions of the matrices.

4.6 Separate vs. Joint Full-Duplex Precoding

This section provides an analytical comparison between the separate and joint FDP schemes. In particular, it investigates conditions under which separate FDP is optimal and conditions under which joint FDP has the potential to improve the performance over the separate approach.

Theorem 4.1. *Separate FDP is optimal if and only if* $\alpha \geq E\left[\left|\left|\hat{\mathbf{G}}_{i,a}\mathbf{V}_{i,\mathrm{F}}\mathbf{x}_i\right|\right|_2\right] / \sqrt{P_{\max,i}}$.

Proof. The proof is provided in Appendix B.1. □

4.7 Self-Interference Pricing

In this section, a utility function-based approach is applied to manage self-interference in FD systems, corresponding to the system model in Section 4.2.1 while also applying postcoding matrices.[8] In order to avoid solving the difficult non-convex sum-rate maximization problem, the utility function-based approach defines a new utility function (i.e., instead of attempting to directly maximize the sum-rate). The new utility function is designed to be easier to solve and the objective is that the result will still provide significant sum-rate improvements. Hence, the goal is for the sum-rate to be improved, while operating at a lower complexity. For this algorithm, both precoding and postcoding are applied. As such, the algorithm must assume some active and/or passive cancellation to ensure the linearity of the LNA and ADC.

The presented approach alternates between fixing and optimizing the precoding and postcoding matrices. The postcoding matrices are applied at the receiver-side after the LNA and ADC. Assuming fixed precoding matrices, $\mathbf{V}_i \in \mathbb{C}^{N_T \times d_i}$, $i = 1, 2$, the following optimization problem can be formulated for the i-th postcoding matrix, $\mathbf{U}_i \in \mathbb{C}^{N_R \times d_i}, i = 1, 2$:

$$\begin{aligned} \max_{\mathbf{U}_i} \quad & \mathcal{U}_i \\ \text{subject to:} \quad & \mathbf{U}_i^\dagger \mathbf{U}_i = \mathbf{I}_{d_i}, \end{aligned} \tag{4.13}$$

where the number of DoF at the i-th node is typically selected as $d_i = \lfloor \min\{N_T, N_R\}/2 \rfloor$ so that SIP can make use of a subspace maximization approach. The objective function is defined as:

$$\mathcal{U}_i \triangleq E\left[\left|\left|\mathbf{U}_i^\dagger \mathbf{H}_j \mathbf{V}_j \mathbf{x}_j\right|\right|_2^2\right] - \mu_i E\left[\left|\left|\mathbf{U}_i^\dagger \hat{\mathbf{G}}_i \mathbf{V}_i \mathbf{x}_i\right|\right|_2^2\right], \tag{4.14}$$

where $j \neq i$ and μ_i is a weighting factor that balances the effects of the forward and self-interference channels. Similarly, for fixed postcoding matrices $\mathbf{U}_i$, $i = 1, 2$, the following optimization problem can be formulated for the i-th precoding matrix:

$$\begin{aligned} \max_{\mathbf{V}_i} \quad & \tilde{\mathcal{U}}_i \\ \text{subject to:} \quad & \mathbf{V}_i^\dagger \mathbf{V}_i = \mathbf{I}_{d_i}, \end{aligned} \tag{4.15}$$

[8] Postcoding was discussed in Section 2.2.

where the objective function is defined as:

$$\tilde{\mathcal{U}}_i \triangleq E\left[\left|\left|\mathbf{V}_i^{\dagger}\mathbf{H}_i^{\dagger}\mathbf{U}_j\mathbf{x}_j\right|\right|_2^2\right] - \tilde{\mu}_i E\left[\left|\left|\mathbf{V}_i^{\dagger}\hat{\mathbf{G}}_i^{\dagger}\mathbf{U}_i\mathbf{x}_i\right|\right|_2^2\right], \tag{4.16}$$

where $j \neq i$ and $\tilde{\mu}_i$ is a weighting factor that balances the effects of the forward and self-interference channels. Note that the objective functions for optimizing the precoding matrices are in terms of the reverse channels.

For fixed values of μ_i and $\tilde{\mu}_i$, optimization problems (4.13) and (4.15) can be solved using a subspace maximization approach [102, p.45], as follows. $\mathcal{U}_i$ can be re-written as:

$$\mathcal{U}_i = \mathrm{Tr}\left[\mathbf{U}_i^{\dagger}\left(\underbrace{\mathbf{H}_j\mathbf{V}_j\mathbf{S}_j\mathbf{V}_j^{\dagger}\mathbf{H}_j^{\dagger} - \mu_i\hat{\mathbf{G}}_i\mathbf{V}_i\mathbf{S}_i\mathbf{V}_i^{\dagger}\hat{\mathbf{G}}_i^{\dagger}}_{\mathbf{\Xi}_{i,j}}\right)\mathbf{U}_i\right]. \tag{4.17}$$

Hence, for fixed $\mathbf{V}_i$ and $\mathbf{S}_i$ $(i = 1, 2)$, the optimal $\mathbf{U}_i$ $(i = 1, 2)$ is selected as the matrix of eigenvectors corresponding to the d_i largest eigenvalues of $\mathbf{\Xi}_{i,j}$. Similarly, $\tilde{\mathcal{U}}_i$ can be re-written as:

$$\tilde{\mathcal{U}}_i = \mathrm{Tr}\left[\mathbf{V}_i^{\dagger}\left(\underbrace{\mathbf{H}_i^{\dagger}\mathbf{U}_j\mathbf{S}_j\mathbf{U}_j^{\dagger}\mathbf{H}_i - \tilde{\mu}_i\hat{\mathbf{G}}_i^{\dagger}\mathbf{U}_i\mathbf{S}_i\mathbf{U}_i^{\dagger}\hat{\mathbf{G}}_i}_{\tilde{\mathbf{\Xi}}_{i,j}}\right)\mathbf{V}_i\right]. \tag{4.18}$$

Hence, for fixed $\mathbf{U}_i$ and $\mathbf{S}_i$ $(i = 1, 2)$, the optimal $\mathbf{V}_i$ $(i = 1, 2)$ is selected as the matrix of eigenvectors corresponding to the d_i largest eigenvalues of $\tilde{\mathbf{\Xi}}_{i,j}$. Clearly, the selection of μ_i and $\tilde{\mu}_i$ $(i = 1, 2)$ will affect the performance of the utility function-based approach.

We propose weighting factors to improve the sum-rate of the system based on a self-interference pricing approach. As such, the weighting factors were re-defined as: $\mu_i = \pi_i/\psi_i$ and $\tilde{\mu}_i = \tilde{\pi}_i/\tilde{\psi}_i$. Note that $\pi_i, \psi_i, \tilde{\pi}_i, \tilde{\psi}_i$ $(i = 1, 2)$ are referred to as pricing functions. This is equivalent to re-writing the objective functions as:

$$\mathcal{U}_i = \mathrm{Tr}\left[\psi_i\mathbf{U}_i^{\dagger}\mathbf{C}_{i,j}\mathbf{U}_i - \pi_i\mathbf{U}_i^{\dagger}\hat{\mathbf{C}}_{i,i}\mathbf{U}_i\right],$$
$$\tilde{\mathcal{U}}_i = \mathrm{Tr}\left[\tilde{\psi}_i\mathbf{V}_i^{\dagger}\tilde{\mathbf{C}}_{i,j}\mathbf{V}_i - \tilde{\pi}_i\mathbf{V}_i^{\dagger}\tilde{\mathbf{C}}_{i,i}\mathbf{V}_i\right],$$

where $\mathbf{C}_{i,j}$ and $\hat{\mathbf{C}}_{i,i}$ are defined in Section 4.2.1 and

$$\tilde{\mathbf{C}}_{i,j} = \mathbf{H}_i^\dagger \mathbf{U}_j \mathbf{S}_j \mathbf{U}_j^\dagger \mathbf{H}_i,$$
$$\tilde{\mathbf{C}}_{i,i} = \hat{\mathbf{G}}_i^\dagger \mathbf{U}_i \mathbf{S}_i \mathbf{U}_i^\dagger \hat{\mathbf{G}}_i.$$

The pricing functions are selected to reflect the effect of each covariance matrix on the achieved sum-rate. In particular, ψ_i and $\tilde{\psi}_i$ represent the sum of squares of marginal gains in sum-rate at node i due to transmission from each antenna pair, respectively. Similarly, π_i and $\tilde{\pi}_i$ represent the sum of squares of marginal losses in sum-rate at node i due to transmission from each antenna pair. Mathematically, these quantities can be defined as:

$$\pi_i \triangleq \left|\left|\frac{-\partial R_i}{\partial \hat{\mathbf{C}}_{i,i}}\right|\right|_F^2, \quad \tilde{\pi}_i \triangleq \left|\left|\frac{-\partial \tilde{R}_i}{\partial \tilde{\mathbf{C}}_{i,i}}\right|\right|_F^2,$$
$$\psi_i \triangleq \left|\left|\frac{\partial R_i}{\partial \mathbf{C}_{i,j}}\right|\right|_F^2, \quad \tilde{\psi}_i \triangleq \left|\left|\frac{\partial \tilde{R}_i}{\partial \tilde{\mathbf{C}}_{i,j}}\right|\right|_F^2,$$

where $\tilde{R}_i = \log_2 \left| \mathbf{I}_{N_T} + \left(\mathbf{\Sigma}_i + \tilde{\mathbf{C}}_{i,i} \right)^{-1} \tilde{\mathbf{C}}_{i,j} \right|$. The pricing functions require computing the derivative of a scalar function with respect to a matrix (i.e., computing the derivative of the sum-rate with respect to a covariance matrix). As such, the optimized pricing functions can be derived using the concept of matrix differentials [100, 101] to be:

$$\pi_i = \left|\left| \frac{1}{\ln(2)} \mathbf{\Phi}_{N,i}^{-1} \mathbf{C}_{i,j} \left[\mathbf{I}_{N_R} + \mathbf{\Phi}_{N,i}^{-1} \mathbf{C}_{i,j} \right]^{-1} \mathbf{\Phi}_{N,i}^{-1} \right|\right|_F^2, \tag{4.19}$$

$$\tilde{\pi}_i = \left|\left| \frac{1}{\ln(2)} \tilde{\mathbf{\Phi}}_{N,i}^{-1} \tilde{\mathbf{C}}_{i,j} \left[\mathbf{I}_{N_T} + \tilde{\mathbf{\Phi}}_{N,i}^{-1} \tilde{\mathbf{C}}_{i,j} \right]^{-1} \tilde{\mathbf{\Phi}}_{N,i}^{-1} \right|\right|_F^2, \tag{4.20}$$

$$\psi_i = \left|\left| \frac{1}{\ln(2)} \left[\mathbf{I}_{N_R} + \mathbf{\Phi}_{N,i}^{-1} \mathbf{C}_{i,j} \right]^{-1} \mathbf{\Phi}_{N,i}^{-1} \right|\right|_F^2, \tag{4.21}$$

$$\tilde{\psi}_i = \left|\left| \frac{1}{\ln(2)} \left[\mathbf{I}_{N_T} + \tilde{\mathbf{\Phi}}_{N,i}^{-1} \tilde{\mathbf{C}}_{i,j} \right]^{-1} \tilde{\mathbf{\Phi}}_{N,i}^{-1} \right|\right|_F^2, \tag{4.22}$$

where $\mathbf{\Phi}_{N,i} = \mathbf{\Sigma}_i + \hat{\mathbf{C}}_{i,i}$ and $\tilde{\mathbf{\Phi}}_{N,i} = \mathbf{\Sigma}_i + \tilde{\mathbf{C}}_{i,i}$. The derivations of (4.19) and (4.21) are given below. The derivations of (4.20) and (4.22) can be similarly derived.

Using the fact that $\mathrm{d}(\ln|\mathbf{X}|) = \mathrm{Tr}[\mathbf{X}^{-1}\mathrm{d}(\mathbf{X})]$ [101] and that $\mathrm{d}(\mathbf{X}^{-1}) = -\mathbf{X}^{-1}\mathrm{d}(\mathbf{X})\mathbf{X}^{-1}$

[101], the differential of $-R_i$ with respect to $\hat{\mathbf{C}}_{i,i}$ can be written as:

$$\begin{aligned}\mathrm{d}(-R_i) =& \frac{1}{\ln(2)}\mathrm{Tr}\left[\left(\mathbf{I}_N + \mathbf{\Phi}_{N,i}^{-1}\mathbf{C}_{i,j}\right)^{-1}\mathbf{\Phi}_{N,i}^{-1}\mathrm{d}(\hat{\mathbf{C}}_{i,i})\mathbf{\Phi}_{N,i}^{-1}\mathbf{C}_{i,j}\right] \\ =& \frac{1}{\ln(2)}\mathrm{Tr}\left[\mathbf{\Phi}_{N,i}^{-1}\mathbf{C}_{i,j}\left(\mathbf{I}_N + \mathbf{\Phi}_{N,i}^{-1}\mathbf{C}_{i,j}\right)^{-1}\mathbf{\Phi}_{N,i}^{-1}\mathrm{d}(\hat{\mathbf{C}}_{i,i})\right],\end{aligned}$$

which gives (4.19), since $\mathrm{d}y = \mathrm{Tr}\left(\mathbf{A}\mathrm{d}\mathbf{X}\right)$ implies that $\mathbf{A}$ is the Jacobian of y with respect to $\mathbf{X}$ [101]. Similarly, the differential of R_i with respect to $\mathbf{C}_{i,j}$ can be written as:

$$\mathrm{d}(R_i) = \frac{1}{\ln(2)}\mathrm{Tr}\left[\left(\mathbf{I}_N + \mathbf{\Phi}_{N,i}^{-1}\mathbf{C}_{i,j}\right)^{-1}\mathbf{\Phi}_{N,i}^{-1}\mathrm{d}(\mathbf{C}_{i,j})\right],$$

which gives (4.21). The SIP algorithm is summarized in Algorithm 4.3.

Algorithm 4.3: FD MIMO point-to-point: self-interference pricing algorithm.

Initialize $\mathbf{V}_i$ $i = 1, 2$ to random unitary matrices. ;
repeat
  Fix $\mathbf{V}_1$ and $\mathbf{V}_2$;
  Compute π_i and ψ_i using (4.19) and (4.21), respectively ;
  Update $\mathbf{U}_1$ and $\mathbf{U}_2$ from (4.17) ;
  Fix $\mathbf{U}_1$ and $\mathbf{U}_2$;
  Compute $\tilde{\pi}_i$ and $\tilde{\psi}_i$ using (4.20) and (4.22), respectively ;
  Update $\mathbf{V}_1$ and $\mathbf{V}_2$ from (4.18) ;
until $\mathcal{U}_i$ *and* $\tilde{\mathcal{U}}_i$ *converge*;

4.8 Self-Interference Pricing Using Full-Duplex Precoding

In this section, the SIP utility function-based approach presented in Section 4.7 is adapted to take advantage of the FDP structure. In order to avoid solving the difficult non-convex sum-rate maximization problem, the SIP approach defines a new utility function. In the original, SIP algorithm, both precoding and postcoding were applied. As such, the original SIP algorithm must assume some active and/or passive cancellation to ensure the linearity of the LNA and ADC. In this section, only precoding is applied since the FDP structure provides additional transmit dimensions. As well, since the cancellation effectively takes place prior to the LNA and ADC, the linearity of the system can be ensured.

The FDP-SIP optimization problem at the i-th node is defined as:

$$\begin{aligned} \max_{\mathbf{V}_i} \quad & \mathcal{U}_i \\ \text{subject to:} \quad & \mathbf{V}_i^{\dagger}\mathbf{V}_i = \mathbf{I}_M, \end{aligned} \tag{4.23}$$

where $\mathbf{V}_i \in \mathbb{C}^{2M \times M}$ and the objective function is defined as:

$$\mathcal{U}_i \triangleq \psi_i \left|\left|\mathbf{H}_i\mathbf{V}_i\right|\right|_F^2 - \pi_i \left|\left|\hat{\mathbf{G}}_i\mathbf{V}_i\right|\right|_F^2, \tag{4.24}$$

where ψ_i and π_i are weighting factors that balances the effects of the forward and self-interference channels and $j \neq i$.

Note that (4.24) can be re-written as:

$$\mathcal{U}_i \triangleq \text{Tr}\left[\mathbf{V}_i^{\dagger}\mathbf{\Xi}_i\mathbf{V}_i\right], \tag{4.25}$$

where $\mathbf{\Xi}_i = \psi_i\mathbf{H}_i^{\dagger}\mathbf{H}_i - \pi_i\hat{\mathbf{G}}_i^{\dagger}\hat{\mathbf{G}}_i$.

For fixed values of ψ_i and π_i optimization problems (4.23) can be solved using a subspace maximization approach [102, p.45], where the optimal $\mathbf{V}_i$ $(i = 1, 2)$ is selected as outlined in Algorithm 4.4.

Algorithm 4.4: Subspace maximization algorithm.

The optimal $\mathbf{V}_i$ $(i = 1, 2)$ is selected as the matrix of eigenvectors corresponding to the M largest eigenvalues of $\mathbf{\Xi}_i = \psi_i\mathbf{H}_i^{\dagger}\mathbf{H}_i - \pi_i\hat{\mathbf{G}}_i^{\dagger}\hat{\mathbf{G}}_i$.

Similarly to in Section 4.7, the weighting factors are selected to improve the sum-rate of the system based on a self-interference pricing approach. The pricing functions are selected to reflect the effect of each covariance matrix on the achieved sum-rate. Mathematically, these quantities can be defined as:

$$\pi_i \triangleq \left|\left|\frac{-\partial R_i}{\partial \hat{\mathbf{C}}_{i,i}}\right|\right|_F^2, \quad \psi_i \triangleq \left|\left|\frac{\partial R_i}{\partial \mathbf{C}_{i,j}}\right|\right|_F^2.$$

The pricing functions require computing the derivative of a scalar function with respect to a matrix (i.e., computing the derivative of the sum-rate with respect to a covariance matrix). Following the derivation in Section 4.7, the optimized pricing functions can be

derived to be (4.19) and (4.21) for π_i and ψ_i, respectively, where the difference lies in terms of the dimensionality of the matrices involved. A summary of the FDP-SIP algorithm for the i-th node is given in Algorithm 4.5.

Algorithm 4.5: FD MIMO point-to-point: FDP-SIP algorithm for node i.

Initialize $\mathbf{V}_i$ to a random unitary matrix. ;
repeat
  Update π_i and ψ_i using (4.19) and (4.21), respectively ;
  Update $\mathbf{V}_i$ from (4.25) ;
until $\mathcal{U}_i$ *converges*;

4.9 Self-Interference Threshold Using Full-Duplex Precoding

This section presents the Self-Interference Threshold (SIT) algorithm which can be applied with or without using the FDP structure, where the difference lies in the dimensionality of the matrices involved. For consistency, when the SIT algorithm is applied to the FDP structure, the algorithm is referred to as FDP-SIT. The SIT approach introduces a maximum self-interference constraint for each node, referred to as the self-interference threshold value, θ_i for $i = 1, 2$.

The SIT optimization problem is defined as:

$$\begin{aligned} \max_{\mathbf{Q}_1,\mathbf{Q}_2} \quad & R_1^{\text{th}} + R_2^{\text{th}} \\ \text{subject to:} \quad & \text{Tr}[\mathbf{Q}_i] \leq P_{\max,i},\ i = 1, 2, \\ & \text{Tr}[\hat{\mathbf{G}}_i \mathbf{Q}_i \hat{\mathbf{G}}_i^{\dagger}] \leq \theta_i,\ i = 1, 2, \\ & \mathbf{Q}_i \succcurlyeq 0,\ i = 1, 2, \end{aligned} \tag{4.26}$$

where θ_i is a fixed self-interference threshold value and R_i^{th} is defined as:

$$R_i^{\text{th}} = \log_2 \left| \mathbf{I}_M + \left(\mathbf{\Sigma}_i + \mathbf{\Theta}_i \right)^{-1} \mathbf{C}_{i,j} \right|,$$

where $j \neq i$ and $\mathbf{\Theta}_i$ is the $M \times M$ matrix with each entry equal to θ_i / M for $i = 1, 2$. Hence, a component-wise upper-bound is applied to the self-interference covariance matrix. Note that for fixed values of θ_i $(i = 1, 2)$, optimization problem (4.26) is convex, and hence, can

be solved using any convex optimization software (e.g., cvx).

The SIT algorithm performs a nested bisection search to optimize the threshold values. Without loss of generality, assume the outer loop performs bisection over θ_1. Then, for a fixed θ_1, Algorithm 4.6 provides a bisection search algorithm for θ_2, where $R_{\text{th}}(\theta_2) = \sum_{i=1}^{2} R_i^{\text{th}}$ when θ_2 is applied.

The full SIT algorithm is summarized in Algorithm 4.7. The outer loop performs a bisection search over θ_1. For each value of θ_1, a bisection search over θ_2 must be performed. Optimization problem (4.26) must be solved after each outer and inner loop update (i.e., after updating the value of θ_1 or θ_2).

For each fixed value of θ_1, the bisection search over θ_2 provides a monotonically increasing rate function; however, since after each θ_1 update, a new bisection search over θ_2 must be run, it is possible that the sum-rate may temporarily drop before monotonically increasing. In other words, the SIT approach exhibits a piece-wise monotonically increasing rate function, where each discontinuity corresponds to an update of the θ_1 parameter (i.e., the start of a new bisection search over θ_2). From an outer-loop perspective (i.e., focusing on the sum-rate changes with respect to changes in θ_1), the SIT algorithm is monotonically increasing, and hence, convergence of the algorithm is guaranteed.

In this chapter, we distinguish between the SIT and the FDP-SIT algorithms. Both SIT and FDP-SIT apply Algorithm 4.7, where the difference lies only in terms of the dimensionality and elements of the channel matrices, as specified in Section 4.2.1.

Algorithm 4.6: SIT: bisection search for θ_2.

Given: $\theta_1 \geq 0$;
Initialize: $\theta_{2,\min} = 0$, $\theta_{2,\max} = 2^3$;
Step 1: Determine max and min bisection values ;
while *1* **do**
  if $R_{\text{th}}(\theta_{2,\min}) \geq R_{\text{th}}(\theta_{2,\max})$ **then**
    break ;
  else
    $\theta_{2,\max} = 2 \times \theta_{2,\max}$;
    if $R_{\text{th}}(\theta_{2,\max}) \leq R_{\text{th}}(\theta_{2,\max}/2)$ **then**
      $\theta_{2,\min} = \theta_{2,\min}/2$;
      break ;
    else
      $\theta_{2,\min} = \theta_{2,\max}$;
    end
  end
end
Step 2: Perform Bisection ;
repeat
  $\theta_2 = (\theta_{2,\min} + \theta_{2,\max})/2$;
  Solve (4.26) using θ_1 and θ_2 for $R_{\text{th}}(\theta_2)$;
  if $R_{\text{th}}(\theta_{2,\min}) \leq R_{\text{th}}(\theta_2) \geq R_{\text{th}}(\theta_{2,\max})$ **then**
    $d_{\min} = R_{\text{th}}(\theta_2) - R_{\text{th}}(\theta_{2,\min})$;
    $d_{\max} = R_{\text{th}}(\theta_2) - R_{\text{th}}(\theta_{2,\max})$;
    if $d_{\min} < d_{\max}$ **then**
      $\theta_{2,\max} = \theta_{2,\max} - (\theta_{2,\max} - \theta_2)/2$;
    else
      $\theta_{2,\min} = \theta_{2,\min} + (\theta_2 - \theta_{2,\min})/2$;
    end
  else if $R_{\text{th}}(\theta_{2,\min}) \leq R_{\text{th}}(\theta_2) \leq R_{\text{th}}(\theta_{2,\max})$ **then**
    $\theta_{2,\min} = \theta_2$;
  else if $R_{\text{th}}(\theta_{2,\min}) \geq R_{\text{th}}(\theta_2) \geq R_{\text{th}}(\theta_{2,\max})$ **then**
    $\theta_{2,\max} = \theta_2$;
  else
    if $R_{\text{th}}(\theta_{2,\max}) > R_{\text{th}}(\theta_{2,\min})$ **then**
      $\theta_{2,\min} = \theta_2$;
    else
      $\theta_{2,\max} = \theta_2$;
    end
  end
until θ_2 *converges*;

Algorithm 4.7: FD MIMO point-to-point: self-interference threshold.

Initialize: $\theta_{1,\min} = 0$, $\theta_{1,\max} = \Lambda_{\max}$;
repeat
  $\theta_1 = (\theta_{1,\min} + \theta_{1,\max})/2$;
  Find optimal θ_2 for fixed θ_1 using Algorithm 4.6 ;
  Solve (4.26) using θ_1 and θ_2 for $\mathbf{Q}_i^\star$;
  Apply the same bisection search updates as in Algorithm 4.6 on $\theta_{1,\min}$ and $\theta_{1,\max}$;
until θ_1 *converges*;
Apply Cholesky decomposition: $\mathbf{Q}_i^\star = \mathbf{L}_i \mathbf{L}_i^\dagger$, $i = 1, 2$;
Solve for $\mathbf{V}_i = \mathbf{L}_i \mathbf{S}_i^{-1/2}$, $i = 1, 2$

4.10 Illustrative Results

This section provides some illustrative results to compare the various FD MIMO point-to-point algorithms and to demonstrate the effectiveness of the proposed FDP structure. For all simulations, the PAs are assumed to have a 30 dB gain, the circulators are assumed to have a 20 dB isolation and the variance of the inter-antenna self-interference is assumed to be 20 dB below that of the direct self-interference paths which affect the signal-to-self-interference ratio and self-interference-to-noise ratio.

Note that in terms of computational complexity, for all SCP algorithms, the main source of algorithm complexity is in solving the convex sub-problems and not in terms of computing the objective function approximations regardless of whether or not the FDP structure is applied. As such, the complexity of computing the objective function approximations is negligible.

4.10.1 FD MIMO Point-to-Point Simulation Results

For MIMO point-to-point systems, the HD optimization problem is convex, and hence, can be easily solved using cvx. The noise was normalized such that $E[\mathbf{z}_i\mathbf{z}_i^\dagger] = \mathbf{I}_M$ $(i = 1, 2)$. Hence, the forward channels, $\tilde{\mathbf{H}}_i$ $(i = 1, 2)$, were generated as zero-mean complex Gaussian random variables with a variance equal to the SNR. Conversely, the self-interference channels, $\tilde{\mathbf{G}}_{i,a}$ $(i = 1, 2)$, were generated as zero-mean complex Gaussian random variables with a variance equal to the self-Interference-to-Noise Ratio (INR_{in}), where $\text{SNR}/\text{INR}_{\text{in}}$ represents the Signal-to-self-Interference Ratio at the receiver input (SIR_{in}) before self-interference cancellation. The simulations assume $M = 4$, and that each node uses an identical power (normalized to one).

Fig. 4.4 shows the FD-to-HD sum-rate ratio vs. α with SNR = 5 dB, $\text{SIR}_{\text{in}} = -40$ dB and $\sigma^2_{\text{err}} = 1$. The results show that for $\alpha < 15$ dB the FDP-SCAMP algorithm (i.e., joint FDP) provides significant performance improvements over the other FD algorithms and optimized HD. For $\alpha < 7$ dB, the FDP-DC algorithm slightly outperforms the FDP-SCAMP algorithm; however, the FDP-DC algorithm tends to have a negative slope with respect to increasing α. This is caused by the fact that the DC approximation significantly approximates the self-interference-plus-noise terms. As such, the FDP-DC algorithm leads to an objective function which has a very poor approximation of the self-interference matrix, which includes the auxiliary cancellation path; hence, the algorithm fails to take advantage

of the potential performance benefits offered by the FDP structure and, instead, becomes destructive as α increases. Conversely, while the FDP-SCAMP algorithm approximates all of the direct, self-interference, and noise signals, the approximations are more spread out, and hence, the FDP-SCAMP algorithm can take advantage of the FDP structure. Due to the inaccuracy of the FDP-DC approximation, it was not included in the remainder of the simulation results.

For $\alpha \geq 15$ dB, there is sufficient power available to cancel the self-interference, and hence, by Theorem 4.1, the separate and joint (i.e., FDP-SCAMP) FDP algorithms have the same performance. The FDP-SIT algorithm provides a sum-rate in between that of the separate FDP and FDP-SCAMP algorithms; however, due to the bisection searches, the FDP-SIT algorithm tends to require many iterations to converge. This will be discussed further in Section 4.10.2. Fig. 4.4 also shows that for sufficiently-large α, the FDP-SIP algorithm provides performance improvements over the SIP algorithm.

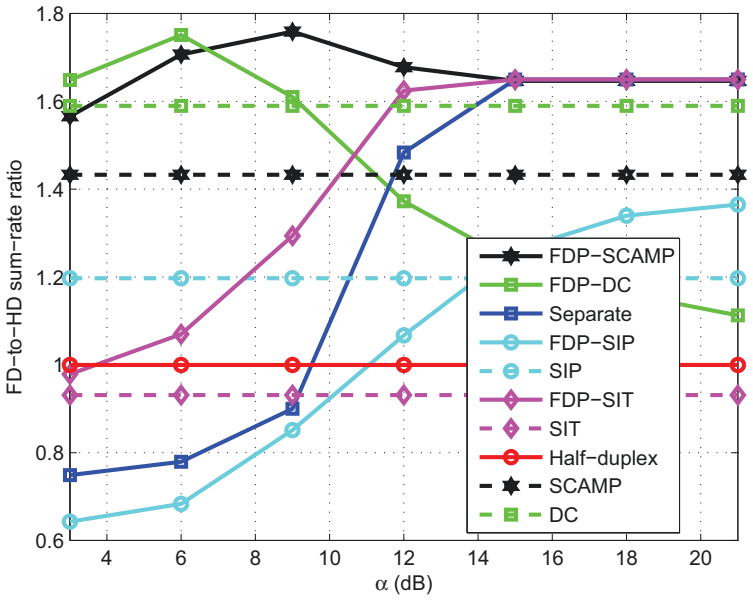

Fig. 4.4 MIMO point-to-point FD-to-HD sum-rate ratio vs. α with SNR = 5 dB, $\text{SIR}_{\text{in}} = -40$ dB, $\sigma^2_{\text{err}} = 1$.

Based on Fig. 4.4, it can be seen that the FDP-SCAMP algorithm exhibits some peaks for α values between 6 and 12 dB. These peaks are due to the inaccurate channel knowledge. Depending on the specific inaccurate channel knowledge, some values of alpha may be more

optimal than others; however, it is impossible to know ahead of time which value of α will be more favourable. However, Fig. 4.4 shows that, in general, the joint FDP-SCAMP algorithm can provide significant sum-rate improvements over the separate FDP algorithm when α is not sufficiently large.

Fig. 4.5 shows the FD-to-HD sum-rate ratio vs. α with SNR = 5 dB, $\text{SIR}_{\text{in}} = -40$ dB and σ^2_{err} = 1e-4 (i.e., ideal channel knowledge). This demonstrates the limitations of the various algorithms due only to the amount of available cancellation power (i.e., α), as opposed to Fig. 4.4 which shows the limitations due to both limited cancellation power and channel knowledge imperfections. As shown in Fig. 4.5, with near-perfect channel knowledge, for sufficiently large α, the algorithms achieve two times the sum-rate of optimized HD, as expected. Note that the FDP-SIP algorithm fails to achieve two-times the optimized HD sum-rate due to the fact that it solves a modified optimization problem which is not directly related to the original non-convex optimization problem. As well, with ideal channel knowledge, the peaks for the FDP-SCAMP algorithm for α between 6 and 12 dB, seen in Fig. 4.4, do not occur.

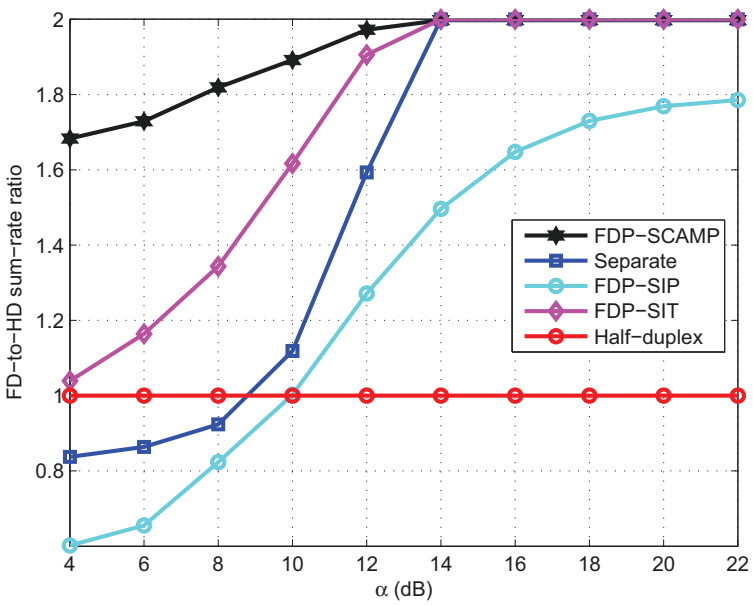

Fig. 4.5 MIMO point-to-point FD-to-HD sum-rate ratio vs. α with SNR = 5 dB, $\text{SIR}_{\text{in}} = -40$ dB, σ^2_{err} = 1e-4.

Fig. 4.6(a) shows the FD-to-HD sum-rate ratio and FD sum-rate vs. SNR with $\text{SIR}_{\text{in}} =$

-40 dB, $\alpha = 15$ dB, $\sigma^2_{\text{err}} = 1$. The results indicate that for low SNR the separate FDP algorithm provides identical performance to the joint FDP-SCAMP algorithm, but as the SNR increases, the performance of the separate approach decreases rapidly. This is caused by the fact that α and SIR_{in} remain fixed. Hence, as the SNR increases, so too does the INR_{in}, but the value of α remains fixed. Therefore, the amount of cancellation power remains fixed while the magnitude of the interference increases.

The joint FDP-SCAMP algorithm can offer a better trade-off between the forward channel sum-rate maximization and the self-interference suppression by adjusting the power allocated to the forward precoding and self-interference cancellation. Effectively trading-off between the two is crucial, especially in the high SNR regime, where higher self-interference is present since α and SIR_{in} remain fixed.

Fig. 4.6(b) indicates that the achieved sum-rate of the separate FDP algorithm increases with SNR for SNR < 10 dB, and then decreases with SNR for SNR > 10 dB. This is due to the fact that as the SNR increases, the quality of the forward channel increases; however, since α and SIR_{in} remain fixed, the interference increases, as well. In particular, the separate FDP algorithm fails to effectively cancel the strong self-interference and since the forward precoder is designed separately, the achievable sum-rate suffers.

Fig. 4.7 shows the FD-to-HD sum-rate ratio vs. SIR_{in} with SNR $= 10$ dB, $\alpha = 15$ dB, $\sigma^2_{\text{err}} = 1$. The results show that when the SIR_{in} is sufficiently large the separate FDP and joint FDP-SCAMP algorithms offer the same sum-rate (i.e., when $\alpha = 15$ dB is sufficiently large to fully cancel the self-interference, as outlined in Theorem 4.1). Likewise, for smaller values of SIR_{in}, corresponding to transmission over greater distances, the benefits of the joint FDP-SCAMP algorithm are significant over the separate FDP, FDP-SIP, FDP-SIT, and the non-FDP approaches (i.e., SCAMP and DC). Intuitively, the joint FDP algorithm allows for the forward paths to assist in the cancellation of the very strong self-interference which results in significant performance improvements over the separate FDP algorithm.

Fig. 4.8 shows the FD-to-HD sum-rate ratio vs. σ^2_{err} with SNR $= 10$ dB, $\text{SIR}_{\text{in}} = -45$ dB, $\alpha = 18$ dB. The results show that the performance of the FDP-based algorithms are more heavily influenced by the effects of imperfect channel knowledge.

While the FDP structure allows for the potential to cancel more self-interference, as σ^2_{err} becomes large, inaccurate channel knowledge can lead to inefficient use of the FDP structure, which may result in larger residual self-interference.

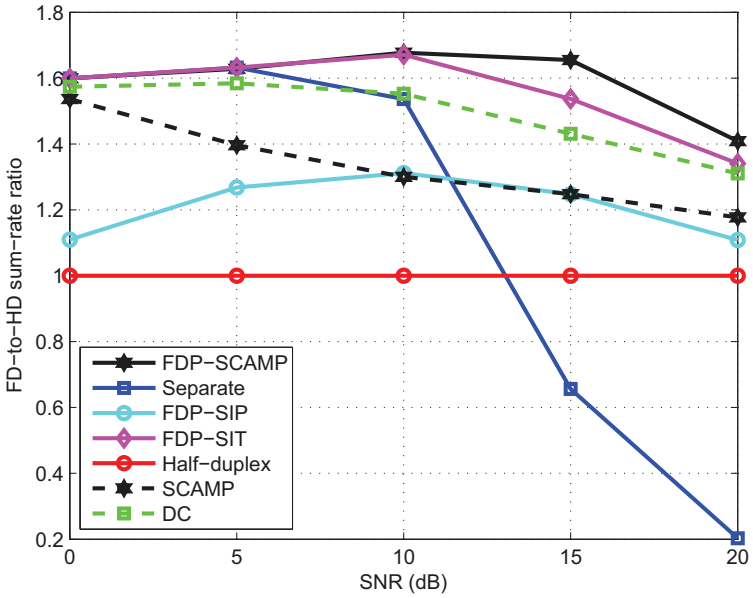

(a) FD-to-HD sum-rate ratio

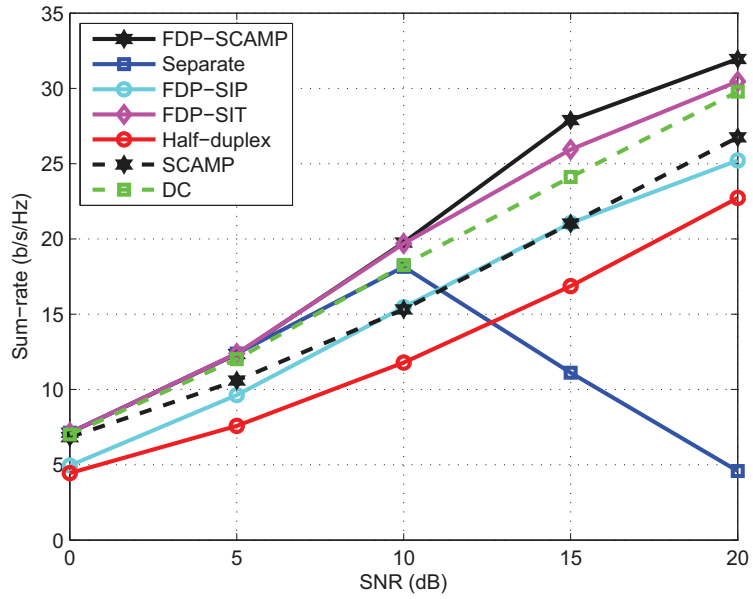

(b) Sum-rate (b/s/Hz)

Fig. 4.6 MIMO point-to-point sum-rate vs. SNR with $\mathrm{SIR}_{\mathrm{in}} = -40$ dB, $\alpha = 15$ dB, $\sigma^2_{\mathrm{err}} = 1$.

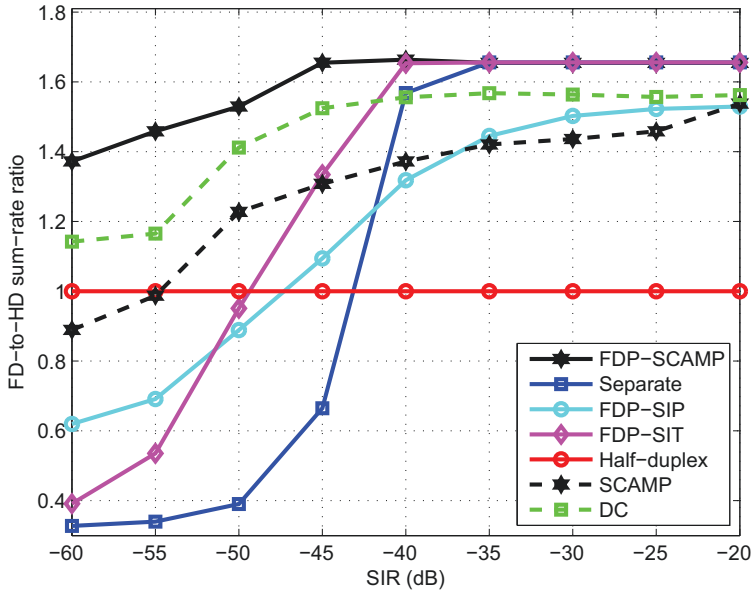

Fig. 4.7 MIMO point-to-point FD-to-HD sum-rate ratio vs. $\mathrm{SIR}_{\mathrm{in}}$ with SNR $= 10$ dB, $\alpha = 15$ dB, $\sigma^2_{\mathrm{err}} = 1$.

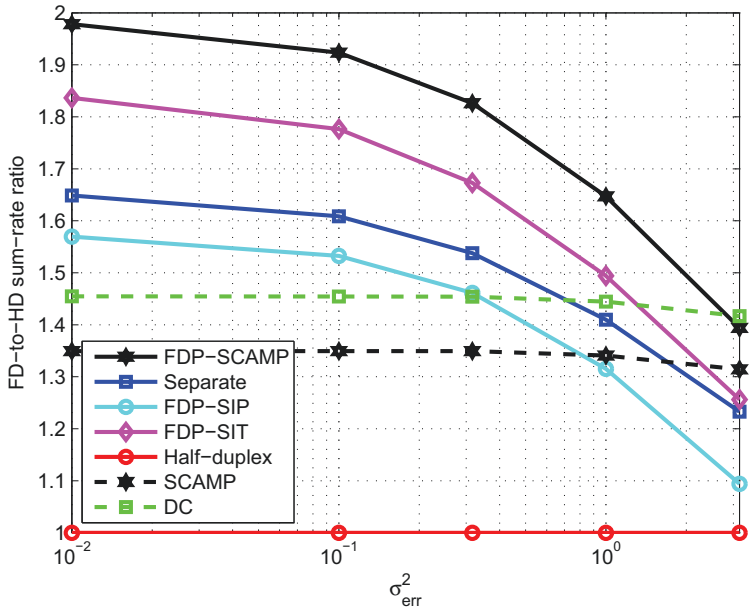

Fig. 4.8 MIMO point-to-point FD-to-HD sum-rate ratio vs. σ^2_{err} with SNR $= 10$ dB, $\mathrm{SIR}_{\mathrm{in}} = -45$ dB, $\alpha = 18$ dB.

4.10.2 FD MIMO Point-to-Point with 2x2 MIMO Measured Data

In this sub-section, the performances of the various algorithms using measured data are compared. The elements of the forward channel matrix, $\mathbf{H}_i$, and self-interference channel matrix, $\mathbf{G}_i$, for both nodes were obtained from the measurement of an experimental FD 2x2 MIMO point-to-point system, where the nodes were separated by 5 m. The measured data represents one snap shot during the daytime (i.e., with students moving around) on the 2.5 GHz carrier. The circulators used had a 20 dB isolation and a 0.2 dB insertion loss. The vector network analyzer transmit power was -10 dBm, the radio frequency amplifier gain was 14.76 dB, the switch insertion loss was 1.9 dB; hence, the transmit power at the circulator *input* was +2.86 dBm.

As before, it was assumed that the self-interference measurements had an associated zero-mean Gaussian estimation error with a variance, σ^2_{err}. Fig. 4.9 shows the FD-to-HD sum-rate ratio vs. α using the measured data with $\sigma^2_{\text{err}} = 1$.

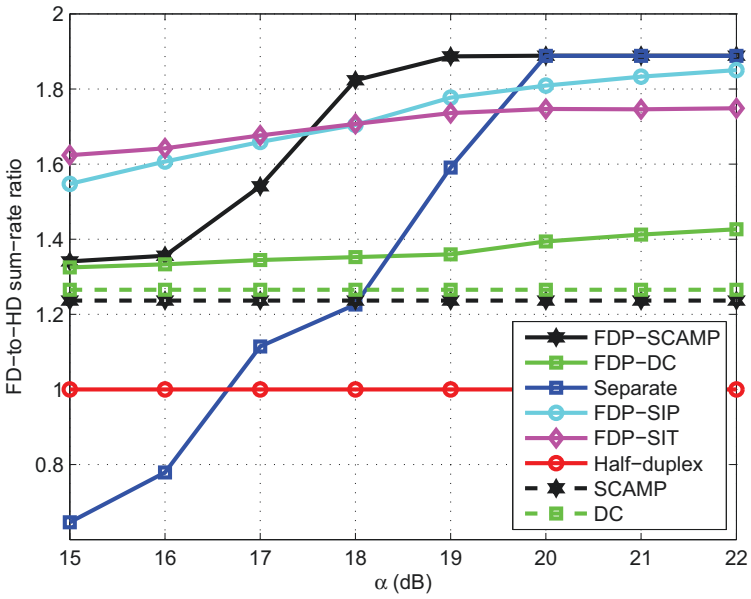

Fig. 4.9 MIMO point-to-point FD-to-HD sum-rate ratio vs. α using measured data on the 2.5 GHz carrier at a distance of 5 m with $\sigma^2_{\text{err}} = 1$.

The results show that for smaller values of α, the FDP-SIP and FDP-SIT algorithms provide the best performance. When α is small, an increased sum-rate is achieved by effectively trading-off between the maximization of the forward and minimization of the

self-interference channels. As such, the FDP-SIP algorithm is able to more effectively balance between them, due to the fact that it does not apply an approximation to its objective function. Likewise, the bisection search of the FDP-SIT algorithm is able to effectively adjust the self-interference threshold value to more effectively balance between them. Conversely, while the joint FDP-SCAMP algorithm attempts to maximize its sum-rate, it must overcome both the insufficient cancellation power (i.e., relatively small α) and the fact that its objective function is approximated.

As α increases, the FDP-SCAMP algorithm can more effectively take advantage of the additional cancellation power, and offers performance improvements over the other algorithms. Clearly, when α is sufficiently large, the separate FDP and joint FDP-SCAMP algorithms become equivalent (i.e., corresponding to $\alpha \geq 20$ dB, on average, in this scenario).

It is interesting to note that based on the simulation results shown in Section 4.10.1, the FDP-DC algorithm is a decreasing function of α, while based on the measured results the FDP-DC algorithm is an increasing function of α. This could be due to the fact that the measured data corresponds to transmission over a short distance (i.e., 5 m), while most of the simulation results assume more pessimistic $\mathrm{SIR}_{\mathrm{in}}$ values.

A convergence comparison of the various algorithms with respect to the final converged optimized HD sum-rate based on a particular realization is given in Fig. 4.10. The FDP-SIP approach required very few iterations to converge (typically ranging from three to six) and the FDP-SIT approach required many iterations for the nested bisection search to converge.

The FDP-SIT approach exhibits a step-like convergence, which is caused by the nested bisection search. In particular, for each fixed value of θ_1, the bisection search for θ_2 provides a monotonically increasing function until it begins to level-off; however, after each additional outer-loop iteration, the bisection search for θ_2 is re-initialized, often resulting in a sudden drop in rate followed by a monotonic increase until it levels-off once again. Due to the nested bisection search, the FDP-SIT approach requires many iterations to converge.

Table 4.1 shows the average number of iterations until convergence for each algorithm (while varying α from 15 dB to 22 dB over multiple realizations). Note that objective function convergence is specified in terms of the number of iterations required for the algorithm's objective function to converge, while sum-rate convergence is specified in terms of the number of iterations required for the algorithm's sum-rate to converge. In either case,

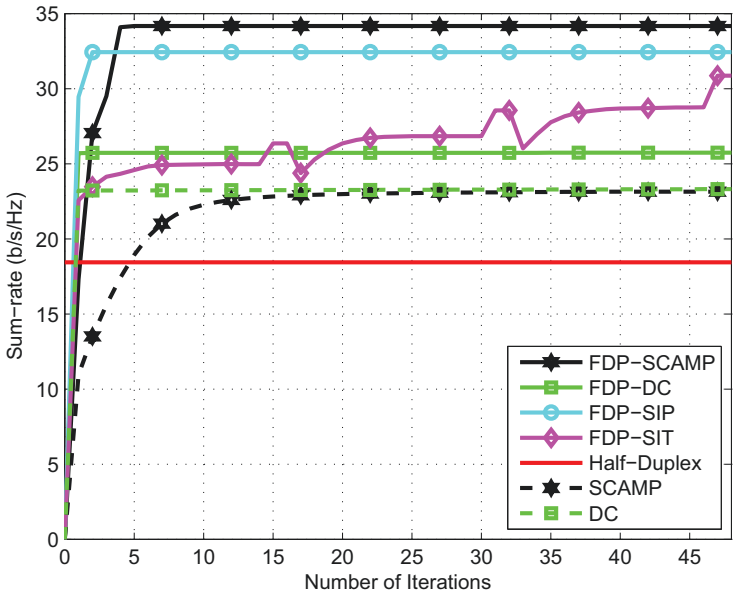

Fig. 4.10 MIMO point-to-point convergence comparison using measured data on the 2.5 GHz carrier at a distance of 5 m with $\alpha = 19$ dB and $\sigma^2_{\text{err}} = 1$.

convergence was defined as when the percentage change between two consecutive iterations was less than 1e-4 (e.g., for the objective function case: $|(f^{(\nu)} - f^{(\nu-1)})/f^{(\nu-1)}| <$ 1e-4, where $f^{(\nu)}$ is the objective function value at the ν-th iteration).

The results show that the FDP-SIP algorithm converges much faster than the other algorithms, on average. It is interesting to note that based on the 2x2 MIMO point-to-point measured data on the 2.5 GHz carrier at a distance of 5 m, the FDP-SIP algorithm provides a very competitive sum-rate while operating at a very low computational complexity and requiring very few iterations to converge.

However, the results of Section 4.10.1 show that the FDP-SCAMP algorithm can provide significant performance gains over the FDP-SIP algorithm in many scenarios. More measured data-based scenarios (e.g., at longer distances, more antennas) need to be explored to better compare the FDP-SIP and FDP-SCAMP algorithms and to see what types of performance benefits the FDP-SCAMP can provide in those environments.

Table 4.1 Average number of iterations until convergence for each algorithm for the 2x2 MIMO point-to-point measured data on the 2.5 GHz carrier at a distance of 5 m with $\sigma^2_{\text{err}} = 1$.

Algorithm	Average Number of Iterations	
	Objective Function Convergence	Sum-Rate Convergence
FDP-SCAMP	70.2	57.1
FDP-DC	219.8	19.3
FDP-SIP	3.8	3.8
FDP-SIT	290.0	289.6
SCAMP	37.6	38.8
DC	299.0	52.4

4.11 Concluding Remarks

This chapter presented a full-duplex precoding transceiver structure which applies joint precoding to control the forward channel precoding and the self-interference cancellation. The new MIMO-OFDM FDP structure allows for different algorithms and optimization objectives to be developed rather than just the typical self-interference minimization. In particular, separate and joint sum-rate maximization design algorithms are proposed. The separate FDP algorithm is similar to a typical adaptive self-interference canceller, where here the cancellation is done by precoding rather than a self-interference replica generator. The joint FDP-SCAMP algorithm make use of sequential convex programming.

This chapter also presented the SIP and SIT (respectively, FDP-SIP and FDP-SIT) algorithms for the FD MIMO point-to-point scenario. The SIP-based algorithms apply a utility-function based approach to avoid the non-convex optimization problem. The SIT-based approaches simplify the non-convex optimization problem by introducing a maximum interference threshold constraint which convexifies the optimization problem. A nested bisection search is performed as part of an outer-loop to optimize the choice of threshold values.

It is shown both analytically and through extensive simulations that when there is sufficient cancellation power at the transceiver (i.e., α is sufficiently large), the separate and joint designs offer a similar sum-rate performance; however, when the amount of cancellation power is limited, the joint approach can provide significant performance improvements.

The simulation results showed that FDP-SCAMP provides between 1.6 and 1.8 times

the spectral efficiency of optimized HD for many of the tested FD MIMO point-to-point scenarios. In conclusion, extensive simulation results using both standard channel models and measured data show that the proposed FDP structure and corresponding algorithms can provide very significant sum-rate improvements over optimized HD for MIMO point-to-point systems.

Chapter 5

Full-Duplex MIMO Point-to-Multi-Point Precoding[1]

5.1 Introduction

Chapter 4 considers precoding design for FD MIMO point-to-point (i.e., FD SU-MIMO) systems. This chapter focuses on precoding design for sum-rate maximization while considering the effects of residual self-interference for FD MIMO point-to-multi-point (i.e., FD MU-MIMO) systems. The FD MIMO point-to-multi-point system presented in this chapter is applicable to the cases of FD UEs, HD UEs, and mixed FD/HD UEs.

The FD MIMO point-to-multi-point system with HD UEs in this chapter generalizes the system model used for precoding design in [67,68]. In particular, while the configuration is similar, the environment is different and more realistic since we include the interference from uplink transmission to downlink UEs. Furthermore, we consider the effects of imperfect channel knowledge. The FD MIMO point-to-multi-point problem formulation leads to a non-convex matrix-variable optimization problem, where we consider two SCP approaches to develop efficient sum-rate maximization algorithms.

The first algorithm takes advantage of the DC structure of the non-convex optimization problem by directly looking at the objective function decomposition. The form of the original objective function naturally lends itself to this choice of DC decomposition. In particular, the MIMO point-to-multi-point DC-based algorithm derived in this chapter

[1]Parts of Chapter 5 have been accepted to be published in the IEEE Transactions on Vehicular Technology [103] and submitted for publication to the IEEE Transactions on Wireless Communications [93].

generalizes the joint precoding scheme presented in [67] and the FD MIMO point-to-point DC-based algorithm presented in Chapter 4, which can be recovered as special cases.

The second algorithm called Sequential Convex Approximations for Matrix-variable Programming (SCAMP) is developed for solving general non-convex matrix-variable optimization problems with logarithmic objective functions. In this chapter, we apply the SCAMP algorithm to FD MIMO point-to-multi-point systems. The SCAMP algorithm approximates the non-convex objective function by first applying a lower-bound and then applying an upper-bound on one of the terms in the lower-bound. The result is a non-convex approximation of the original non-convex objective function. First-order approximations are applied to the non-convex terms of the approximation function in order to ensure that the approximate objective function satisfies the Disciplined Convex Programming (DCP) ruleset [104]. The FD MIMO point-to-point SCAMP algorithm presented in Chapter 4 can be recovered as a special case.

Finally, analytical expressions for the loss in sum-rate incurred due to the effect of the residual self-interference are derived. The residual self-interference results due to the effects of imperfect channel knowledge.

The illustrative results in this chapter consider a wireless cellular environment. Chapter 4 only considers FD point-to-point systems, whereas in this chapter, we focus on FD point-to-multi-point systems, where a FD BS services UEs which can operate in either HD or FD mode. In particular, the point-to-multi-point system with a FD BS and HD UEs has very practical applications, specifically to cellular systems. For such systems it is beneficial to let the MSs operate in HD mode. Specifically, it is very rare that the MS uses the whole frequency allocated to the system and requiring FD UEs provides significantly more challenges from both a design and an implementation perspective. Conversely, it is quite feasible to consider BSs operating in FD mode while using its antennas to serve various HD users. The illustrative results demonstrate the effectiveness of the proposed SCP algorithms for FD MIMO point-to-multi-point systems, while exploring the effects with and without the FDP structure presented in Chapter 4.

5.2 System Model

This section presents the FD MIMO point-to-multi-point system model which is applicable to FD MIMO point-to-multi-point systems with HD, FD, or mixed FD/HD UEs.

5.2.1 Full-Duplex MIMO Point-to-Multi-Point System with HD UEs

The FD MU-MIMO system, shown in Fig. 5.1, is a point-to-multi-point system with a FD MIMO BS serving a number of HD UEs. Let the number of downlink UEs be K_{DL} and the number of uplink UEs be K_{UL}. It is assumed that each of the UEs are equipped with $N_{\mathrm{UE},T}$ transmit and $N_{\mathrm{UE},R}$ receive antennas, respectively. Hence, it is assumed that the BS is equipped with $N_{\mathrm{BS},T} = K_{\mathrm{DL}}N_{\mathrm{UE},R}$ transmit and $N_{\mathrm{BS},R} = K_{\mathrm{UL}}N_{\mathrm{UE},T}$ receive antennas, respectively.[2]

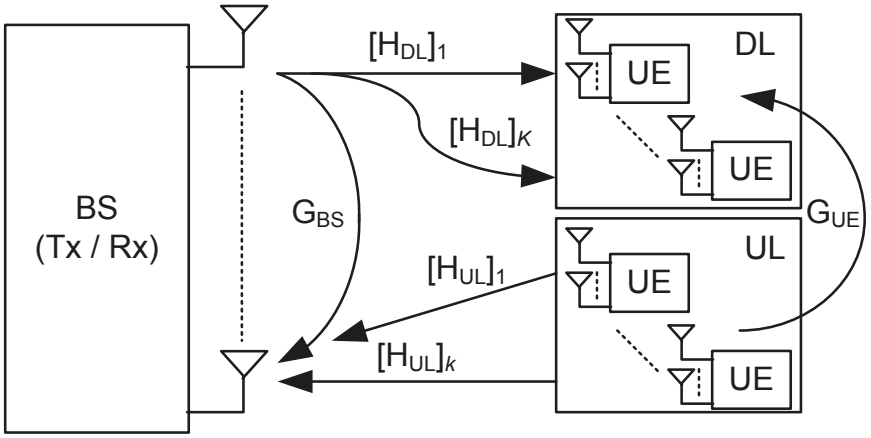

Fig. 5.1 Full-duplex MIMO point-to-multi-point system with HD UEs.

The received signal at the BS can be written as:

$$\mathbf{y}_{\mathrm{BS}} = \sum_{u\in\mathcal{I}_{\mathcal{U}}} [\mathbf{H}_{\mathrm{UL}}]_u \mathbf{V}_{\mathrm{UE},u}\mathbf{x}_{\mathrm{UE},u} + \sum_{k\in\mathcal{I}_{\mathcal{D}}} \mathbf{G}_{\mathrm{BS}}\mathbf{V}_{\mathrm{BS},k}\mathbf{x}_{\mathrm{BS},k} + \mathbf{z}_{\mathrm{BS}}, \tag{5.1}$$

where $\mathcal{I}_{\mathcal{U}}$ denotes the set of uplink UEs, $\mathcal{I}_{\mathcal{D}}$ denotes the set of downlink UEs, $[\mathbf{H}_{\mathrm{UL}}]_u \in \mathbb{C}^{N_{\mathrm{BS},R}\times N_{\mathrm{UE},T}}$ is the channel matrix from the u-th UE to the BS, $\mathbf{V}_{\mathrm{UE},u} \in \mathbb{C}^{N_{\mathrm{UE},T}\times N_{\mathrm{UE},T}}$ is the precoding matrix for the u-th UE, $\mathbf{x}_{\mathrm{UE},u} \in \mathbb{C}^{N_{\mathrm{UE},T}\times 1}$ vector of uplink data symbols for the u-th UE, $\mathbf{G}_{\mathrm{BS}} \in \mathbb{C}^{N_{\mathrm{BS},R}\times N_{\mathrm{BS},T}}$ is the BS self-interference matrix, $\mathbf{V}_{\mathrm{BS},k} \in \mathbb{C}^{N_{\mathrm{BS},T}\times N_{\mathrm{BS},T}}$ is the precoding matrix for the k-th user at the BS, $\mathbf{x}_{\mathrm{BS},k} \in \mathbb{C}^{N_{\mathrm{BS},T}\times 1}$ vector of transmitted symbols from the BS to the k-th UE, and $\mathbf{z}_{\mathrm{BS}} \in \mathbb{C}^{N_{\mathrm{BS},R}\times 1}$ is the additive white Gaussian noise.

[2]This assumption implies that the scheduling has been previously completed.

Similarly, the received signal at the k-th UE ($k \in \mathcal{I}_{\mathcal{D}}$) can be written as:

$$\mathbf{y}_k = [\mathbf{H}_{\mathrm{DL}}]_k \mathbf{V}_{\mathrm{BS},k} \mathbf{x}_{\mathrm{BS},k} + \sum_{l \in \mathcal{I}_{\mathcal{D}} \setminus \{k\}} [\mathbf{H}_{\mathrm{DL}}]_k \mathbf{V}_{\mathrm{BS},l} \mathbf{x}_{\mathrm{BS},l} + \sum_{u \in \mathcal{I}_{\mathcal{U}}} [\mathbf{G}_{\mathrm{UE}}]_{k,u} \mathbf{V}_{\mathrm{UE},u} \mathbf{x}_{\mathrm{UE},u} + \mathbf{z}_k, \tag{5.2}$$

where $[\mathbf{H}_{\mathrm{DL}}]_k \in \mathbb{C}^{N_{\mathrm{UE},R} \times N_{\mathrm{BS},T}}$ is the channel matrix from the BS to the k-th UE, $[\mathbf{G}_{\mathrm{UE}}]_{k,u} \in \mathbb{C}^{N_{\mathrm{UE},R} \times N_{\mathrm{UE},T}}$ is the interference matrix from the u-th uplink UE to the k-th downlink UE, and $\mathbf{z}_k \in \mathbb{C}^{N_{\mathrm{UE},R} \times 1}$ is the additive white Gaussian noise. Note that it is assumed that $k \in \mathcal{I}_{\mathcal{D}}$.

Hence, the downlink sum-rate can be written as:

$$R_{\mathrm{DL}} = \sum_{k \in \mathcal{I}_{\mathcal{D}}} \log_2 \left| \mathbf{I}_{N_{\mathrm{UE},R}} + \left(\mathbf{\Sigma}_k + \tilde{\mathbf{C}}_{\mathrm{DL},k} \right)^{-1} \mathbf{C}_{\mathrm{DL},k} \right|,$$

where $\mathbf{\Sigma}_k = E[\mathbf{z}_k \mathbf{z}_k^{\dagger}]$, $\tilde{\mathbf{C}}_{\mathrm{DL},k}$ and $\mathbf{C}_{\mathrm{DL},k}$ are the downlink receive covariance matrices for the interference and direct channels, respectively, defined as:

$$\begin{aligned} \mathbf{C}_{\mathrm{DL},k} &= [\mathbf{H}_{\mathrm{DL}}]_k \mathbf{Q}_{\mathrm{BS},k} [\mathbf{H}_{\mathrm{DL}}]_k^{\dagger}, \\ \tilde{\mathbf{C}}_{\mathrm{DL},k} &= \sum_{l \in \mathcal{I}_{\mathcal{D}} \setminus \{k\}} [\mathbf{H}_{\mathrm{DL}}]_k \mathbf{Q}_{\mathrm{BS},l} [\mathbf{H}_{\mathrm{DL}}]_k^{\dagger} + \sum_{u \in \mathcal{I}_{\mathcal{U}}} [\mathbf{G}_{\mathrm{UE}}]_{k,u} \mathbf{Q}_{\mathrm{UE},u} [\mathbf{G}_{\mathrm{UE}}]_{k,u}^{\dagger}, \end{aligned}$$

where the transmit covariance matrices $\mathbf{Q}_{\mathrm{BS},k}$ and $\mathbf{Q}_{\mathrm{UE},u}$ are defined as:

$$\begin{aligned} \mathbf{Q}_{\mathrm{BS},k} &= \mathbf{V}_{\mathrm{BS},k} \mathbf{S}_{\mathrm{BS},k} \mathbf{V}_{\mathrm{BS},k}^{\dagger}, \quad k \in \mathcal{I}_{\mathcal{D}}, \\ \mathbf{Q}_{\mathrm{UE},u} &= \mathbf{V}_{\mathrm{UE},u} \mathbf{S}_{\mathrm{UE},u} \mathbf{V}_{\mathrm{UE},u}^{\dagger}, \quad u \in \mathcal{I}_{\mathcal{U}}, \end{aligned}$$

where $\mathbf{S}_{\mathrm{BS},k} = E[\mathbf{x}_{\mathrm{BS},k} \mathbf{x}_{\mathrm{BS},k}^{\dagger}]$ and $\mathbf{S}_{\mathrm{UE},u} = E[\mathbf{x}_{\mathrm{UE},u} \mathbf{x}_{\mathrm{UE},u}^{\dagger}]$. Similarly, the uplink sum-rate can be written as:

$$R_{\mathrm{UL}} = \log_2 \left| \mathbf{I}_{N_{\mathrm{BS},R}} + \left(\mathbf{\Sigma}_{\mathrm{BS}} + \tilde{\mathbf{C}}_{\mathrm{UL}} \right)^{-1} \mathbf{C}_{\mathrm{UL}} \right|,$$

where $\mathbf{\Sigma}_{\mathrm{BS}} = E[\mathbf{z}_{\mathrm{BS}} \mathbf{z}_{\mathrm{BS}}^{\dagger}]$, $\tilde{\mathbf{C}}_{\mathrm{UL}}$ and $\mathbf{C}_{\mathrm{UL}}$ are the uplink receive covariance matrices for the

interference and direct channels, respectively, defined as:

$$\mathbf{C}_{\mathrm{UL}} = \sum_{u \in \mathcal{I}_{\mathcal{U}}} [\mathbf{H}_{\mathrm{UL}}]_u \mathbf{Q}_{\mathrm{UE},u} [\mathbf{H}_{\mathrm{UL}}]_u^{\dagger},$$
$$\tilde{\mathbf{C}}_{\mathrm{UL}} = \sum_{k \in \mathcal{I}_{\mathcal{D}}} \mathbf{G}_{\mathrm{BS}} \mathbf{Q}_{\mathrm{BS},k} \mathbf{G}_{\mathrm{BS}}^{\dagger}.$$

The self-interference channels, $\mathbf{G}_{\mathrm{BS}}$ and $\mathbf{G}_{\mathrm{UE}}$, are assumed to be estimated, while the forward channels, $\mathbf{H}_{\mathrm{DL}}$ and $\mathbf{H}_{\mathrm{UL}}$, are assumed to be known perfectly, in order to more easily compare with HD transmission. More specifically, it is assumed that:

$$\mathbf{G}_{\mathrm{BS}} = \hat{\mathbf{G}}_{\mathrm{BS}} + \Delta\mathbf{G}_{\mathrm{BS}},$$
$$\mathbf{G}_{\mathrm{UE}} = \hat{\mathbf{G}}_{\mathrm{UE}} + \Delta\mathbf{G}_{\mathrm{UE}},$$

where $\mathbf{G}_{\mathrm{BS}}$ and $\mathbf{G}_{\mathrm{UE}}$ are the true channel matrices, $\hat{\mathbf{G}}_{\mathrm{BS}}$ and $\hat{\mathbf{G}}_{\mathrm{UE}}$ are the estimated channel matrices, and $\Delta\mathbf{G}_{\mathrm{BS}}$ and $\Delta\mathbf{G}_{\mathrm{UE}}$ are the channel estimation error matrices, with zero mean and variance σ_{err}^2. Similarly, $\hat{R}_{\mathrm{DL}}$ and $\hat{R}_{\mathrm{UL}}$ are the estimates of R_{DL} and R_{UL} and are defined as:

$$\hat{R}_{\mathrm{DL}} = \sum_{k \in \mathcal{I}_{\mathcal{D}}} \log_2 \left| \mathbf{I}_{N_{\mathrm{UE},R}} + \left(\mathbf{\Sigma}_k + \hat{\mathbf{C}}_{\mathrm{DL},k} \right)^{-1} \mathbf{C}_{\mathrm{DL},k} \right|,$$
$$\hat{R}_{\mathrm{UL}} = \log_2 \left| \mathbf{I}_{N_{\mathrm{BS},R}} + \left(\mathbf{\Sigma}_{\mathrm{BS}} + \hat{\mathbf{C}}_{\mathrm{UL}} \right)^{-1} \mathbf{C}_{\mathrm{UL}} \right|,$$

where $\hat{\mathbf{C}}_{\mathrm{DL},k}$ and $\hat{\mathbf{C}}_{\mathrm{UL}}$ are the estimates of the covariance matrices $\tilde{\mathbf{C}}_{\mathrm{DL},k}$ and $\tilde{\mathbf{C}}_{\mathrm{UL}}$, respectively, and are given by:

$$\hat{\mathbf{C}}_{\mathrm{DL},k} = \sum_{l \in \mathcal{I}_{\mathcal{D}} \setminus \{k\}} [\mathbf{H}_{\mathrm{DL}}]_k \mathbf{Q}_{\mathrm{BS},l} [\mathbf{H}_{\mathrm{DL}}]_k^{\dagger} + \sum_{u \in \mathcal{I}_{\mathcal{U}}} [\hat{\mathbf{G}}_{\mathrm{UE}}]_{k,u} \mathbf{Q}_{\mathrm{UE},u} [\hat{\mathbf{G}}_{\mathrm{UE}}]_{k,u}^{\dagger},$$
$$\hat{\mathbf{C}}_{\mathrm{UL}} = \sum_{k \in \mathcal{I}_{\mathcal{D}}} \hat{\mathbf{G}}_{\mathrm{BS}} \mathbf{Q}_{\mathrm{BS},k} \hat{\mathbf{G}}_{\mathrm{BS}}^{\dagger}.$$

The non-convex sum-rate maximization problem can be written as:

$$\begin{aligned} \max_{\substack{\mathbf{V}_{\mathrm{BS},k},\mathbf{V}_{\mathrm{UE},u},\\ k\in\mathcal{I}_{\mathcal{D}},\, u\in\mathcal{I}_{\mathcal{U}}}} \quad & \hat{R}_{\mathrm{DL}} + \hat{R}_{\mathrm{UL}} \\ \text{subject to:} \quad & \mathrm{Tr}\left[\mathbf{V}_{\mathrm{UE},u}\mathbf{S}_{\mathrm{UE},u}\mathbf{V}_{\mathrm{UE},u}^{\dagger}\right] \leq P_{\max,u},\ u\in\mathcal{I}_{\mathcal{U}} \\ & \sum_{k\in\mathcal{I}_{\mathcal{D}}} \mathrm{Tr}\left[\mathbf{V}_{\mathrm{BS},k}\mathbf{S}_{\mathrm{BS},k}\mathbf{V}_{\mathrm{BS},k}^{\dagger}\right] \leq P_{\max,\mathrm{BS}}. \end{aligned} \tag{5.3}$$

5.2.2 Full-Duplex MIMO Point-to-Multi-Point System with FD UEs

The FD MIMO point-to-multi-point system model with FD UEs is shown in Fig. 5.2. In this system, a FD BS services K FD UEs. The received signals at the BS and UEs are identical to that of (5.1) and (5.2), respectively, when $\mathcal{I}_{\mathcal{U}} = \mathcal{I}_{\mathcal{D}} = \{1,\ldots,K\}$. As such, the FD MIMO point-to-multi-point system with FD UEs can be recovered as a special case of the FD MIMO point-to-multi-point with HD UEs derivations provided in this chapter.

Furthermore, a system where the BS operates in FD-mode while some UEs operate in HD-mode and some UEs operate in FD-mode (i.e., a mixed HD/FD UE scenario) can also be recovered as a special case of the FD MIMO point-to-multi-point with HD UEs derivations provided in this chapter, where each FD UE is an element of the set $\mathcal{I}_{\mathcal{U}} \cap \mathcal{I}_{\mathcal{D}}$.

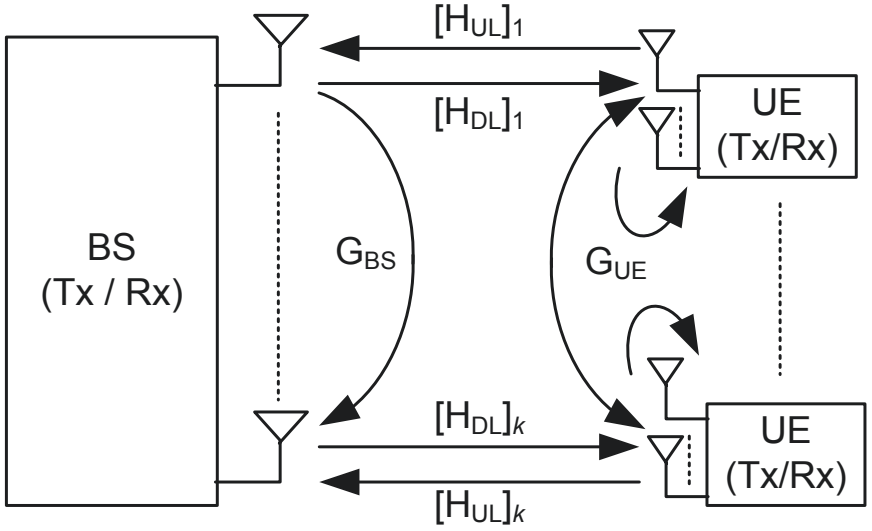

Fig. 5.2 Full-duplex MIMO point-to-multi-point system model with FD UEs.

5.2.3 Full-Duplex Precoding for MIMO Point-to-Multi-Point Systems

The FD MIMO point-to-multi-point system model using the FDP structure is very similar to the system model in Section 5.2.1, where the main differences are in terms of the dimensionality of the matrices involved. It is also assumed that the BS is equipped with $M = N_{\mathrm{BS,R}} = N_{\mathrm{BS,T}}$ physical antennas, where $M = K_{\mathrm{DL}} N_{\mathrm{UE},R} = K_{\mathrm{UL}} N_{\mathrm{UE},T}$.

Hence, when using the FDP structure, $[\mathbf{H}_{\mathrm{UL}}]_u \in \mathbb{C}^{M \times N_{\mathrm{UE},T}}$, $\mathbf{V}_{\mathrm{BS},k} \in \mathbb{C}^{2M \times M}$ is the FDP matrix for the k-th user at the BS, and $\mathbf{G}_{\mathrm{BS}} \in \mathbb{C}^{M \times 2M}$ is the FDP BS self-interference matrix which, as in Chapter 4, has the following form:

$$\mathbf{G}_{\mathrm{BS}} = \begin{bmatrix} \tilde{\mathbf{G}}_{\mathrm{BS},a} & \alpha \mathbf{I}_M \end{bmatrix},$$

where $\tilde{\mathbf{G}}_{\mathrm{BS},a} \in \mathbb{C}^{M \times M}$ and it is assumed that the paths are numbered such that the first M paths correspond to forward transmission, while the second M paths correspond to the auxiliary paths (i.e., the paths which are not transmitted). As in Section 4.2.4, $\tilde{\mathbf{G}}_{\mathrm{BS},a}$ is assumed to be estimated while α is assumed to be known perfectly since its exact effects can be measured off-line.

Similarly, $[\mathbf{H}_{\mathrm{DL}}]_k \in \mathbb{C}^{M \times 2M}$ is the FDP channel matrix from the BS to the k-th UE which has the following form:

$$[\mathbf{H}_{\mathrm{DL}}]_k = \begin{bmatrix} [\tilde{\mathbf{H}}_{\mathrm{DL}}]_k & \mathbf{0}_M \end{bmatrix},$$

where $[\tilde{\mathbf{H}}_{\mathrm{DL}}]_k \in \mathbb{C}^{M \times M}$ since it is assumed that the paths are numbered such that the first M paths correspond to forward transmission, while the second M paths correspond to the auxiliary paths (i.e., the paths which are not transmitted).

The transmission equations and sum-rate expressions are identical to those in Section 5.2.1 with these new definitions of $[\mathbf{H}_{\mathrm{DL}}]_k$ ($k \in \mathcal{I}_{\mathcal{D}}$) and $\mathbf{G}_{\mathrm{BS}}$ (with the corresponding appropriately sized matrices and vectors).

5.2.4 Full-Duplex MIMO Point-to-Multi-Point: Sum-Rate Maximization

Optimization problem (5.3) can be re-written as:

$$\max_{\substack{\mathbf{Q}_{\mathrm{BS},k},\mathbf{Q}_{\mathrm{UE},u},\\ k\in\mathcal{I}_{\mathcal{D}},\, u\in\mathcal{I}_{\mathcal{U}}}} \quad \hat{R}_{\mathrm{DL}} + \hat{R}_{\mathrm{UL}} \tag{5.4a}$$

$$\text{subject to:} \quad \mathrm{Tr}\left[\mathbf{Q}_{\mathrm{UE},u}\right] \leq P_{\max,u},\ u \in \mathcal{I}_{\mathcal{U}}, \tag{5.4b}$$

$$\sum_{k\in\mathcal{I}_{\mathcal{D}}} \mathrm{Tr}\left[\mathbf{Q}_{\mathrm{BS},k}\right] \leq P_{\max,\mathrm{BS}}, \tag{5.4c}$$

$$\mathbf{Q}_{\mathrm{BS},k} \succcurlyeq 0,\ k \in \mathcal{I}_{\mathcal{D}}, \tag{5.4d}$$

$$\mathbf{Q}_{\mathrm{UE},u} \succcurlyeq 0,\ u \in \mathcal{I}_{\mathcal{U}}, \tag{5.4e}$$

where the constraints on the transmit covariance matrices (i.e., (5.4d)-(5.4e)) to be positive semi-definite ensure the feasibility of the solution. Once optimization problem (5.4) is solved, the corresponding precoding matrices can be recovered using the Cholesky decomposition. In particular, $\mathbf{Q}_{\mathrm{UE},u} = \mathbf{L}_{\mathrm{UE},u}\mathbf{L}_{\mathrm{UE},u}^{\dagger}$, $\mathbf{Q}_{\mathrm{BS},k} = \mathbf{L}_{\mathrm{BS},k}\mathbf{L}_{\mathrm{BS},k}^{\dagger}$, and hence, the precoding matrices can be computed as:

$$\mathbf{V}_{\mathrm{UE},u} = \mathbf{L}_{\mathrm{UE},u}\mathbf{S}_{\mathrm{UE},u}^{-1/2}, \tag{5.5}$$

$$\mathbf{V}_{\mathrm{BS},k} = \mathbf{L}_{\mathrm{BS},k}\mathbf{S}_{\mathrm{BS},k}^{-1/2}. \tag{5.6}$$

This section presents the DC-based and SCAMP SCP algorithms for FD MIMO point-to-multi-point systems. As discussed in Section 5.2.2, the derivation applies to the cases of FD MIMO point-to-multi-point systems with HD UEs, FD UEs, and mixed FD/HD UEs. As well, the algorithms also generalize the DC-based and SCAMP algorithms for the FD MIMO point-to-point system, presented in Chapter 4, which can be recovered as a special case when $\mathcal{I}_{\mathcal{D}} = \mathcal{I}_{\mathcal{U}} = \{1\}$.

5.3 FD MIMO Point-to-Multi-Point: DC-Based Algorithm

This section presents the DC-based SCP algorithm for FD MIMO point-to-multi-point systems. As discussed in Section 5.2.2, the derivation applies to the cases of MIMO point-to-multi-point systems with HD UEs, FD UEs, and mixed FD/HD UEs. As well, the algorithm also generalizes the DC-based algorithm for the FD MIMO point-to-point system,

presented in Chapter 4, which can be recovered as a special case when $\mathcal{I}_{\mathcal{D}} = \mathcal{I}_{\mathcal{U}} = \{1\}$.

The DC-based algorithm applies SCP by writing the non-convex optimization problem as a DC (i.e., $f = g - h$, where g and h are convex) and applying a first-order approximation to h to make the objective function convex. The objective function lends itself naturally to a particular choice of DC decomposition. First, we re-write the objective function as a minimization problem:

$$\begin{aligned} \min_{\substack{\mathbf{Q}_{\mathrm{BS},k}, \mathbf{Q}_{\mathrm{UE},u}, \\ k \in \mathcal{I}_{\mathcal{D}},\, u \in \mathcal{I}_{\mathcal{U}}}} \quad & f \\ \text{subject to:} \quad & (5.4b) - (5.4e) \end{aligned} \tag{5.7}$$

where $f = -\hat{R}_{\mathrm{DL}} - \hat{R}_{\mathrm{UL}}$ and where $\hat{R}_{\mathrm{DL}}$ and $\hat{R}_{\mathrm{UL}}$ are the estimates of R_{DL} and R_{UL} and are defined in Section 5.2.1.

f is a non-convex function but can be written as a difference of convex functions by writing $-\hat{R}_{\mathrm{DL}}$ and $-\hat{R}_{\mathrm{UL}}$ as a difference of convex functions. $-\hat{R}_{\mathrm{DL}}$ can be re-written as:

$$\begin{aligned} -\hat{R}_{\mathrm{DL}} &= \sum_{k \in \mathcal{I}_{\mathcal{D}}} \log_2 \left| \mathbf{\Sigma}_k + \hat{\mathbf{C}}_{\mathrm{DL},k} \right| - \sum_{k \in \mathcal{I}_{\mathcal{D}}} \log_2 \left| \mathbf{\Sigma}_k + \hat{\mathbf{C}}_{\mathrm{DL},k} + \mathbf{C}_{\mathrm{DL},k} \right| \\ &= g_{\mathrm{DL}} - h_{\mathrm{DL}} \end{aligned}$$

where g_{DL} and h_{DL} are defined as follows:

$$g_{\mathrm{DL}} = -\sum_{k \in \mathcal{I}_{\mathcal{D}}} \log_2 \left| \mathbf{\Sigma}_k + \sum_{l \in \mathcal{I}_{\mathcal{D}}} [\mathbf{H}_{\mathrm{DL}}]_k \mathbf{Q}_{\mathrm{BS},l} [\mathbf{H}_{\mathrm{DL}}]_k^{\dagger} + \sum_{u \in \mathcal{I}_{\mathcal{U}}} [\hat{\mathbf{G}}_{\mathrm{UE}}]_{k,u} \mathbf{Q}_{\mathrm{UE},u} [\hat{\mathbf{G}}_{\mathrm{UE}}]_{k,u}^{\dagger} \right|,$$

$$h_{\mathrm{DL}} = -\sum_{k \in \mathcal{I}_{\mathcal{D}}} \log_2 \left| \mathbf{\Sigma}_k + \sum_{l \in \mathcal{I}_{\mathcal{D}} \setminus \{k\}} [\mathbf{H}_{\mathrm{DL}}]_k \mathbf{Q}_{\mathrm{BS},l} [\mathbf{H}_{\mathrm{DL}}]_k^{\dagger} + \sum_{u \in \mathcal{I}_{\mathcal{U}}} [\hat{\mathbf{G}}_{\mathrm{UE}}]_{k,u} \mathbf{Q}_{\mathrm{UE},u} [\hat{\mathbf{G}}_{\mathrm{UE}}]_{k,u}^{\dagger} \right|,$$

where both g_{DL} and h_{DL} are convex (since $\log |\mathbf{X}|$ is concave for $\mathbf{X} \succcurlyeq 0$, $|\mathbf{X}| \neq 0$); however, their difference, $-\hat{R}_{\mathrm{DL}}$, is not. Similarly, $-\hat{R}_{\mathrm{UL}}$ can be re-written as:

$$-\hat{R}_{\mathrm{UL}} = g_{\mathrm{UL}} - h_{\mathrm{UL}},$$

where g_{UL} and h_{UL} are defined as follows:

$$g_{\mathrm{UL}} = -\log_2 \left| \mathbf{\Sigma}_{\mathrm{BS}} + \sum_{l \in \mathcal{I}_{\mathcal{D}}} \hat{\mathbf{G}}_{\mathrm{BS}} \mathbf{Q}_{\mathrm{BS},l} \hat{\mathbf{G}}_{\mathrm{BS}}^{\dagger} + \sum_{u \in \mathcal{I}_{\mathcal{U}}} [\mathbf{H}_{\mathrm{UL}}]_u \mathbf{Q}_{\mathrm{UE},u} [\mathbf{H}_{\mathrm{UL}}]_u^{\dagger} \right|$$

$$h_{\mathrm{UL}} = -\log_2 \left| \mathbf{\Sigma}_{\mathrm{BS}} + \sum_{k \in \mathcal{I}_{\mathcal{D}}} \hat{\mathbf{G}}_{\mathrm{BS}} \mathbf{Q}_{\mathrm{BS,k}} \hat{\mathbf{G}}_{\mathrm{BS}}^{\dagger} \right|,$$

where both g_{UL} and h_{UL} are convex; however, their difference, $-\hat{R}_{\mathrm{UL}}$, is not.

Hence, f can be written as a difference of convex functions, $f = g - h$, where

$$g = g_{\mathrm{DL}} + g_{\mathrm{UL}} \tag{5.8}$$

$$h = h_{\mathrm{DL}} + h_{\mathrm{UL}}. \tag{5.9}$$

On the ν-th iteration, the DC-based algorithm approximates f by $\tilde{f}_{\mathrm{MU-DC}}(\nu) = g - \tilde{h}(\nu)$, where $\tilde{h}(\nu)$ is the first-order Taylor's series approximation [105, p. 69] of h corresponding to the ν-th iteration. The first-order Taylor's series approximation for the function $\log_2 |\mathbf{A}+\mathbf{X}|$ is given by (5.10):

$$\log_2 |\mathbf{A} + \mathbf{X}| \geq \log_2 |\mathbf{A} + \mathbf{X}_0| + \frac{1}{\ln(2)} \mathrm{Tr}\left[(\mathbf{A} + \mathbf{X}_0)^{-1} (\mathbf{X} - \mathbf{X}_0) \right]. \tag{5.10}$$

Hence, $\tilde{h}(\nu)$ can be written as:

$$\tilde{h}(\nu) = \tilde{h}_{\mathrm{DL}}(\nu) + \tilde{h}_{\mathrm{UL}}(\nu), \tag{5.11}$$

where the expressions for $\tilde{h}_{\mathrm{DL}}(\nu)$ and $\tilde{h}_{\mathrm{UL}}(\nu)$ are obtained by applying (5.10) to h_{DL} and h_{UL}, respectively, centered around the point $\left(\mathbf{Q}_{\mathrm{BS},k}^{(\nu)}, \mathbf{Q}_{\mathrm{UE},u}^{(\nu)} \right)$ for $k \in \mathcal{I}_{\mathcal{D}}$ and $u \in \mathcal{I}_{\mathcal{U}}$, where the superscript (ν) refers to the covariance matrix associated with the ν-th iteration, and

are given by:

$$\tilde{h}_{\mathrm{DL}}(\nu) = \sum_{k\in\mathcal{I}_{\mathcal{D}}} \mathrm{Tr}\left[\frac{\left(\mathbf{\Omega}_{\mathrm{DL},k}(\nu)\right)^{-1}}{\ln(2)} \sum_{u\in\mathcal{I}_{\mathcal{U}}} [\hat{\mathbf{G}}_{\mathrm{UE}}]_{k,u}\left(\mathbf{Q}_{\mathrm{UE},u} - \mathbf{Q}_{\mathrm{UE},u}^{(\nu)}\right)[\hat{\mathbf{G}}_{\mathrm{UE}}]_{k,u}^{\dagger}\right]$$
$$+ \sum_{k\in\mathcal{I}_{\mathcal{D}}} \mathrm{Tr}\left[\frac{\left(\mathbf{\Omega}_{\mathrm{DL},k}(\nu)\right)^{-1}}{\ln(2)} \sum_{l\in\mathcal{I}_{\mathcal{D}}\backslash\{k\}} [\mathbf{H}_{\mathrm{DL}}]_k \left(\mathbf{Q}_{\mathrm{BS},l} - \mathbf{Q}_{\mathrm{BS},l}^{(\nu)}\right)[\mathbf{H}_{\mathrm{DL}}]_k^{\dagger}\right] - \sum_{k\in\mathcal{I}_{\mathcal{D}}} \log_2\left|\mathbf{\Omega}_{\mathrm{DL},k}(\nu)\right|,$$

$$\tilde{h}_{\mathrm{UL}}(\nu) = -\log_2\left|\mathbf{\Omega}_{\mathrm{UL}}(\nu)\right| - \mathrm{Tr}\left[\frac{\left(\mathbf{\Omega}_{\mathrm{UL}}(\nu)\right)^{-1}}{\ln(2)} \sum_{k\in\mathcal{I}_{\mathcal{D}}} \hat{\mathbf{G}}_{\mathrm{BS}}\left(\mathbf{Q}_{\mathrm{BS,k}} - \mathbf{Q}_{\mathrm{BS,k}}^{(\nu)}\right)\hat{\mathbf{G}}_{\mathrm{BS}}^{\dagger}\right],$$

and where $\mathbf{\Omega}_{\mathrm{DL},k}(\nu)$ and $\mathbf{\Omega}_{\mathrm{UL}}(\nu)$ are given by:

$$\mathbf{\Omega}_{\mathrm{DL},k}(\nu) = \mathbf{\Sigma}_k + \sum_{l\in\mathcal{I}_{\mathcal{D}}\backslash\{k\}} [\mathbf{H}_{\mathrm{DL}}]_k \mathbf{Q}_{\mathrm{BS},l}^{(\nu)} [\mathbf{H}_{\mathrm{DL}}]_k^{\dagger} + \sum_{u\in\mathcal{I}_{\mathcal{U}}} [\hat{\mathbf{G}}_{\mathrm{UE}}]_{k,u} \mathbf{Q}_{\mathrm{UE},u}^{(\nu)} [\hat{\mathbf{G}}_{\mathrm{UE}}]_{k,u}^{\dagger},$$
$$\mathbf{\Omega}_{\mathrm{UL}}(\nu) = \mathbf{\Sigma}_{\mathrm{BS}} + \sum_{l\in\mathcal{I}_{\mathcal{D}}} \hat{\mathbf{G}}_{\mathrm{BS}} \mathbf{Q}_{\mathrm{BS,l}}^{(\nu)} \hat{\mathbf{G}}_{\mathrm{BS}}^{\dagger}.$$

$\tilde{f}_{\mathrm{MU-DC}}(\nu)$ is a convex function since it is the difference between a convex function, g, and an affine function, $\tilde{h}(\nu)$. As such, the non-convex optimization problem (5.7) can be locally approximated, around the point $\left(\mathbf{Q}_{\mathrm{BS},k}^{(\nu)}, \mathbf{Q}_{\mathrm{UE},u}^{(\nu)}\right)$ for $k \in \mathcal{I}_{\mathcal{D}}$ and $u \in \mathcal{I}_{\mathcal{U}}$, by convex optimization problem (5.12).

$$\begin{aligned} \min_{\substack{\mathbf{Q}_{\mathrm{BS},k}, \mathbf{Q}_{\mathrm{UE},u}, \\ k\in\mathcal{I}_{\mathcal{D}},\, u\in\mathcal{I}_{\mathcal{U}}}} \quad & \tilde{f}_{\mathrm{MU-DC}}(\nu) \\ \text{subject to:} \quad & (5.4b) - (5.4e) \end{aligned} \tag{5.12}$$

The DC-based algorithm is described in Algorithm 5.1. A sequence of convex semi-definite programming optimization problems are solved where the objective function is updated for each iteration to locally approximate the original non-convex optimization problem. Note that each convex sub-problem can be solved using cvx [98,99]. Convergence to a local optimum is guaranteed since after each iteration the objective function is non-increasing and the optimization problem is bounded below (i.e., the negative of the total system sum-rate).

Algorithm 5.1: DC-based algorithm.

Randomly initialize $\mathbf{Q}_{\mathrm{BS},k}^{(0)},\ k \in \mathcal{I}_{\mathcal{D}}$;
Randomly initialize $\mathbf{Q}_{\mathrm{UE},u}^{(0)},\ u \in \mathcal{I}_{\mathcal{U}}$;
Initialize $\nu = 0$;
repeat
  Update $\tilde{h}$ using (5.11), around the point $\left(\mathbf{Q}_{\mathrm{BS},k}^{(\nu)}, \mathbf{Q}_{\mathrm{UE},u}^{(\nu)}\right),\ k \in \mathcal{I}_{\mathcal{D}},\ u \in \mathcal{I}_{\mathcal{U}}$;
  Update $\tilde{f}_{\mathrm{MU-DC}}(\nu) = g - \tilde{h}(\nu)$;
  Solve (5.12) for $\left(\mathbf{Q}_{\mathrm{BS},k}^{\star}, \mathbf{Q}_{\mathrm{UE},u}^{\star}\right),\ k \in \mathcal{I}_{\mathcal{D}},\ u \in \mathcal{I}_{\mathcal{U}}$;
  $\nu = \nu + 1$;
  Update $\mathbf{Q}_{\mathrm{UE},u}^{(\nu)} = \mathbf{Q}_{\mathrm{UE},u}^{\star},\ u \in \mathcal{I}_{\mathcal{U}}$;
  Update $\mathbf{Q}_{\mathrm{BS},k}^{(\nu)} = \mathbf{Q}_{\mathrm{BS},k}^{\star},\ k \in \mathcal{I}_{\mathcal{D}}$;
until $\tilde{f}_{\mathrm{MU-DC}}(\nu)$ *converges*;
Apply Cholesky decomposition: $\mathbf{Q}_{\mathrm{UE},u}^{\star} = \mathbf{L}_{\mathrm{UE},u}\mathbf{L}_{\mathrm{UE},u}^{\dagger}$;
Apply Cholesky decomposition: $\mathbf{Q}_{\mathrm{BS},k}^{\star} = \mathbf{L}_{\mathrm{BS},k}\mathbf{L}_{\mathrm{BS},k}^{\dagger}$;
Solve for $\mathbf{V}_{\mathrm{UE},u}$ using (5.5), $u \in \mathcal{I}_{\mathcal{U}}$;
Solve for $\mathbf{V}_{\mathrm{BS},k}$ using (5.6), $k \in \mathcal{I}_{\mathcal{D}}$;

5.3.1 FD MIMO Point-to-Multi-Point: SCAMP Algorithm

This section presents a scheme developed for solving general non-convex matrix-variable optimization problems with logarithmic objective functions applied to the FD MIMO point-to-multi-point scenario. The SCAMP algorithm results in an alternate objective function approximation to the DC-based algorithm. As discussed in Section 5.2.2, the derivation applies to the cases of MIMO point-to-multi-point systems with HD UEs, FD UEs, and mixed FD/HD UEs. As well, the algorithm also generalizes the SCAMP algorithm for the FD MIMO point-to-point system, presented in Chapter 4, which can be recovered as a special case when $\mathcal{I}_{\mathcal{D}} = \mathcal{I}_{\mathcal{U}} = \{1\}$.

The SCAMP approximation is derived by combining the first-order Taylor's approximations [105, p. 69] of the functions $\log_2|\mathbf{A}+\mathbf{X}|$, given by (5.10), and $\log_2|\mathbf{X}|$, which can be expressed as:

$$\log_2|\mathbf{X}| \geq \log_2|\mathbf{X}_0| + \frac{1}{\ln(2)}\mathrm{Tr}\left[\mathbf{X}_0^{-1}\left(\mathbf{X}-\mathbf{X}_0\right)\right]. \tag{5.13}$$

The inverse of a sum of two matrices can be written as [106]:

$$(\mathbf{A}+\mathbf{X}_0)^{-1} = \mathbf{X}_0^{-1} - \mathbf{X}_0^{-1}\left(\mathbf{I}+\mathbf{A}\mathbf{X}_0^{-1}\right)^{-1}\mathbf{A}\mathbf{X}_0^{-1}. \tag{5.14}$$

Hence, substituting (5.14) into (5.10) gives:

$$\begin{aligned}\log_2|\mathbf{A}+\mathbf{X}| \geq \log_2|\mathbf{A}+\mathbf{X}_0| + \tfrac{1}{\ln(2)}\mathrm{Tr}\left[\mathbf{X}_0^{-1}(\mathbf{X}-\mathbf{X}_0)\right] \\ - \tfrac{1}{\ln(2)}\mathrm{Tr}\left[\mathbf{X}_0^{-1}\left(\mathbf{I}+\mathbf{A}\mathbf{X}_0^{-1}\right)^{-1}\mathbf{A}\mathbf{X}_0^{-1}(\mathbf{X}-\mathbf{X}_0)\right].\end{aligned} \tag{5.15}$$

Next, by substituting for the common term $\mathrm{Tr}\left[\mathbf{X}_0^{-1}(\mathbf{X}-\mathbf{X}_0)\right]$, (5.13) and (5.15) can be combined to give:

$$\log_2|\mathbf{A}+\mathbf{X}| \approx \log_2|\mathbf{X}| - \tfrac{1}{\ln(2)}\mathrm{Tr}\left[\mathbf{\Phi}\mathbf{X}\right] + \beta, \tag{5.16}$$

where Φ and β are given by:

$$\mathbf{\Phi} = \mathbf{X}_0^{-1}\left(\mathbf{I}+\mathbf{A}\mathbf{X}_0^{-1}\right)^{-1}\mathbf{A}\mathbf{X}_0^{-1}, \tag{5.17}$$

$$\beta = \log_2|\mathbf{A}+\mathbf{X}_0| + \tfrac{1}{\ln(2)}\mathrm{Tr}\left[\mathbf{X}_0^{-1}\left(\mathbf{I}+\mathbf{A}\mathbf{X}_0^{-1}\right)^{-1}\mathbf{A}\right] - \log_2|\mathbf{X}_0|. \tag{5.18}$$

The following definitions will assist in the derivation of the FD MIMO point-to-multi-point SCAMP algorithm.

$$\mathbf{\Upsilon}_{\mathrm{DL},k} = \mathbf{\Sigma}_k + \hat{\mathbf{C}}_{\mathrm{DL},k}, \tag{5.19}$$

$$\mathbf{\Upsilon}_{\mathrm{UL}} = \mathbf{\Sigma}_{\mathrm{BS}} + \hat{\mathbf{C}}_{\mathrm{UL}}, \tag{5.20}$$

where $\hat{\mathbf{C}}_{\mathrm{DL},k}$ and $\hat{\mathbf{C}}_{\mathrm{UL}}$ are defined as in Section 5.2.1 to be the estimates of $\tilde{\mathbf{C}}_{\mathrm{DL},k}$ and $\tilde{\mathbf{C}}_{\mathrm{UL}}$, respectively.

As well, $\mathbf{\Upsilon}_{\mathrm{DL},k}^{(\nu)}$, $\hat{\mathbf{C}}_{\mathrm{DL},k}^{(\nu)}$, $\mathbf{C}_{\mathrm{DL},k}^{(\nu)}$, $\mathbf{\Upsilon}_{\mathrm{UL}}^{(\nu)}$, $\hat{\mathbf{C}}_{\mathrm{UL}}^{(\nu)}$, and $\mathbf{C}_{\mathrm{UL}}^{(\nu)}$ refer to each respective expression evaluated at the point $\left(\mathbf{Q}_{\mathrm{BS},k}^{(\nu)}, \mathbf{Q}_{\mathrm{UE},u}^{(\nu)}\right)$ for $k \in \mathcal{I}_{\mathcal{D}}$ and $u \in \mathcal{I}_{\mathcal{U}}$, where ν refers to the covariance matrix associated with the ν-th iteration.

On the ν-th iteration, applying the SCAMP approximation, (5.16), to $\hat{R}_{\mathrm{DL}}$ gives the

following equation:

$$-\hat{R}_{\mathrm{DL}} \approx \sum_{k\in\mathcal{I}_{\mathcal{D}}} \left\{ \eta_{\mathrm{DL},k} + \varphi_{\mathrm{DL},k} + \tfrac{1}{\ln(2)} t_{\mathrm{DL},k} - \beta_{\mathrm{DL},k} \right\},$$

where $\beta_{\mathrm{DL},k}$ is defined as in (5.18) with $\mathbf{A}=\mathbf{I}$ and $\mathbf{X}_0 = \left(\boldsymbol{\Upsilon}_{\mathrm{DL},k}^{(\nu)}\right)^{-1} \mathbf{C}_{\mathrm{DL},k}^{(\nu)}$. As well, $\eta_{\mathrm{DL},k}$, $\varphi_{\mathrm{DL},k}$, and $t_{\mathrm{DL},k}$ are defined as follows:

$$\eta_{\mathrm{DL},k} = -\log_2 \left| \mathbf{C}_{\mathrm{DL},k} \right|, \tag{5.21}$$

$$\varphi_{\mathrm{DL},k} = \log_2 \left| \boldsymbol{\Upsilon}_{\mathrm{DL},k} \right|, \tag{5.22}$$

$$t_{\mathrm{DL},k} = \mathrm{Tr}\left[\boldsymbol{\Phi}_{\mathrm{DL},k} \boldsymbol{\Upsilon}_{\mathrm{DL},k}^{-1} \mathbf{C}_{\mathrm{DL},k} \right], \tag{5.23}$$

where $\boldsymbol{\Phi}_{\mathrm{DL},k}$ is given by (5.17) with $\mathbf{A}=\mathbf{I}$ and $\mathbf{X}_0 = \left(\boldsymbol{\Upsilon}_{\mathrm{DL},k}^{(\nu)}\right)^{-1} \mathbf{C}_{\mathrm{DL},k}^{(\nu)}$.

In order to ensure that the convex approximation to $-\hat{R}_{\mathrm{DL}}$ satisfies the DCP ruleset [104], on the ν-th iteration, $\varphi_{\mathrm{DL},k}$ and $t_{\mathrm{DL},k}$ were replaced by their respective first-order Taylor's series approximations. The Taylor's series approximations applied are given by (5.10) for $\varphi_{\mathrm{DL},k}$, and by (5.24) for $t_{\mathrm{DL},k}$.

$$\mathrm{Tr}\left[\mathbf{A}\mathbf{X}^{-1}\mathbf{Y}\right] \approx \mathrm{Tr}\left[\mathbf{A}\mathbf{X}_0^{-1}\mathbf{Y}_0\right] + \mathrm{Tr}\left[\left(\mathbf{A}\mathbf{X}_0^{-1}\right)^{\dagger}\left(\mathbf{Y}-\mathbf{Y}_0\right)\right] - \mathrm{Tr}\left[\left(\mathbf{X}_0^{-1}\mathbf{Y}_0\mathbf{A}\mathbf{X}_0^{-1}\right)^{\dagger}\left(\mathbf{X}-\mathbf{X}_0\right)\right], \tag{5.24}$$

which can be computed using the concept of matrix differentials [100, 101].

Hence, the Taylor's series approximations of $\varphi_{\mathrm{DL},k}$ and $t_{\mathrm{DL},k}$, on the ν-th iteration, centered around the point $\left(\mathbf{Q}_{\mathrm{BS},k}^{(\nu)}, \mathbf{Q}_{\mathrm{UE},u}^{(\nu)}\right)$, for $k \in \mathcal{I}_{\mathcal{D}}$ and $u \in \mathcal{I}_{\mathcal{U}}$, are denoted by $\tilde{\varphi}_{\mathrm{DL},k}(\nu)$ and $\tilde{t}_{\mathrm{DL},k}(\nu)$ and are given by (5.25) and (5.26), respectively.

$$\tilde{\varphi}_{\mathrm{DL},k}(\nu) = \log_2\left|\boldsymbol{\Upsilon}_{\mathrm{DL},k}^{(\nu)}\right| + \mathrm{Tr}\left[\frac{\left(\boldsymbol{\Upsilon}_{\mathrm{DL},k}^{(\nu)}\right)^{-1}}{\ln(2)}\left(\hat{\mathbf{C}}_{\mathrm{DL},k} - \hat{\mathbf{C}}_{\mathrm{DL},k}^{(\nu)}\right)\right], \tag{5.25}$$

$$\begin{aligned}\tilde{t}_{\mathrm{DL},k}(\nu) = t_{\mathrm{DL},k}^{(\nu)} &+ \mathrm{Tr}\left[\left(\boldsymbol{\Phi}_{\mathrm{DL},k}\left(\boldsymbol{\Upsilon}_{\mathrm{DL},k}^{(\nu)}\right)^{-1}\right)^{\dagger}\left(\mathbf{C}_{\mathrm{DL},k} - \mathbf{C}_{\mathrm{DL},k}^{(\nu)}\right)\right] \\ &- \mathrm{Tr}\left[\left(\left(\boldsymbol{\Upsilon}_{\mathrm{DL},k}^{(\nu)}\right)^{-1}\mathbf{C}_{\mathrm{DL},k}^{(\nu)}\boldsymbol{\Phi}_{\mathrm{DL},k}\left(\boldsymbol{\Upsilon}_{\mathrm{DL},k}^{(\nu)}\right)^{-1}\right)^{\dagger}\left(\hat{\mathbf{C}}_{\mathrm{DL},k} - \hat{\mathbf{C}}_{\mathrm{DL},k}^{(\nu)}\right)\right],\end{aligned} \tag{5.26}$$

where $t_{\mathrm{DL},k}^{(\nu)}$ refers to (5.23) evaluated at the point $\left(\mathbf{Q}_{\mathrm{BS},k}^{(\nu)}, \mathbf{Q}_{\mathrm{UE},u}^{(\nu)}\right)$, for $k \in \mathcal{I}_{\mathcal{D}}$ and $u \in \mathcal{I}_{\mathcal{U}}$.

Hence, on the ν-th iteration, the DCP approximation to $\hat{R}_{\mathrm{DL}}$, denoted by $\tilde{R}_{\mathrm{DL}}(\nu)$, is given by:

$$-\tilde{R}_{\mathrm{DL}}(\nu) = \sum_{k \in \mathcal{I}_{\mathcal{D}}} \left\{ \eta_{\mathrm{DL},k} + \tilde{\varphi}_{\mathrm{DL},k}(\nu) + \tfrac{1}{\ln(2)} \tilde{t}_{\mathrm{DL},k}(\nu) - \beta_{\mathrm{DL},k} \right\}, \tag{5.27}$$

where $\eta_{\mathrm{DL},k}$ is given by (5.21), $\tilde{\varphi}_{\mathrm{DL},k}(\nu)$ is given by (5.25), $\tilde{t}_{\mathrm{DL},k}(\nu)$ is given by (5.26), and $\beta_{\mathrm{DL},k}$ is given by (5.18) with $\mathbf{A} = \mathbf{I}$ and $\mathbf{X}_0 = \left(\boldsymbol{\Upsilon}_{\mathrm{DL},k}^{(\nu)}\right)^{-1} \mathbf{C}_{\mathrm{DL},k}^{(\nu)}$.

Similar to the downlink case, on the ν-th iteration, applying the SCAMP approximation, (5.16), to $\hat{R}_{\mathrm{UL}}$ gives the following equation:

$$-\hat{R}_{\mathrm{UL}} \approx \eta_{\mathrm{UL}} + \varphi_{\mathrm{UL}} + \tfrac{1}{\ln(2)} t_{\mathrm{UL}} - \beta_{\mathrm{UL}},$$

where β_{UL} is defined as in (5.18) with $\mathbf{A} = \mathbf{I}$ and $\mathbf{X}_0 = \left(\boldsymbol{\Upsilon}_{\mathrm{UL}}^{(\nu)}\right)^{-1} \mathbf{C}_{\mathrm{UL}}^{(\nu)}$. As well, η_{UL}, φ_{UL}, and t_{UL} are defined as follows:

$$\eta_{\mathrm{UL}} = -\log_2 \left| \mathbf{C}_{\mathrm{UL}} \right|, \tag{5.28}$$

$$\varphi_{\mathrm{UL}} = \log_2 \left| \boldsymbol{\Upsilon}_{\mathrm{UL}} \right|, \tag{5.29}$$

$$t_{\mathrm{UL}} = \mathrm{Tr}\left[\boldsymbol{\Phi}_{\mathrm{UL}} \boldsymbol{\Upsilon}_{\mathrm{UL}}^{-1} \mathbf{C}_{\mathrm{UL}} \right], \tag{5.30}$$

where $\boldsymbol{\Phi}_{\mathrm{UL}}$ is given by (5.17) with $\mathbf{A} = \mathbf{I}$ and $\mathbf{X}_0 = \left(\boldsymbol{\Upsilon}_{\mathrm{UL}}^{(\nu)}\right)^{-1} \mathbf{C}_{\mathrm{UL}}^{(\nu)}$.

Similar to the downlink case, on the ν-th iteration, in order to ensure that the convex approximation to $\hat{R}_{\mathrm{UL}}$ satisfies the DCP ruleset, φ_{UL} and t_{UL} were replaced by their respective first-order Taylor's series approximations.

$$\tilde{\varphi}_{\mathrm{UL}}(\nu) = \log_2 \left| \boldsymbol{\Upsilon}_{\mathrm{UL}}^{(\nu)} \right| + \tfrac{1}{\ln(2)} \mathrm{Tr}\left[\left(\boldsymbol{\Upsilon}_{\mathrm{UL}}^{(\nu)} \right)^{-1} \left(\hat{\mathbf{C}}_{\mathrm{UL}} - \hat{\mathbf{C}}_{\mathrm{UL}}^{(\nu)} \right) \right], \tag{5.31}$$

$$\begin{aligned} \tilde{t}_{\mathrm{UL}}(\nu) = t_{\mathrm{UL}}^{(\nu)} &+ \mathrm{Tr}\left[\left(\boldsymbol{\Phi}_{\mathrm{UL}} \left(\boldsymbol{\Upsilon}_{\mathrm{UL}}^{(\nu)} \right)^{-1} \right)^{\dagger} \left(\mathbf{C}_{\mathrm{UL}} - \mathbf{C}_{\mathrm{UL}}^{(\nu)} \right) \right] \\ &- \mathrm{Tr}\left[\left(\left(\boldsymbol{\Upsilon}_{\mathrm{UL}}^{(\nu)} \right)^{-1} \mathbf{C}_{\mathrm{UL}}^{(\nu)} \boldsymbol{\Phi}_{\mathrm{UL}} \left(\boldsymbol{\Upsilon}_{\mathrm{UL}}^{(\nu)} \right)^{-1} \right)^{\dagger} \left(\hat{\mathbf{C}}_{\mathrm{UL}} - \hat{\mathbf{C}}_{\mathrm{UL}}^{(\nu)} \right) \right], \end{aligned} \tag{5.32}$$

where $t_{\mathrm{UL}}^{(\nu)}$ is given by (5.30) evaluated at the point $\left(\mathbf{Q}_{\mathrm{BS},k}^{(\nu)}, \mathbf{Q}_{\mathrm{UE},u}^{(\nu)}\right)$, $k \in \mathcal{I}_{\mathcal{D}}, u \in \mathcal{I}_{\mathcal{U}}$.

Hence, on the ν-th iteration, the DCP approximation to $\hat{R}_{\mathrm{UL}}$, denoted by $\tilde{R}_{\mathrm{UL}}(\nu)$, is given by:

$$-\tilde{R}_{\mathrm{UL}}(\nu) = \eta_{\mathrm{UL}} + \tilde{\varphi}_{\mathrm{UL}}(\nu) + \tfrac{1}{\ln(2)}\tilde{t}_{\mathrm{UL}}(\nu) - \beta_{\mathrm{UL}}, \tag{5.33}$$

where η_{UL} is given by (5.28), $\tilde{\varphi}_{\mathrm{UL}}(\nu)$ is given by (5.31), $\tilde{t}_{\mathrm{UL}}(\nu)$ is given by (5.32), and β_{UL} is given by (5.18) with $\mathbf{A} = \mathbf{I}$ and $\mathbf{X}_0 = \left(\boldsymbol{\Upsilon}_{\mathrm{UL}}^{(\nu)}\right)^{-1}\mathbf{C}_{\mathrm{UL}}^{(\nu)}$.

Note that the SCAMP optimization problem can be written as:

$$\begin{aligned} \min_{\substack{\mathbf{Q}_{\mathrm{BS},k},\mathbf{Q}_{\mathrm{UE},u},\\ k\in\mathcal{I}_{\mathcal{D}},\, u\in\mathcal{I}_{\mathcal{U}}}} \quad & \tilde{f}_{\mathrm{MU-SCAMP}}(\nu) \\ \text{subject to:} \quad & (5.4b) - (5.4e), \end{aligned} \tag{5.34}$$

where $\tilde{f}_{\mathrm{MU-SCAMP}}(\nu) = -\tilde{R}_{\mathrm{DL}}(\nu) - \tilde{R}_{\mathrm{UL}}(\nu)$. Note that optimization problems (5.12) and (5.34) only differ in the selection of their convex objective function approximations (i.e., $\tilde{f}_{\mathrm{MU-DC}}(\nu)$ and $\tilde{f}_{\mathrm{MU-SCAMP}}(\nu)$, respectively).

By construction, optimization problem (5.34) is convex and satisfies the DCP ruleset. The SCAMP algorithm is described in Algorithm 5.2. As with the DC-based algorithm, optimization problem (5.34) can be solved using cvx [98, 99]. As well, it can be seen that the SCAMP algorithm converges to a locally optimal point of the original non-convex optimization problem by using a similar argument to that of Section 5.3.

5.4 Effect of Estimation Error on the Sum-Rate

This section investigates the effect of channel estimation error on the achievable sum-rate. The derivation is provided in Appendix C.1. In particular, it provides analytical results to express the loss incurred due to inaccurate channel knowledge resulting in residual self-interference.

Let the superscript $\star$ refer to the particular matrices corresponding to the transmit covariance matrices $\left(\mathbf{Q}_{\mathrm{BS},k}^{\star}, \mathbf{Q}_{\mathrm{UE},u}^{\star}\right)$, for $k \in \mathcal{I}_{\mathcal{D}}$ and $u \in \mathcal{I}_{\mathcal{U}}$. Then, the true sum-rate corresponding to the transmit covariance matrices $\left(\mathbf{Q}_{\mathrm{BS},k}^{\star}, \mathbf{Q}_{\mathrm{UE},u}^{\star}\right)$, for $k \in \mathcal{I}_{\mathcal{D}}$ and $u \in \mathcal{I}_{\mathcal{U}}$ can be written as:

$$R^{\star} = \hat{R}^{\star} + \Delta R,$$

where ΔR is the loss incurred due to inaccurate channel knowledge resulting in residual

Algorithm 5.2: SCAMP algorithm.

Randomly initialize $\mathbf{Q}_{\mathrm{BS},k}^{(\nu)},\ k \in \mathcal{I}_{\mathcal{D}}$;
Randomly initialize $\mathbf{Q}_{\mathrm{UE},u}^{(\nu)},\ u \in \mathcal{I}_{\mathcal{U}}$;
Initialize $\nu = 0$;
repeat
  Update $\boldsymbol{\Upsilon}_{\mathrm{DL},k}^{(\nu)}$, $\hat{\mathbf{C}}_{\mathrm{DL},k}^{(\nu)}$, $\mathbf{C}_{\mathrm{DL},k}^{(\nu)}$, $\boldsymbol{\Upsilon}_{\mathrm{UL}}^{(\nu)}$, $\hat{\mathbf{C}}_{\mathrm{UL}}^{(\nu)}$, and $\mathbf{C}_{\mathrm{UL}}^{(\nu)}$ centered around the point $\left(\mathbf{Q}_{\mathrm{BS},k}^{(\nu)}, \mathbf{Q}_{\mathrm{UE},u}^{(\nu)}\right)$, $k \in \mathcal{I}_{\mathcal{D}}$, $u \in \mathcal{I}_{\mathcal{U}}$;
  Update $\tilde{\varphi}_{\mathrm{DL},k}(\nu)$ using (5.25), $\tilde{t}_{\mathrm{DL,k}}(\nu)$ using (5.26), $\tilde{\varphi}_{\mathrm{UL}}(\nu)$ using (5.31), and $\tilde{t}_{\mathrm{UL}}(\nu)$ using (5.32). ;
  Update $-\tilde{R}_{\mathrm{DL}}(\nu)$ using (5.27) and $-\tilde{R}_{\mathrm{UL}}(\nu)$ using (5.33) ;
  Solve (5.34) for $\left(\mathbf{Q}_{\mathrm{BS},k}^{\star}, \mathbf{Q}_{\mathrm{UE},u}^{\star}\right)$, $k \in \mathcal{I}_{\mathcal{D}}$, $u \in \mathcal{I}_{\mathcal{U}}$;
  $\nu = \nu + 1$;
  Update $\mathbf{Q}_{\mathrm{UE},u}^{(\nu)} = \mathbf{Q}_{\mathrm{UE},u}^{\star},\ u \in \mathcal{I}_{\mathcal{U}}$;
  Update $\mathbf{Q}_{\mathrm{BS},k}^{(\nu)} = \mathbf{Q}_{\mathrm{BS},k}^{\star},\ k \in \mathcal{I}_{\mathcal{D}}$;
until $\tilde{f}_{\mathrm{MU-SCAMP}}(\nu)$ *converges*;
Apply Cholesky decomposition: $\mathbf{Q}_{\mathrm{UE},u}^{\star} = \mathbf{L}_{\mathrm{UE},u}\mathbf{L}_{\mathrm{UE},u}^{\dagger}$;
Apply Cholesky decomposition: $\mathbf{Q}_{\mathrm{BS},k}^{\star} = \mathbf{L}_{\mathrm{BS},k}\mathbf{L}_{\mathrm{BS},k}^{\dagger}$;
Solve for $\mathbf{V}_{\mathrm{UE},u}$ using (5.5), $u \in \mathcal{I}_{\mathcal{U}}$;
Solve for $\mathbf{V}_{\mathrm{BS},k}$ using (5.6), $k \in \mathcal{I}_{\mathcal{D}}$;

self-interference derived in Appendix C.1 to be:

$$\Delta R = \Delta R_{\mathrm{UL}} + \sum_{k \in \mathcal{I}_{\mathcal{D}}} \Delta R_{\mathrm{DL},k},$$

where ΔR_{UL} and $\Delta R_{\mathrm{DL},k}$ are given by:

$$\Delta R_{\mathrm{UL}} = \log_2 \left| \mathbf{I}_{N_{\mathrm{BS},R}} - \boldsymbol{\Psi}_{\mathrm{UL}}^{-1} \left(\mathbf{I}_{N_{\mathrm{BS},R}} + \Delta\tilde{\mathbf{C}}_{\mathrm{UL}}^{\star} \boldsymbol{\Upsilon}_{\mathrm{UL}}^{-1} \right)^{-1} \Delta\tilde{\mathbf{C}}_{\mathrm{UL}}^{\star} \boldsymbol{\Upsilon}_{\mathrm{UL}}^{-1} \mathbf{C}_{\mathrm{UL}}^{\star} \right|,$$

$$\Delta R_{\mathrm{DL},k} = \log_2 \left| \mathbf{I}_{N_{\mathrm{UE},R}} - \boldsymbol{\Psi}_{\mathrm{DL},k}^{-1} \left(\mathbf{I}_{N_{\mathrm{UE},R}} + \Delta\tilde{\mathbf{C}}_{\mathrm{DL},k}^{\star} \boldsymbol{\Upsilon}_{\mathrm{DL},k}^{-1} \right)^{-1} \Delta\tilde{\mathbf{C}}_{\mathrm{DL},k}^{\star} \boldsymbol{\Upsilon}_{\mathrm{DL},k}^{-1} \mathbf{C}_{\mathrm{DL},k}^{\star} \right|,$$

where $\boldsymbol{\Psi}_{\mathrm{UL}} = \boldsymbol{\Upsilon}_{\mathrm{UL}} \left(\mathbf{I} + \boldsymbol{\Upsilon}_{\mathrm{UL}}^{-1} \mathbf{C}_{\mathrm{UL}}^{\star} \right)$, $\boldsymbol{\Upsilon}_{\mathrm{UL}} = \boldsymbol{\Sigma}_{\mathrm{BS}} + \hat{\mathbf{C}}_{\mathrm{UL}}^{\star}$, $\boldsymbol{\Psi}_{\mathrm{DL},k} = \boldsymbol{\Upsilon}_{\mathrm{DL},k} \left(\mathbf{I} + \boldsymbol{\Upsilon}_{\mathrm{DL},k}^{-1} \mathbf{C}_{\mathrm{DL},k}^{\star} \right)$, and $\boldsymbol{\Upsilon}_{\mathrm{DL},k} = \boldsymbol{\Sigma}_k + \hat{\mathbf{C}}_{\mathrm{DL},k}^{\star}$.

5.5 Illustrative Results

This section provides some illustrative results for FD MIMO point-to-multi-point systems with HD UEs. In particular, Section 5.5.1 provides some simulation results that compare the SCP algorithms without using the FDP structure. Section 5.5.2 provides simulation and environmental comparisons between the FD MIMO point-to-point and point-to-multi-point environments. Finally, Section 5.5.3 demonstrates the potential benefits of including the FDP structure for FD MIMO point-to-multi-point systems.

As in Chapter 4, for all SCP algorithms, the main source of algorithm complexity is in solving the convex sub-problems, and as such, the complexity of computing the objective function approximations is negligible.

5.5.1 FD MIMO Point-to-Multi-Point without FDP Structure

This sub-section compares the performance of the DC-based and SCAMP algorithms without using the FDP structure to the optimized HD and the joint design proposed in [67] for the MIMO point-to-multi-point system with HD UEs shown in Fig. 5.1. Note that for the MIMO point-to-multi-point system with HD UEs, the HD optimization problem is non-convex and can be solved by using SCP. The noise was normalized such that $E[\mathbf{z}_{\mathrm{BS}}\mathbf{z}_{\mathrm{BS}}^{\dagger}] = \mathbf{I}_{N_{R,\mathrm{BS}}}$ and $E[\mathbf{z}_k\mathbf{z}_k^{\dagger}] = \mathbf{I}_{N_{R,\mathrm{UE}}}$, for $k \in \mathcal{I}_{\mathcal{D}}$, and $\mathbf{H}_{\mathrm{DL}}$ and $\mathbf{H}_{\mathrm{UL}}$ were generated as zero-mean complex Gaussian random variables with a variance equal to the SNR. Conversely, the self-interference channel, $\mathbf{G}_{\mathrm{BS}}$, was generated as a zero-mean complex Gaussian random variable with a variance equal to the self-Interference-to-Noise Ratio at the Base Station ($\mathrm{INR}_{\mathrm{BS,in}}$), where $\mathrm{SNR}/\mathrm{INR}_{\mathrm{BS,in}}$ represents the Signal-to-self-Interference Ratio at the BS receiver input ($\mathrm{SIR}_{\mathrm{BS,in}}$) before interference cancellation.

Similarly, $[\mathbf{G}_{\mathrm{UE}}]_{k,u}$ for $k \in \mathcal{I}_{\mathcal{D}}$, $u \in \mathcal{I}_{\mathcal{U}}$ was generated as a zero-mean complex Gaussian random variable with a variance equal to the co-channel Interference-to-Noise Ratio at the UE ($\mathrm{INR}_{\mathrm{UE,in}}$), where $\mathrm{SNR}/\mathrm{INR}_{\mathrm{UE,in}}$ represents the Signal-to-co-channel-Interference Ratio at the UE receiver input ($\mathrm{SIR}_{\mathrm{UE,in}}$) before interference cancellation. Note that since the BS antennas are co-located, they suffer from very strong self-interference, whereas since the downlink and uplink UEs are geographically separated, they suffer from a weaker interference. Hence, $\mathrm{INR}_{\mathrm{BS,in}} > \mathrm{INR}_{\mathrm{UE,in}}$.

The simulations assume $K_{\mathrm{dl}} = K_{\mathrm{ul}} = 3$, $N_{\mathrm{UE},T} = N_{\mathrm{UE},R} = 2$, $N_{\mathrm{BS},R} = N_{\mathrm{BS},T} = 6$, $P_{\max,u} = 23$ dBm for all $u \in \mathcal{I}_{\mathcal{U}}$, and $P_{\max,\mathrm{BS}} = 30$ dBm in accordance with the 3GPP LTE

(Release 9) simulation baseline parameters for a picocell deployment [107, p.59].

Fig. 5.3 shows the FD-to-HD sum-rate ratio vs. SNR with $\mathrm{SIR}_{\mathrm{BS,in}} = -15$ dB, $\mathrm{SIR}_{\mathrm{UE,in}} = -5$ dB, and $\sigma^2_{\mathrm{err}} = 1$. The results show that the SCAMP algorithm can offer 15–25% sum-rate improvements over optimized HD for a wide-range of realistic SNR values. In particular, it is interesting to note that the SCAMP algorithm outperforms the DC-based algorithm for all SNR values.

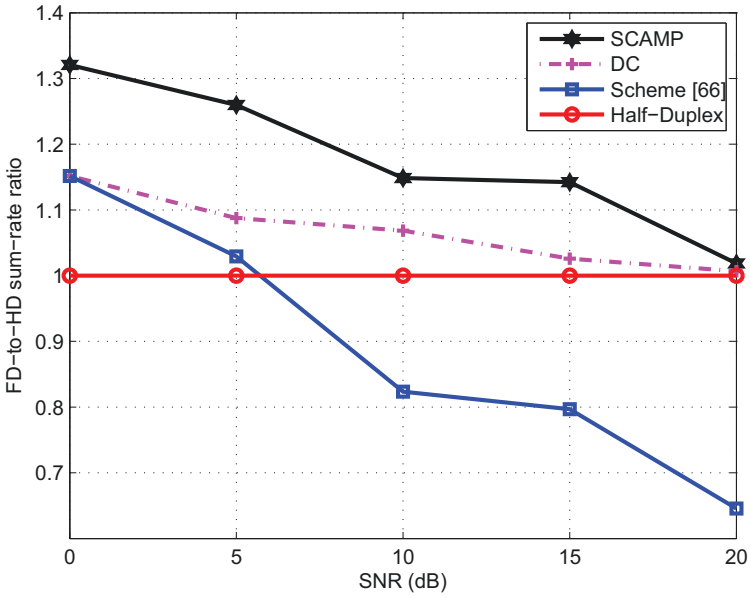

Fig. 5.3 FD-to-HD sum-rate ratio vs. SNR with $\mathrm{SIR}_{\mathrm{BS,in}} = -15$ dB, $\mathrm{SIR}_{\mathrm{UE,in}} = -5$ dB, and $\sigma^2_{\mathrm{err}} = 1$.

Fig. 5.4 shows the FD-to-HD sum-rate ratio vs. $\mathrm{SIR}_{\mathrm{BS,in}}$ with SNR = 5 dB, $\mathrm{SIR}_{\mathrm{UE,in}} = -5$ dB, and $\sigma^2_{\mathrm{err}} = 1$. The results show that the SCAMP algorithm provides about 20–30% sum-rate improvements over optimized HD for a wide-range of $\mathrm{SIR}_{\mathrm{BS,in}}$ values. In particular, for $\mathrm{SIR}_{\mathrm{BS,in}} > -25$ dB, the SCAMP algorithm provides significantly better sum-rate than the other candidate SCP algorithms. Furthermore, with $\mathrm{SIR}_{\mathrm{BS,in}} = -40$ dB, the SCAMP algorithm still provides performance improvements over the optimized HD approach.

Fig. 5.5 shows the FD-to-HD sum-rate ratio vs. σ^2_{err} with SNR = 5 dB, $\mathrm{SIR}_{\mathrm{BS,in}} = -20$ dB, and $\mathrm{SIR}_{\mathrm{UE,in}} = -5$ dB. The results show that the SCAMP algorithm is capable of achieving more than 20% sum-rate improvements over optimized HD for some reasonable

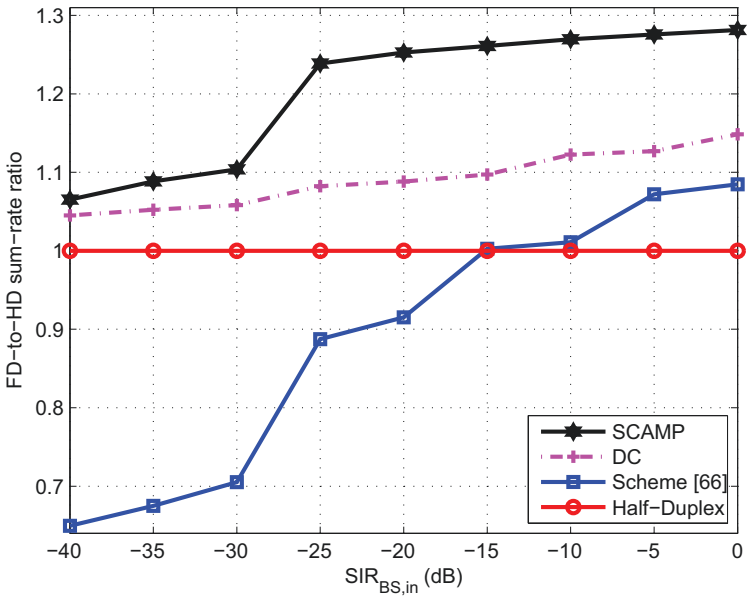

Fig. 5.4 FD-to-HD sum-rate ratio vs. $\mathrm{SIR}_{\mathrm{BS,in}}$ with SNR = 5 dB, $\mathrm{SIR}_{\mathrm{UE,in}} = -5$ dB, and $\sigma^2_{\mathrm{err}} = 1$.

values of σ^2_{err}. In addition, when $\sigma^2_{\mathrm{err}} = 10$, corresponding to large inaccuracies in the channel knowledge, the SCAMP algorithm was still capable of providing 5% performance improvements over optimized HD.

Fig. 5.6 shows the convergence of the SCP algorithms compared to the converged optimized HD value for two different realizations with SNR = 5 dB, $\mathrm{SIR}_{\mathrm{BS,in}} = -20$ dB, $\mathrm{SIR}_{\mathrm{UE,in}} = -5$ dB, and $\sigma^2_{\mathrm{err}} = 1$. It is important to note that the optimized HD also requires multiple iterations; however, here we only show the final converged value of the optimized HD approach to highlight the convergence of the FD SCP-based algorithms.

The results show that the DC-based algorithm tends to initially outperform the SCAMP algorithm but, in general, the SCAMP algorithm outperforms the DC-based algorithm at convergence. As well, it was observed that the SCP algorithms periodically have a step-like convergence where the algorithm will level-off for some iterations before increasing significantly and beginning to level-off again. This is due to the internal convex optimization solver, since occasionally cvx [98,99] will fail to find an optimal point or will return a point which is considered an inaccurate solution; however, after slightly tuning the initial points to the convex solver (i.e., after several more iterations), an optimal point can be found,

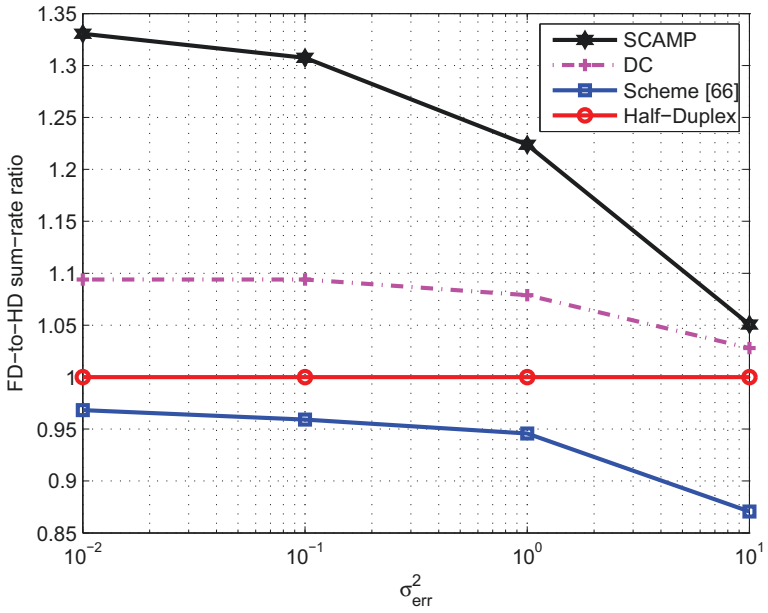

Fig. 5.5 FD-to-HD sum-rate ratio vs. σ^2_{err} with SNR $= 5$ dB, $\text{SIR}_{\text{BS,in}} = -20$ dB, and $\text{SIR}_{\text{UE,in}} = -5$ dB.

resulting in a sudden sum-rate increase and the step-like convergence.

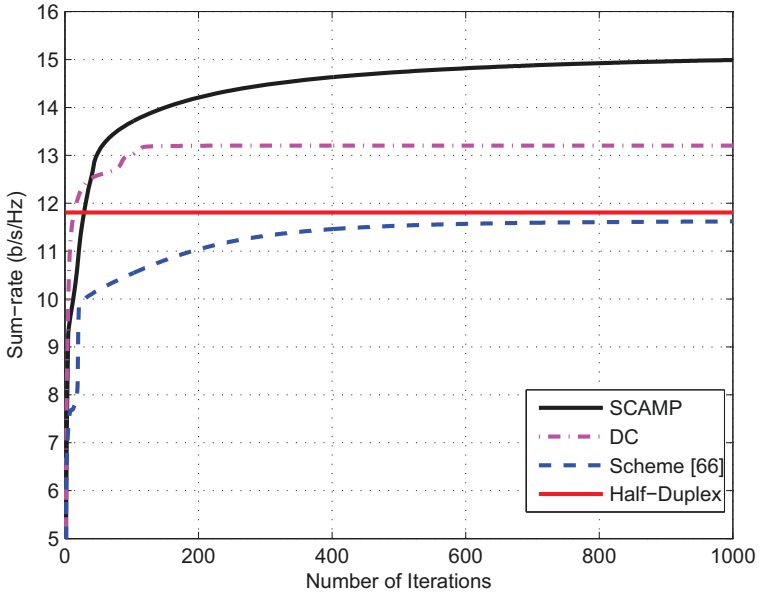

(a) Realization 1

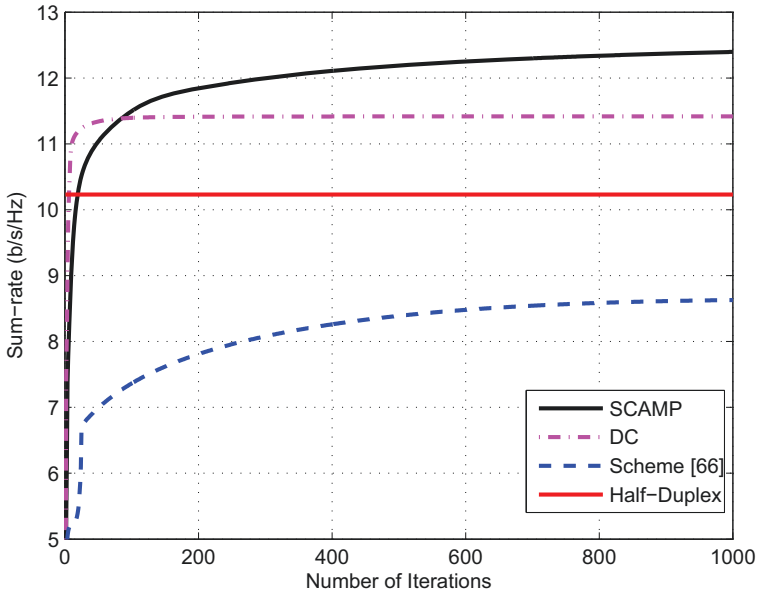

(b) Realization 2

Fig. 5.6 Convergence comparison for SNR = 5 dB, $\mathrm{SIR}_{\mathrm{BS,in}} = -20$ dB, $\mathrm{SIR}_{\mathrm{UE,in}} = -5$ dB, and $\sigma^2_{\mathrm{err}} = 1$.

5.5.2 Comparison with FD MIMO Point-to-Point

It is interesting to note that in Section 5.5.1, for each FD MIMO point-to-multi-point scenario tested, the SCAMP algorithm outperformed the DC-based algorithm. However, results in Chapter 4 without using the FDP structure indicate that the DC-based algorithm offers a better sum-rate than the SCAMP algorithm for the FD MIMO point-to-point scenario.

This is due to the method by which the DC-based and SCAMP algorithms approximate their respective objective functions. In particular, the DC-based algorithm only approximates the interference-plus-noise terms, and hence, has a perfect approximation of the forward channels. Conversely, the SCAMP approach approximates each of the forward, interference, and noise terms but it spreads out the approximations over multiple terms. As such, for FD MIMO point-to-point systems, where there is fewer sources of interference (self or otherwise), an accurate forward channel is more important, leading to superior performance for the DC-based algorithm (i.e., the DC-based algorithm better approximates the FD MIMO point-to-point system than the SCAMP algorithm). However, for FD MIMO point-to-multi-point systems, there are many forms of interference (e.g., many self-interference terms and uplink co-channel interference) which results in the SCAMP algorithm better-approximating the FD MIMO point-to-multi-point environment than the DC-based algorithm.

Note that when applying the FDP structure for FD MIMO point-to-point systems, the FDP-SCAMP algorithm outperformed the FDP-DC algorithm. The potential benefit of the FDP structure is embedded in the modified self-interference matrix, and as such, the SCAMP algorithm is better suited to leverage its potential. This observation can be further extended to FD MIMO point-to-multi-point systems with the FDP structure, and hence, the FDP-DC algorithm was omitted from the simulations provided in Section 5.5.3.

5.5.3 MIMO Point-to-Multi-Point with FDP Structure

This sub-section provides some illustrative results to demonstrate the effectiveness of the proposed FDP structure for FD MIMO point-to-multi-point systems. In particular, the performance of FDP-SCAMP (i.e., the SCAMP algorithm when using the FDP structure from Chapter 4) is compared to optimized HD and the DC-based and SCAMP algorithms without using the FDP structure for FD MIMO point-to-multi-point systems with HD

UEs. For this scenario, only the joint FDP structure was applied since even when applying a separate design, the resulting optimization problem is non-convex. Thus, the separate approach would require a similar computational complexity to the joint approach. As well, the HD optimization problem is non-convex, and hence, was also optimized using SCP.

The simulation parameters are set up as in Section 5.5.1, with the following exceptions. The elements of $[\tilde{\mathbf{H}}_{\mathrm{DL}}]_k$ ($k \in \mathcal{I}_{\mathcal{D}}$) were generated as zero-mean complex Gaussian random variables with a variance equal to the SNR. The elements of the self-interference channel, $\tilde{\mathbf{G}}_{\mathrm{BS},a}$, were generated as zero-mean complex Gaussian random variables with a variance equal to $\mathrm{INR}_{\mathrm{BS,in}}$, where $\mathrm{SNR}/\mathrm{INR}_{\mathrm{BS,in}}$ represents the $\mathrm{SIR}_{\mathrm{BS,in}}$ before interference cancellation. As well, the PAs are assumed to have a 30 dB gain, the circulators are assumed to have a 20 dB isolation and the variance of the inter-antenna self-interference is assumed to be 20 dB below that of the direct self-interference paths.

Fig. 5.7 shows the FD-to-HD sum-rate ratio vs. SNR with $\mathrm{SIR}_{\mathrm{BS,in}} = -40$ dB, $\mathrm{SIR}_{\mathrm{UE,in}} = -5$ dB, $\alpha = 15$ dB, $\sigma^2_{\mathrm{err}} = 1$. The results show that the FDP structure provides a significant performance improvement over the non-FDP algorithms over a wide-range of SNR values (e.g., approximately 8% at low SNR and 10% at high SNR).

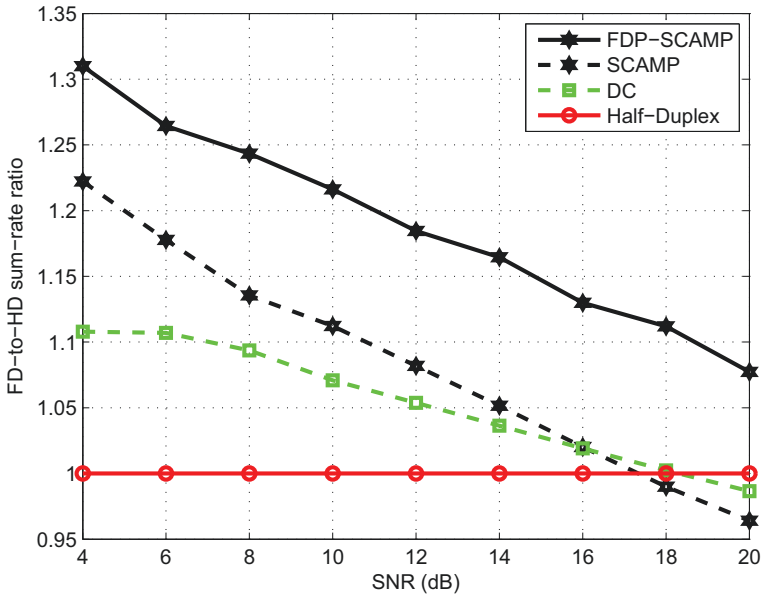

Fig. 5.7 MIMO point-to-multi-point FD-to-HD sum-rate ratio vs. SNR with $\mathrm{SIR}_{\mathrm{BS,in}} = -40$ dB, $\mathrm{SIR}_{\mathrm{UE,in}} = -5$ dB, $\alpha = 15$ dB, $\sigma^2_{\mathrm{err}} = 1$.

Fig. 5.8 shows the FD-to-HD sum-rate ratio vs. $\mathrm{SIR}_{\mathrm{BS,in}}$ with SNR = 10 dB, $\mathrm{SIR}_{\mathrm{UE,in}} = -5$ dB, $\alpha = 15$ dB, $\sigma^2_{\mathrm{err}} = 1$. The results show that the FDP structure provides an approximately 10% sum-rate improvement over the non-FDP algorithms.

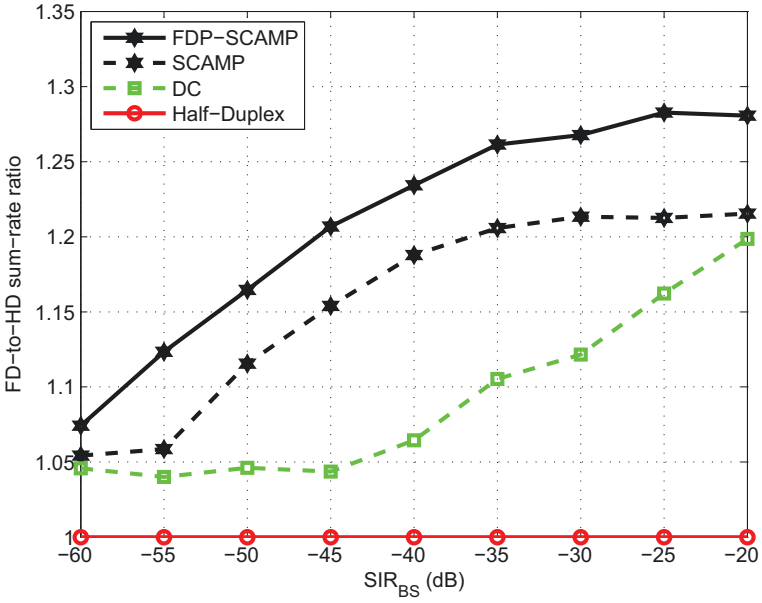

Fig. 5.8 MIMO point-to-multi-point FD-to-HD sum-rate ratio vs. $\mathrm{SIR}_{\mathrm{BS,in}}$ with SNR = 10 dB, $\mathrm{SIR}_{\mathrm{UE,in}} = -5$ dB, $\alpha = 15$ dB, $\sigma^2_{\mathrm{err}} = 1$.

Fig. 5.9 shows the FD-to-HD sum-rate ratio vs. σ^2_{err} with SNR = 5 dB, $\mathrm{SIR}_{\mathrm{BS,in}} = -40$ dB, $\mathrm{SIR}_{\mathrm{UE,in}} = -5$ dB, $\alpha = 15$ dB. The results indicate that even for larger values of σ^2_{err} the FDP structure provides a performance improvement over the non-FDP approaches without substantially increasing the complexity.

5.6 Concluding Remarks

This chapter presented two SCP-based algorithms for solving the non-convex sum-rate maximization problem with matrix variables for FD MIMO point-to-multi-point systems. The DC-based algorithm is based on the fact that the structure of the problem naturally lends itself to a particular DC decomposition. The SCAMP algorithm is a general technique proposed for solving non-convex optimization problems with a logarithmic objective function which is applied to FD MIMO point-to-multi-point systems. The SCAMP algo-

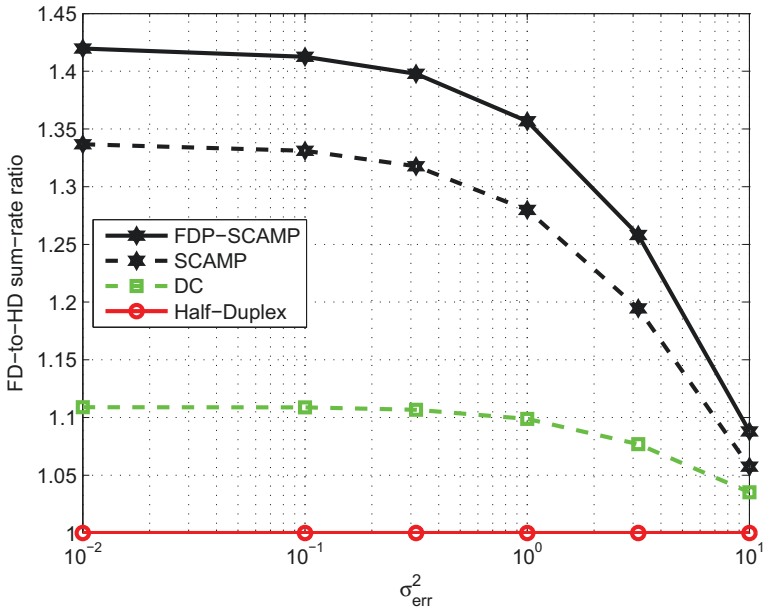

Fig. 5.9 MIMO point-to-multi-point FD-to-HD sum-rate ratio vs. σ^2_{err} with SNR $= 5$ dB, $\text{SIR}_{\text{BS,in}} = -40$ dB, $\text{SIR}_{\text{UE,in}} = -5$ dB, $\alpha = 15$ dB.

rithm is a multi-step procedure that begins by applying a non-convex approximation to the non-convex objective function and then proceeds to convexify the non-convex approximation. The two SCP-based algorithms result in two different convex approximations to the non-convex sum-rate maximization problem. An analytical expression for the estimation error of the sum-rate was derived, which provides an analytical result to express the loss incurred due to inaccurate channel knowledge resulting in residual self-interference.

Illustrative results with and without the FDP structure showed that the SCAMP algorithm provides approximately 1.2–1.3 times the sum-rate of optimized HD in a wide-range of FD MIMO point-to-multi-point system scenarios. Hence, even in the presence of high self-interference, the SCAMP algorithm is capable of providing significant sum-rate improvements over existing optimized HD techniques for FD MIMO point-to-multi-point systems.

Chapter 6

Concluding Remarks

6.1 Summary

Increasing the amount of resource sharing in a system generates additional interference but, at the same time, offers potential spectral efficient benefits if the interference can be effectively managed. As such, effective interference management for interference-limited systems will play a critical role in the development of next-generation wireless and wireline communication systems. This thesis focused on the design of HD and FD scalar and vectored DRA algorithms for improving the spectral efficiency with specific applications to DSL and FD wireless systems.

In Chapter 3, a HD near-optimal low-complexity distributed scalar DRA algorithm referred to as the constant offset ASB-MRU was developed. The constant offset ASB-MRU introduces the concept of a virtual network of reference users to provide approximate global channel knowledge using only local channel knowledge resulting in a near-ideal balance between performance, complexity, and sensitivity to users entering/leaving the system. Sufficient conditions for convergence, existence, and efficiency of the constant offset algorithm were provided. Chapter 3 also derived a lower-bound on the expected sum-rate which provides better insight into the actual spectral efficiency of the system than existing models.

In Chapter 4, a MIMO-OFDM FDP transceiver structure was proposed which applies precoding to jointly control the forward channel precoding and the self-interference cancellation. The FDP structure allows for different algorithms and optimization objectives to be developed. In particular, focusing on the objective of sum-rate maximization, separate

and joint design algorithms were proposed. Simulation results using both standard channel models and measured data showed that using the proposed FDP structure, between 1.6 to 1.8 times the spectral efficiency of optimized HD systems is achievable in a wide-range of FD MIMO point-to-point scenarios.

In Chapter 5, two SCP-based algorithms for solving the non-convex sum-rate maximization problem with matrix variables for FD MIMO point-to-multi-point systems were developed. In particular, the SCAMP algorithm is a general technique proposed for solving non-convex optimization problems with a logarithmic objective function which is applied to FD MIMO point-to-multi-point systems. Chapter 5 also derived an analytical expression for the estimation error of the sum-rate, which provided an analytical result to express the loss incurred due to inaccurate channel knowledge resulting in residual self-interference. Simulation results indicated that the SCAMP algorithm provides between 1.2 to 1.3 times the sum-rate of optimized HD in a wide-range of FD MIMO point-to-multi-point system scenarios.

6.2 Potential Future Work

The main focus of this Ph.D. thesis has been on improving the spectral efficiency of wireless and wireline communication systems. This section discusses some potential future work related to the work proposed in this thesis.

The FDP structure proposed in Chapter 4 allows for different optimization objectives to be developed rather than solely focusing on self-interference minimization. This thesis focused on the optimization objective of sum-rate maximization, and hence, all the developed algorithms solve sum-rate maximization-based optimization problems. Areas of potential future work include alternative optimization objectives (e.g., power minimization, energy efficiency, bit-error rate minimization). Several approaches similar to those proposed in this thesis, as well as many approaches unique to the specific optimization objective, could be developed for each optimization objective.

Furthermore, the results of Chapter 5 showed that the SCAMP algorithm is an effective tool for solving non-convex matrix variable optimization problems with a logarithmic objective function. In particular, Chapter 5 showed that the SCAMP algorithm effectively solved the non-convex sum-rate maximization problem for FD MIMO point-to-multi-point systems. The SCAMP algorithm is a general scheme, and as such, it may be a useful tool

to efficiently solve many different optimization problems in many different fields of study, including other communication systems, and potentially, to solve non-convex optimization problems in other disciplines, as well.

While the SCAMP algorithm was shown to converge fairly quickly for FD MIMO point-to-point systems in Chapter 4, the main limitation of the SCAMP algorithm in FD MIMO point-to-multi-point systems (i.e., for more complicated systems) is that often many iterations were required for the algorithm to converge. An interesting area for future work would be investigating methods to reduce the computational time of the SCAMP algorithm and, more generally, SCP-based algorithms. One particularly interesting area of research would be investigating the choice of starting point. More specifically, the complexity benefits of the constant offset ASB-MRU algorithm from Chapter 3 come from its initialization phase and, essentially, the fact that it generates a very efficient starting point for the algorithm, leading to fast convergence. Perhaps a more complicated and/or similar approach can be implemented for the SCAMP algorithm, whereby the choice of initial point can be vastly improved to significantly reduce the number of iterations required, and hence, improve its practical implementation benefits for FD MIMO point-to-multi-point systems.

Appendix A

A.1 Computational Complexity Analysis

The computational complexity represents the number of operations required for the execution of an algorithm. In particular, it demonstrates the behaviour of different algorithms as the parameters (e.g., number of users, sub-carriers) increase. This is represented using big-O notation (i.e., $\mathcal{O}(\cdot)$), which shows the limiting behaviour of a function when the arguments tend towards infinity. Mathematically, the big-O notation is described as follows:

$$f(x) = \mathcal{O}(g(x)) \Longleftrightarrow |f(x)| \leq c|g(x)| \quad \forall \quad x > x_0,$$

where $c > 0$ is some constant and $x_0 \in \mathbb{R}$. Suppose two algorithms are dependent on a variable X, where one algorithm has a complexity of $\mathcal{O}(X)$ while the other has a complexity of $\mathcal{O}(X^2)$. Then, the big-O notation implies that the $\mathcal{O}(X)$ algorithm will converge faster than the $\mathcal{O}(X^2)$ algorithm for sufficiently large X. The convergence time of an algorithm is said to be exponential if it is $\mathcal{O}(a^X)$ and is said to be polynomial if it is $\mathcal{O}(X^a)$ for some $a > 1$. In algorithmic terms, exponential time is generally significantly slower than polynomial time. One key factor which the big-O notation fails to capture is the value of the constants in front of the key terms (e.g., the number of iterations required for the algorithm to be run) since it only looks at the behaviour of the algorithms as the parameters tend towards infinity. Hence, for a fixed value of X, it is possible for a $\mathcal{O}(X)$ algorithm to take longer to converge than a $\mathcal{O}(X^2)$ algorithm. More specifically, for a fixed value of X, suppose the number of iterations required to run the $\mathcal{O}(X)$ algorithm is denoted by ν_1 and the number of iterations required to run the $\mathcal{O}(X^2)$ algorithm is ν_2. It is possible that $\nu_1 X > \nu_2 X^2$, for some values of X; however, for sufficiently large X, the $\mathcal{O}(X)$ algorithm

will run faster than the $\mathcal{O}(X^2)$.

For DRA purposes, there are two main parameters: the number of users K, and the number of frequency sub-carriers, F. Hence, almost all the algorithms will be of the form $\mathcal{O}(f(K,F))$ for some function $f(K,F)$. The only exception is the constant offset ASB-MRU algorithm, which also has the parameter for the number of reference users in the virtual network, denoted as K_R, hence it will be of the form $\mathcal{O}(f(K,F,K_R))$.

Due to the total power constraint, the coupling between sub-carriers requires the transmit powers be searched for jointly over all frequency sub-carriers. Solving an X-dimensional exhaustive search has a computational complexity of $O(a^X)$, assuming a discrete search space of a elements for each dimension. Therefore, solving the DRA optimal resource allocation using an exhaustive search over both the number of users and the number of sub-carriers has a complexity of $O(a^{KF})$, which is computationally intractable for large K and/or F.

Another source of algorithm complexity is the message passing requirements, depending on structure of the algorithm (i.e., centralized, semi-centralized, or distributed). In general, centralized algorithms require some initial message passing to gain global channel knowledge from all users, semi-centralized algorithms require per-iteration message passing, and distributed algorithms require no message passing.

A.1.1 IWF Computational Complexity

The IWF algorithm is a distributed algorithm which consists of two loops. The outer loop cycles through all the K users, while the inner loop performs water-filling for the k-th user over the F sub-carriers. The water-filling process involves a simple bisection search. Assuming the number of outer iterations required for convergence is ν and assuming the bisection loop is run until an accuracy of ϵ is achieved, the total number of iterations required will be $\nu \times \log_2(1/\epsilon)$. Therefore, the overall complexity of the IWF algorithm is $\nu \times \log_2(1/\epsilon) \times K \times F$, which implies:

$$C_{\text{IWF}} = \mathcal{O}(FK).$$

A.1.2 SCALE Computational Complexity

The SCALE algorithm complexity is broken down into the complexity at each user and the complexity at the SMC. Each user optimizes their transmit power, measures their total interference-plus-noise and sends the corresponding F values to the SMC. Each user then waits for an F-dimensional message from the SMC before re-updating their transmit power. Hence, the SCALE algorithm requires the exchange of $2F$ messages per-iteration. Assuming that ω is the number of operations required to update each user's transmit power, the complexity at each user is given by ωF.

The SMC receives a message from each user and generates the messages required for each user. Generating the message for each user requires $F \times K$ additions. This process must be repeated for each of the K users. Hence, the complexity at the SMC is given by FK^2. Therefore, assuming the number of iterations for the transmit powers of each user to converge is ν, the overall complexity of the SCALE algorithm is $\nu \times (FK^2 + \omega K)$, which implies:

$$C_{\text{SCALE}} = \mathcal{O}(FK^2).$$

A.1.3 DSB Computational Complexity

The DSB algorithm consists of each user measuring their channel and sending an F-dimensional message to the SMC (one per sub-carrier). On each iteration, the SMC combines the received messages from all K users and computes each user's updated Lagrange multiplier offset for each sub-carrier. Each user then updates their transmit power on each of the F sub-carriers using the updated received offset values. Hence, the DSB algorithm requires the exchange of $2F$ messages per-iteration. The process is repeated until the offset values for each user on each sub-carrier converge. Assuming the ω is the number of operations required to update each user's transmit power, the complexity at each user is given by ωF.

Calculating the message that the SMC sends to each user requires a summation over $K - 1$ users of the product between the corresponding interference channel gain and the received message from that particular user. Hence, the generation of the message for each user requires $F \times (K-1)$ additions. The process is repeated for each of the K users, leading to a complexity of $FK^2 - FK$ at the SMC. Therefore, aassuming the number of iterations for the transmit powers of each user to converge is ν, the complexity of the DSB algorithm

is $\nu \times (FK^2 - FK + \omega F)$, which implies:

$$C_{\text{DSB}} = \mathcal{O}(FK^2).$$

A.2 Proof of Theorem 3.1

The proof provided in this section generalizes the convergence proof of the ASB-S2 algorithm (ASB algorithm with a high SNR approximation), derived in [15] for the symmetric transmission case (and [16] for the asymmetric transmission case). In particular, the convergence of the ASB-MRU, IWF, and ASB-S2 algorithms can be recovered as special cases.

The convergence proof is obtained by showing that there exists a norm for which the sequence of constant offset iterates forms a Cauchy sequence, and hence, converges to a fixed point. Intuitively, a Cauchy sequence is a sequence whose elements become arbitrarily close to each other as the sequence progresses, with respect to some distance metric (e.g., some norm). More formally, a Cauchy sequence is defined below, where $d(\cdot, \cdot)$ defines some distance measure.

Definition A.1. *A sequence $\{x(t)\}$ is a Cauchy sequence if and only if for all $\epsilon > 0$ there exists a T, such that for all $t, \tau \geq T$, $d(x(t), x(\tau)) < \epsilon$.*

The following proposition will assist in proving that the sequence of constant offset iterates forms a Cauchy sequence.

Proposition A.1. *Suppose that for some feasible fixed initial value $x(0)$: $||x(t+1) - x(t)|| \leq \xi \, ||x(t) - x(t-1)||$ for all $t \geq 1$, where $\xi \in [0, 1)$. Then, $x(t)$ is a Cauchy sequence.*

Proof.

$$||x(t+1) - x(t)|| \leq \xi \, ||x(t) - x(t-1)|| \,, \tag{A.1}$$

for all $t \geq 1$, where $\xi \in [0, 1)$. This implies that:

$$||x(t+1) - x(t)|| \leq \xi^t \, ||x(1) - x(0)|| \,,$$

for all $t \geq 0$. Therefore, for every $t \geq 0$ and $\Delta t \geq 1$, we have:

$$||x(t+\Delta t) - x(t)|| = \left|\left| \sum_{i=1}^{\Delta t} \{x(t+i) - x(t+i-1)\} \right|\right| \tag{A.2}$$

$$\leq \sum_{i=1}^{\Delta t} ||x(t+i) - x(t+i-1)|| \tag{A.3}$$

$$\leq \sum_{i=1}^{\Delta t} \xi^{t+i-1} ||x(1) - x(0)||$$

$$= \xi^t \left(1 + \xi + \cdots + \xi^{\Delta t - 1}\right) ||x(1) - x(0)||$$

$$\leq \frac{\xi^t}{1-\xi} ||x(1) - x(0)||, \tag{A.4}$$

where (A.2) is obtained by adding and subtracting all the terms in between $x(t+\Delta t)$ and $x(t)$, (A.3) follows from the triangle inequality, and (A.4) comes from the fact that $\sum_{i=1}^{\infty} \xi^i = \frac{1}{1-\xi}$, hence $\sum_{i=1}^{a} \xi^i \leq \sum_{i=1}^{\infty} \xi^i = \frac{1}{1-\xi}$ for any a. Suppose $\epsilon > 0$ is given. Since $\xi \in [0, 1)$, we can always find a T is large enough so that for all $t > T$, the following is satisfied:

$$\xi^t < \frac{\epsilon(1-\xi)}{||x(1) - x(0)||}.$$

Then by setting $\tau = t + \Delta t$, we have for for all $t, \tau \geq T$:

$$||x(\tau) - x(t)|| \leq \frac{\xi^t}{1-\xi} ||x(1) - x(0)|| < \epsilon.$$

Hence, the sequence $\{x(t)\}$ is a Cauchy sequence, and therefore, converges to a fixed point, if (A.1) is satisfied for some norm. □

Next, we define our sequence of constant offset iterates.

Definition A.2. *For any iteration, $v \geq 1$, the transmit power of user k on frequency sub-carrier f is given by:* $p_f^{k,v} = \left[\frac{w_k}{\lambda_k^v + \Delta\lambda_f^k} - \frac{\Gamma(\sum_{l \neq k} p_f^{k,v-1} |h_f^{k,l}|^2 + \sigma_f^k)}{|h_f^{k,k}|^2} \right]_0^{p_f^{k,\text{mask}}}$.

Next, we must select an appropriate norm. Since the choice of norm in this proof is unusual, we will formally prove that it is, in fact, a valid norm. Lemma A.1 will be used in the proof of Claim A.1, that the choice of norm is valid.

Lemma A.1. *If* $A, B, C, D \geq 0$*, then* $\max\{A+B, C+D\} \leq \max\{A, C\} + \max\{B, D\}$

Proof. There are four cases:

Case 1. If $A \geq C$ and $B \geq D$, $\max\{A, C\} + \max\{B, D\} = A + B = \max\{A+B, C+D\}$.

Case 2. If $A \leq C$ and $B \leq D$, $\max\{A, C\} + \max\{B, D\} = C + D = \max\{A+B, C+D\}$.

Case 3. If $A \geq C$ and $B \leq D$, $\max\{A, C\} + \max\{B, D\} = A + D$
$\implies \max\{A+B, C+D\} \leq \max\{A+D, A+D\} = A+D = \max\{A, C\}+\max\{B, D\}$.

Case 4. If $A \leq C$ and $B \geq D$, $\max\{A, C\} + \max\{B, D\} = C + B$
$\implies \max\{A+B, C+D\} \leq \max\{C+B, C+B\} = C+B = \max\{A, C\}+\max\{B, D\}$.

□

Claim A.1. $d : \mathbb{R}^F \to \mathbb{R}$ *defined as:* $d(\mathbf{x}) = \max\left\{\sum_f [x_f]_0, \sum_f [-x_f]_0\right\}$ *defines a norm.*

Proof. Let $d : \mathbb{R}^F \to \mathbb{R}$ be a function defined as: $d(\mathbf{x}) = \max\left\{\sum_f [x_f]_0, \sum_f [-x_f]_0\right\}$. $d(\mathbf{x})$ is a norm if it satisfies the following three properties:

1. $d(a\mathbf{x}) = |a| d(\mathbf{x})$, for all $a \in \mathbb{R}$.
2. $d(\mathbf{x} + \mathbf{y}) \leq d(\mathbf{x}) + d(\mathbf{y})$, for all $\mathbf{x}, \mathbf{y} \in \mathbb{R}^F$.
3. $d(\mathbf{x}) = 0$ if and only if $\mathbf{x} = \mathbf{0}$.

Proof of 1.

$$\begin{aligned} d(a\mathbf{x}) &= \max\left\{\sum_f [ax_f]_0, \sum_f [-ax_f]_0\right\} \\ &= \max\left\{\sum_f |a|[x_f]_0, \sum_f |a|[-x_f]_0\right\} \\ &= |a| \max\left\{\sum_f [x_f]_0, \sum_f [-x_f]_0\right\} \\ &= |a| d(\mathbf{x}) \end{aligned} \tag{A.5}$$

where (A.5) holds because if $a > 0$, $\sum_f \max(\pm a x_f, 0) = |a| \sum_f \max(\pm x_f, 0)$, and if $a < 0$, $\sum_f \max(\pm a x_f, 0) = |a| \sum_f \max(\mp x_f, 0)$.

Proof of 2.

$$
\begin{aligned}
d(\mathbf{x}+\mathbf{y}) &= \max\left\{\sum_f [x_f + y_f]_0, \sum_f [-(x_f+y_f)]_0\right\} \\
&\leq \max\left\{\sum_f [x_f]_0 + [y_f]_0, \sum_f [-x_f]_0 + [-y_f]_0\right\} && \text{(A.6)} \\
&= \max\left\{\sum_f [x_f]_0 + \sum_f [y_f]_0, \sum_f [-x_f]_0 + \sum_f [-y_f]_0\right\} \\
&\leq \max\left\{\sum_f [x_f]_0, \sum_f [-x_f]_0\right\} + \max\left\{\sum_f [y_f]_0, \sum_f [-y_f]_0\right\} && \text{(A.7)} \\
&= d(\mathbf{x}) + d(\mathbf{y})
\end{aligned}
$$

where (A.6) holds since $[a+b]_0 \leq [a]_0 + [b]_0$ and (A.7) holds by Lemma A.1.

Proof of 3.

$$
\begin{aligned}
& d(\mathbf{x}) = 0 \iff \max\left\{\sum_f [x_f]_0, \sum_f [-x_f]_0\right\} = 0 \\
& \iff \max(x_f, 0) = \max(-x_f, 0),\ \forall\ f && \text{(A.8)} \\
& \iff x_f = 0,\ \forall\ f
\end{aligned}
$$

where (A.8) holds since $[\pm x_f]_0 = \max\{\pm x_f, 0\} \geq 0$. □

Now that we have proven that it is a valid norm, for the remainder of this proof, let $||\mathbf{x}|| = \max\left\{\sum_f [x_f]_0, \sum_f [-x_f]_0\right\}$. Next, we need to prove that the sequence of constant offset iterates forms a Cauchy sequence (i.e., using Proposition A.1) for each user. The following lemmas will assist in proving that the sequence is Cauchy.

Lemma A.2. *Let $f(x)$ and $g(x)$ be non-increasing and non-decreasing functions, respectively. If there exists an x^* such that $f(x^*) = g(x^*)$, and $f(x)$ and $g(x)$ are strictly decreasing and strictly increasing at $x = x^*$, respectively, then $x^* = \arg\min_x \{\max\{f(x), g(x)\}\}$.*

Proof. For $\Delta x > 0$, $f(x^* + \Delta x) < f(x^*) = g(x^*) < g(x^* + \Delta x)$.
For $\Delta x < 0$, $f(x^* + \Delta x) > f(x^*) = g(x^*) > g(x^* + \Delta x)$.

Therefore, as $\Delta x \to 0^+, \max\{f(x^* + \Delta x), g(x^* + \Delta x)\} = g(x^* + \Delta x)$
and as $\Delta x \to 0^-, \max\{f(x^* + \Delta x), g(x^* + \Delta x)\} = f(x^* + \Delta x)$

As such, when we solve the min-max problem: $\arg\min_x \max\{f(x), g(x)\}$,
if $f(x) < g(x)$, we minimize $\max\{f(x), g(x)\} = g(x)$ by decreasing the value of x (since $g(x)$ is a non-decreasing function) until we reach x^*, since afterwards $f(x) > g(x)$.
When $f(x) > g(x)$, we minimize $\max\{f(x), g(x)\} = f(x)$ by increasing the value of x (since $f(x)$ is a non-increasing function) until we reach x^*, since afterwards $f(x) < g(x)$.

Therefore, the optimal point will be: $x^* = \arg\min_x \max\{f(x), g(x)\}$. □

Lemma A.3. *Some properties of* $[x]_0$*:*

(i) $[[x]_0 - [y]_0]_0 \leq [x - y]_0$

(ii) $[-([x]_0 - [y]_0)]_0 \leq [-(x - y)]_0$

Proof. The proofs are shown below:

(i) There are four possible cases:

Case 1. If $x \geq 0$ and $y \geq 0$, then $[[x]_0 - [y]_0]_0 = [x - y]_0$.

Case 2. If $x \leq 0$ and $y \leq 0$, then $[[x]_0 - [y]_0]_0 = 0 \leq [x - y]_0$.

Case 3. If $x \geq 0$ and $y \leq 0$, then $[[x]_0 - [y]_0]_0 = x \leq x - y = [x - y]_0$.

Case 4. If $x \leq 0$ and $y \geq 0$, then $[[x]_0 - [y]_0]_0 = 0 = [x - y]_0$.

(ii) $[-([x]_0 - [y]_0)]_0 = [[y]_0 - [x]_0]_0 \leq [y - x]_0 = [-(x - y)]_0$,
where the inequality holds from part (i).

□

Lemma A.4. $\max_k \max\left\{\sum_f \left[p_f^{k,v+1} - p_f^{k,v}\right]_0, \sum_f \left[-\left(p_f^{k,v+1} - p_f^{k,v}\right)\right]_0\right\} \leq$
$\max_k \max\left\{\sum_f \left[\sum_{l \neq k} \frac{|h_f^{k,l}|^2}{|h_f^{k,l}|^2}\left(p_f^{l,v} - p_f^{l,v-1}\right)\right]_0, \sum_k \left[-\left(\sum_{l \neq k} \frac{|h_f^{k,l}|^2}{|h_f^{k,k}|^2}\left(p_f^{l,v} - p_f^{l,v-1}\right)\right)\right]_0\right\}$

Proof. To begin, we define:

$$f^{k,v}(x) \triangleq \sum_f \left[\left[\frac{w_k}{x + \Delta\lambda_f^k} - \frac{\Gamma(\sum_{l \neq k} p_f^{l,v} |h_f^{k,l}|^2 + \sigma_f^k)}{|h_f^{k,k}|^2} \right]_0 - p_f^{k,v} \right]_0$$

$$g^{k,v}(x) \triangleq \sum_f \left[- \left(\left[\frac{w_k}{x + \Delta\lambda_f^k} - \frac{\Gamma(\sum_{l \neq k} p_f^{l,v} |h_f^{k,l}|^2 + \sigma_f^k)}{|h_f^{k,k}|^2} \right]_0 - p_f^{k,v} \right) \right]_0$$

Clearly, $f^{k,v}(x)$ is non-increasing in x, since as x increases, $\frac{w_k}{x+\Delta\lambda_f^k}$ decreases, shrinking the magnitude of the expression (which is positive). Similarly, $g^{k,v}(x)$ is non-decreasing in x, since as x increases, $\frac{w_k}{x+\Delta\lambda_f^k}$ decreases, causing the expression to become less negative.

If λ_k^{v+1} has not yet converged, then $f^{k,v}(x)$ is strictly increasing at $x = \lambda_k^{v+1}$ and $g^{k,v}(x)$ is strictly decreasing at $x = \lambda_k^{v+1}$.

$$\begin{aligned}
&\max_k \max \left\{ \sum_f [p_f^{k,v+1} - p_f^{k,v}]_0, \sum_f [-(p_f^{k,v+1} - p_f^{k,v})]_0 \right\} \\
&= \max_k \max \left\{ f^{k,v}(\lambda_k^{v+1}), g^{k,v}(\lambda_k^{v+1}) \right\} \qquad \text{(A.9)} \\
&\leq \max_k \max \left\{ f^{k,v}(\lambda_k^{v}), g^{k,v}(\lambda_k^{v}) \right\}, \qquad \text{(A.10)}
\end{aligned}$$

where (A.9) follows from the definition of $f^{k,v}(x)$ and $g^{k,v}(x)$, and (A.10) follows from Lemma A.2 and the fact that: $\lambda_k^{v+1} = \arg\min_x \{\max\{f^{k,v}(x), g^{k,v}(x)\}\}$, thus:

$$\max\{f^{k,v}(\lambda_k^{v+1}), g^{k,v}(\lambda_k^{v+1})\} \leq \max\{f^{k,v}(x), g^{k,v}(x)\} \quad \forall\, x,$$

where here we substitute $x = \lambda_k^v$. Let X and Y be defined as follows:

$$X \triangleq \frac{w_k}{\lambda_k^v + \Delta\lambda_f^k} - \frac{\Gamma(\sum_{l \neq k} p_f^{l,v} |h_f^{k,l}|^2 + \sigma_f^k)}{|h_f^{k,k}|^2},$$

$$Y \triangleq \frac{w_k}{\lambda_k^v + \Delta\lambda_f^k} - \frac{\Gamma(\sum_{l \neq k} p_f^{l,v-1} |h_f^{k,l}|^2 + \sigma_f^k)}{|h_f^{k,k}|^2}.$$

Then, by construction, $f^{k,v}(\lambda_k^v)$ and $g^{k,v}(\lambda_k^v)$ can be re-written as:

$$\begin{aligned} f^{k,v}(\lambda_k^v) &= \sum_f [([X]_0 - [Y]_0)]_0 \\ &\leq \sum_f [(X-Y)]_0, \text{ by Lemma A.3-i.} \\ g^{k,v}(\lambda_k^v) &= \sum_f [-([X]_0 - [Y]_0)]_0 \\ &\leq \sum_f [-(X-Y)]_0, \text{ by Lemma A.3-ii.} \end{aligned}$$

Hence, applying the above upper-bounds to (A.10), we get:

$$\begin{aligned} &\max\{f^{k,v}(\lambda_k^v), g^{k,v}(\lambda_k^v)\} \\ &\leq \max\left\{\sum_f [(X-Y)]_0, \sum_f [-(X-Y)]_0\right\} \\ &= \max\left\{\sum_f \left[-\sum_{l\neq k} \frac{\Gamma|h_f^{k,l}|^2}{|h_f^{k,k}|^2}\left(p_f^{l,v} - p_f^{l,v-1}\right)\right]_0, \sum_f \left[\sum_{l\neq k} \frac{\Gamma|h_f^{k,l}|^2}{|h_f^{k,k}|^2}\left(p_f^{l,v} - p_f^{l,v-1}\right)\right]_0\right\} \\ &= \max\left\{\sum_f \left[\sum_{l\neq k} \frac{\Gamma|h_f^{k,l}|^2}{|h_f^{k,k}|^2}\left(p_f^{l,v} - p_f^{l,v-1}\right)\right]_0, \sum_f \left[-\sum_{l\neq k} \frac{\Gamma|h_f^{k,l}|^2}{|h_f^{k,k}|^2}\left(p_f^{l,v} - p_f^{l,v-1}\right)\right]_0\right\} \end{aligned}$$

Therefore, applying the above upper-bound to (A.10) gives:

$$\begin{aligned} &\max_f \max\left\{\sum_f \left[p_f^{k,v+1} - p_f^{k,v}\right]_0, \sum_f \left[-\left(p_f^{k,v+1} - p_f^{k,v}\right)\right]_0\right\} \leq \\ &\max_f \max\left\{\sum_f \left[\sum_{l\neq k} \frac{\Gamma|h_f^{k,l}|^2}{|h_f^{k,k}|^2}\left(p_f^{l,v} - p_f^{l,v-1}\right)\right]_0, \sum_f \left[-\left(\sum_{l\neq k} \frac{\Gamma|h_f^{k,l}|^2}{|h_f^{k,k}|^2}\left(p_f^{l,v} - p_f^{l,v-1}\right)\right)\right]_0\right\} \end{aligned}$$

□

Finally, we are ready to prove Theorem 3.1. By Proposition A.1, if we show that $\max_k ||\mathbf{p}^{k,v+1} - \mathbf{p}^{k,v}|| \leq \max_k ||\mathbf{p}^{k,v} - \mathbf{p}^{k,v-1}||$, then $\mathbf{p}^k$ is a Cauchy sequence for all k, and

therefore, each user's transmit power will converges to a fixed point.

$$
\begin{aligned}
&\max_k \left|\left|\mathbf{p}^{k,v+1}-\mathbf{p}^{k,v}\right|\right| \\
&= \max_k \max\left\{\left[\mathbf{p}^{k,v+1}-\mathbf{p}^{k,v}\right]_0, \left[-\left(\mathbf{p}^{k,v+1}-\mathbf{p}^{k,v}\right)\right]_0\right\} \\
&\leq \max_k \max\left\{\sum_f\left[\sum_{l\neq k}\frac{\Gamma|h_f^{k,l}|^2}{|h_f^{k,k}|^2}\left(p_f^{l,v}-p_f^{l,v-1}\right)\right]_0, \sum_f\left[-\left(\sum_{l\neq k}\frac{\Gamma|h_f^{k,l}|^2}{|h_f^{k,k}|^2}\left(p_f^{l,v}-p_f^{l,v-1}\right)\right)\right]_0\right\} \quad \text{(A.11)} \\
&\leq \max_k \max\left\{\sum_f\left[(K-1)\max_{l\neq k}\frac{\Gamma|h_f^{k,l}|^2}{|h_f^{k,k}|^2}\left(p_f^{l,v}-p_f^{l,v-1}\right)\right]_0,\right. \\
&\qquad\qquad \left.\sum_f\left[-\left((K-1)\min_{l\neq k}\frac{\Gamma|h_f^{k,l}|^2}{|h_f^{k,k}|^2}\left(p_f^{l,v}-p_f^{l,v-1}\right)\right)\right]_0\right\} \\
&\leq \max_k \max\left\{(K-1)\max_{l\neq k}\left(\frac{\Gamma|h_f^{k,l}|^2}{|h_f^{k,k}|^2}\sum_f\left[p_f^{l,v}-p_f^{l,v-1}\right]_0\right),\right. \\
&\qquad\qquad \left.(K-1)\min_{l\neq k}\left(\frac{\Gamma|h_f^{k,l}|^2}{|h_f^{k,k}|^2}\sum_f\left[-\left(p_f^{l,v}-p_f^{l,v-1}\right)\right]_0\right)\right\} \\
&\leq (K-1)\max_{f,k}\max_{l\neq k}\left(\frac{\Gamma|h_f^{k,l}|^2}{|h_f^{k,k}|^2}\max\left\{\sum_f\left[p_f^{l,v}-p_f^{l,v-1}\right]_0, \sum_k\left[-\left(p_f^{l,v}-p_f^{l,v-1}\right)\right]_0\right\}\right) \\
&\leq (K-1)\max_{f,k,l\neq k}\left(\frac{\Gamma|h_f^{k,l}|^2}{|h_f^{k,k}|^2}\right)\max_l\left(\max\left\{\sum_f\left[p_f^{l,v}-p_f^{l,v-1}\right]_0, \sum_f\left[-\left(p_f^{l,v}-p_f^{l,v-1}\right)\right]_0\right\}\right) \\
&< \max_l \max\left\{\sum_f\left[p_f^{l,v}-p_f^{l,v-1}\right]_0, \sum_f\left[-\left(p_f^{l,v}-p_f^{l,v-1}\right)\right]_0\right\} \quad \text{(A.12)} \\
&= \max_k \left|\left|\mathbf{p}^{k,v}-\mathbf{p}^{k,v-1}\right|\right|
\end{aligned}
$$

where (A.11) holds because of Lemma A.4, and (A.12) holds by assumption. This completes the proof of Theorem 3.1 since we have shown that $\max_k \left|\left|\mathbf{p}^{k,v+1}-\mathbf{p}^{k,v}\right|\right| < \max_k \left|\left|\mathbf{p}^{k,v}-\mathbf{p}^{k,v-1}\right|\right|$, which based on Proposition A.1 implies that each user's transmit power sequences are Cauchy, and therefore, converge to a fixed point.

A.3 Proof of Theorem 3.2

Let the set of converged offsets and converged transmit powers at the KKT point of the rate adaptive optimization problem outlined in (3.2) be given by $\{\Delta\lambda_f^{k,\mathrm{KKT}}\}$ and $\{p_f^{k,\mathrm{KKT}}\}$, respectively. By Theorem 3.1, for a fixed set of offsets, the constant offset algorithm (Algorithm 3.4) will converge to a fixed point. Hence, there is a one-to-one correspondence between $\{\Delta\lambda_f^{k,\mathrm{KKT}}\}$ and $\{p_f^{k,\mathrm{KKT}}\}$.

Suppose that the virtual network for each user is constructed using the other $K-1$ users. That is, each interfering user $l \neq k$ is represented by a unique reference user. Furthermore, suppose that the transmit power of the reference users are selected as the transmit powers corresponding to their respective $p_f^{k,\mathrm{KKT}}$. Let the set of constant offsets, $\{\Delta\lambda_f^k\}$ (corresponding to the converged set of points $\{(p_f^k)^*\}$), be computed based on the virtual network as in Algorithm 3.3, with the following modification:

$$\mathrm{int}_f^r = \sigma_f^k + \sum_{u\in\mathcal{R}\setminus r} |h_f^{r,u}|^2 p_f^u + |h_f^{r,k}|^2 p_f^{k,\mathrm{KKT}}.$$

By construction, for each user, the set of reference users perfectly represent the other $K-1$ users and their corresponding transmit power at the KKT point. Hence, for each user, the constant offsets generated by Algorithm 3.3 (i.e., $\{\Delta\lambda_f^k\}$) will correspond to that of the final converged offset (i.e., $\{\Delta\lambda_f^{k,\mathrm{KKT}}\}$). Therefore, $\{(p_f^k)^*\}$ will correspond to $\{p_f^{k,\mathrm{KKT}}\}$.

Appendix B

B.1 Proof of Theorem 4.1

As before, let $\hat{\mathbf{G}}_i = \begin{bmatrix} \hat{\mathbf{G}}_{i,a} & \alpha \mathbf{I}_M \end{bmatrix}$. First, we remark that Separate FDP is optimal if and only if the cancellation power constraint is sufficiently large (i.e., the total power constraint is sufficiently large so that solving the unconstrained optimization problem is equivalent to solving the constrained optimization problem).

For the forward direction of the remark we use a transposition argument (i.e., equivalent to proving that when the cancellation power constraint is not sufficiently large, separate FDP is not optimal). When the cancellation power constraint is not sufficiently large, after optimizing both $\mathbf{V}_{i,\mathrm{F}}$ and $\mathbf{V}_{i,\mathrm{S}}$ there will be some residual self-interference. As such, the assumption of no self-interference when $\mathbf{V}_{i,\mathrm{F}}$ was optimized is no longer valid. Hence, a new optimization problem for $\mathbf{V}_{i,\mathrm{F}}$ could be constructed whereby the objective function includes this residual self-interference and the optimization of $\mathbf{V}_{i,\mathrm{F}}$ could further balance between forward channel maximization and self-interference suppression. As such, the optimal solution to the modified optimization problem will provide an improvement over the separate approach. This implies that the separate FDP approach is not optimal.

For the reverse direction of the remark, if the cancellation power constraint is sufficiently large, all self-interference can be cancelled by $\mathbf{V}_{i,\mathrm{S}}$ alone. Hence, since $\mathbf{V}_{i,\mathrm{F}}$ is optimized to maximize the forward channel sum-rate assuming no self-interference and $\mathbf{V}_{i,\mathrm{S}}$ can cancel all the self-interference, separate FDP is optimal.

Following the remark, separate FDP is optimal if and only if α is large enough such that all cancellation can be done by using only $\mathbf{V}_{i,\mathrm{S}}$ (i.e., we are not limited by the cancellation power constraint). That is equivalent to $\lambda_i = 0$ since when $\lambda_i = 0$ the total power constraint

does not need to be satisfied.

$$\mathrm{Tr}\left[\mathbf{V}_{i,\mathrm{S}}\mathbf{S}_i\mathbf{V}_{i,\mathrm{S}}^{\dagger}\right]=\frac{\alpha^2}{\left(\alpha^2+\lambda_i^2\right)^2}\mathrm{Tr}\left[\hat{\mathbf{G}}_{i,a}\mathbf{V}_{i,\mathrm{F}}\mathbf{S}_i\mathbf{V}_{i,\mathrm{F}}^{\dagger}\hat{\mathbf{G}}_{i,a}^{\dagger}\right]\leq P_{\max,i},$$

where substituting $\lambda_i = 0$ gives:

$$\begin{aligned}
\alpha^2 &\geq \mathrm{Tr}\left[\hat{\mathbf{G}}_{i,a}\mathbf{V}_{i,\mathrm{F}}\mathbf{S}_i\mathbf{V}_{i,\mathrm{F}}^{\dagger}\hat{\mathbf{G}}_{i,a}^{\dagger}\right]/P_{\max,i}\\
\alpha^2 &\geq \mathrm{Tr}\left[\hat{\mathbf{G}}_{i,a}\mathbf{V}_{i,\mathrm{F}}E\left[\mathbf{x}_i\mathbf{x}_i^{\dagger}\right]\mathbf{V}_{i,\mathrm{F}}^{\dagger}\hat{\mathbf{G}}_{i,a}^{\dagger}\right]/P_{\max,i}\\
\alpha^2 &\geq E\left[\mathrm{Tr}\left[\hat{\mathbf{G}}_{i,a}\mathbf{V}_{i,\mathrm{F}}\mathbf{x}_i\mathbf{x}_i^{\dagger}\mathbf{V}_{i,\mathrm{F}}^{\dagger}\hat{\mathbf{G}}_{i,a}^{\dagger}\right]\right]/P_{\max,i}\\
\alpha^2 &\geq E\left[\mathrm{Tr}\left[\left(\hat{\mathbf{G}}_{i,a}\mathbf{V}_{i,\mathrm{F}}\mathbf{x}_i\right)\left(\hat{\mathbf{G}}_{i,a}\mathbf{V}_{i,\mathrm{F}}\mathbf{x}_i\right)^{\dagger}\right]\right]/P_{\max,i}\\
\alpha &\geq \sqrt{E\left[\left|\left|\hat{\mathbf{G}}_{i,a}\mathbf{V}_{i,\mathrm{F}}\mathbf{x}_i\right|\right|_2^2\right]}/\sqrt{P_{\max,i}}, \qquad \text{(B.1)}
\end{aligned}$$

where the inequality in (B.1) is obtained using the fact that for a vector $\mathbf{a}$, $||\mathbf{a}||_2^2 = \sum_j [\mathbf{a}]_j [\mathbf{a}]_j^{\dagger} = \mathrm{Tr}\left[\mathbf{a}\mathbf{a}^{\dagger}\right]$. Then, using the fact that for a random variable X (i.e., $X = \left|\left|\hat{\mathbf{G}}_{i,a}\mathbf{V}_{i,\mathrm{F}}\mathbf{x}_i\right|\right|_2$ in this case), we have:

$$\begin{aligned}
E\left[X^2\right] &= E\left[X\right]^2 + \mathrm{Var}(X)\\
\implies E\left[X^2\right] &\geq E\left[X\right]^2\\
\implies \sqrt{E\left[X^2\right]} &\geq E\left[X\right].
\end{aligned}$$

Substituting for X gives: $\sqrt{E\left[\left|\left|\hat{\mathbf{G}}_{i,a}\mathbf{V}_{i,\mathrm{F}}\mathbf{x}_i\right|\right|_2^2\right]} \geq E\left[\left|\left|\hat{\mathbf{G}}_{i,a}\mathbf{V}_{i,\mathrm{F}}\mathbf{x}_i\right|\right|_2\right]$, which can be substituted into (B.1), resulting in:

$$\alpha \geq E\left[\left|\left|\hat{\mathbf{G}}_{i,a}\mathbf{V}_{i,\mathrm{F}}\mathbf{x}_i\right|\right|_2\right]/\sqrt{P_{\max,i}}.$$

Appendix C

C.1 Effect of Estimation Error on the Sum-Rate

Let $R^{\star}_{\mathrm{DL}}$ and $\hat{R}^{\star}_{\mathrm{DL}}$ (respectively, $R^{\star}_{\mathrm{UL}}$ and $\hat{R}^{\star}_{\mathrm{UL}}$) be the downlink (respectively, uplink) true and expected sum-rates corresponding to the transmit covariance matrices $\left(\mathbf{Q}^{\star}_{\mathrm{BS},k}, \mathbf{Q}^{\star}_{\mathrm{UE},u}\right)$, for $k \in \mathcal{I}_{\mathcal{D}}$ and $u \in \mathcal{I}_{\mathcal{U}}$.

Similarly, let $\mathbf{C}^{\star}_{\mathrm{DL},k}$ and $\tilde{\mathbf{C}}^{\star}_{\mathrm{DL},k}$ (respectively, $\mathbf{C}^{\star}_{\mathrm{UL}}$ and $\tilde{\mathbf{C}}^{\star}_{\mathrm{UL}}$) be the downlink (respectively, uplink) transmit covariance matrices corresponding to the transmit covariance matrices $\left(\mathbf{Q}^{\star}_{\mathrm{BS},k}, \mathbf{Q}^{\star}_{\mathrm{UE},u}\right)$, for $k \in \mathcal{I}_{\mathcal{D}}$ and $u \in \mathcal{I}_{\mathcal{U}}$. Hence, $\tilde{\mathbf{C}}^{\star}_{\mathrm{DL},k}$ and $\tilde{\mathbf{C}}^{\star}_{\mathrm{UL}}$ are given by:

$$\begin{aligned}\tilde{\mathbf{C}}^{\star}_{\mathrm{DL},k} &= \hat{\mathbf{C}}^{\star}_{\mathrm{DL},k} + \Delta\tilde{\mathbf{C}}^{\star}_{\mathrm{DL},k},\\ \tilde{\mathbf{C}}^{\star}_{\mathrm{UL}} &= \hat{\mathbf{C}}^{\star}_{\mathrm{UL}} + \Delta\tilde{\mathbf{C}}^{\star}_{\mathrm{UL}},\end{aligned}$$

where $\hat{\mathbf{C}}^{\star}_{\mathrm{DL},k}$, $\Delta\tilde{\mathbf{C}}^{\star}_{\mathrm{DL},k}$, $\hat{\mathbf{C}}^{\star}_{\mathrm{UL}}$, and $\Delta\tilde{\mathbf{C}}^{\star}_{\mathrm{UL}}$ are given by:

$$\begin{aligned}\hat{\mathbf{C}}^{\star}_{\mathrm{DL},k} &= \sum_{l\in\mathcal{I}_{\mathcal{D}}\setminus\{k\}} [\mathbf{H}_{\mathrm{DL}}]_k \mathbf{Q}^{\star}_{\mathrm{BS},l} [\mathbf{H}_{\mathrm{DL}}]_k^{\dagger} + \sum_{u\in\mathcal{I}_{\mathcal{U}}} [\hat{\mathbf{G}}_{\mathrm{UE}}]_{k,u} \mathbf{Q}^{\star}_{\mathrm{UE},u} [\hat{\mathbf{G}}_{\mathrm{UE}}]_{k,u}^{\dagger},\\ \Delta\tilde{\mathbf{C}}^{\star}_{\mathrm{DL},k} &= \sum_{u\in\mathcal{I}_{\mathcal{U}}} \Big\{ [\Delta\mathbf{G}_{\mathrm{UE}}]_{k,u} \mathbf{Q}^{\star}_{\mathrm{UE},u} [\Delta\mathbf{G}_{\mathrm{UE}}]_{k,u}^{\dagger} + [\hat{\mathbf{G}}_{\mathrm{UE}}]_{k,u} \mathbf{Q}^{\star}_{\mathrm{UE},u} [\Delta\mathbf{G}_{\mathrm{UE}}]_{k,u}^{\dagger}\\ &\qquad + [\Delta\mathbf{G}_{\mathrm{UE}}]_{k,u} \mathbf{Q}^{\star}_{\mathrm{UE},u} [\hat{\mathbf{G}}_{\mathrm{UE}}]_{k,u}^{\dagger} \Big\},\\ \hat{\mathbf{C}}^{\star}_{\mathrm{UL}} &= \sum_{k\in\mathcal{I}_{\mathcal{D}}} \hat{\mathbf{G}}_{\mathrm{BS}} \mathbf{Q}^{\star}_{\mathrm{BS},k} \hat{\mathbf{G}}_{\mathrm{BS}}^{\dagger},\\ \Delta\tilde{\mathbf{C}}^{\star}_{\mathrm{UL}} &= \sum_{k\in\mathcal{I}_{\mathcal{D}}} \Big\{ \Delta\mathbf{G}_{\mathrm{BS}} \mathbf{Q}^{\star}_{\mathrm{BS},k} \Delta\mathbf{G}_{\mathrm{BS}}^{\dagger} + \Delta\mathbf{G}_{\mathrm{BS}} \mathbf{Q}^{\star}_{\mathrm{BS},k} \hat{\mathbf{G}}_{\mathrm{BS}}^{\dagger} + \hat{\mathbf{G}}_{\mathrm{BS}} \mathbf{Q}^{\star}_{\mathrm{BS},k} \Delta\mathbf{G}_{\mathrm{BS}}^{\dagger} \Big\}.\end{aligned}$$

Hence, the uplink sum-rate can be written as:

$$R^{\star}_{\mathrm{UL}} = \log_2 \left| \mathbf{I}_{N_{\mathrm{BS},R}} + \left(\mathbf{\Sigma}_{\mathrm{BS}} + \hat{\mathbf{C}}^{\star}_{\mathrm{UL}} + \Delta\tilde{\mathbf{C}}^{\star}_{\mathrm{UL}} \right)^{-1} \mathbf{C}^{\star}_{\mathrm{UL}} \right|.$$

Using (5.14), $\left(\mathbf{\Sigma}_{\mathrm{BS}} + \hat{\mathbf{C}}^{\star}_{\mathrm{UL}} + \Delta\tilde{\mathbf{C}}^{\star}_{\mathrm{UL}} \right)^{-1}$ can be re-written as:

$$\left(\mathbf{\Upsilon}_{\mathrm{UL}} + \Delta\tilde{\mathbf{C}}^{\star}_{\mathrm{UL}} \right)^{-1} = \mathbf{\Upsilon}^{-1}_{\mathrm{UL}} - \mathbf{\Upsilon}^{-1}_{\mathrm{UL}} \left(\mathbf{I}_{N_{\mathrm{BS},R}} + \Delta\tilde{\mathbf{C}}^{\star}_{\mathrm{UL}} \mathbf{\Upsilon}^{-1}_{\mathrm{UL}} \right)^{-1} \Delta\tilde{\mathbf{C}}^{\star}_{\mathrm{UL}} \mathbf{\Upsilon}^{-1}_{\mathrm{UL}},$$

where $\mathbf{\Upsilon}_{\mathrm{UL}} = \mathbf{\Sigma}_{\mathrm{BS}} + \hat{\mathbf{C}}^{\star}_{\mathrm{UL}}$. As such, $R^{\star}_{\mathrm{UL}}$ can be re-written as:

$$R^{\star}_{\mathrm{UL}} = \log_2 \left| \underbrace{\mathbf{I}_{N_{\mathrm{BS},R}} + \mathbf{\Upsilon}^{-1}_{\mathrm{UL}} \mathbf{C}^{\star}_{\mathrm{UL}}}_{\mathbf{A}} - \underbrace{\mathbf{\Upsilon}^{-1}_{\mathrm{UL}} \left(\mathbf{I}_{N_{\mathrm{BS},R}} + \Delta\tilde{\mathbf{C}}^{\star}_{\mathrm{UL}} \mathbf{\Upsilon}^{-1}_{\mathrm{UL}} \right)^{-1} \Delta\tilde{\mathbf{C}}^{\star}_{\mathrm{UL}} \mathbf{\Upsilon}^{-1}_{\mathrm{UL}} \mathbf{C}^{\star}_{\mathrm{UL}}}_{\mathbf{B}} \right|. \tag{C.1}$$

Then, using the fact that $\log_2 |\mathbf{A} - \mathbf{B}| = \log_2 |\mathbf{A}| + \log_2 |\mathbf{I} - \mathbf{A}^{-1}\mathbf{B}|$, (C.1) can be re-written as:

$$R^{\star}_{\mathrm{UL}} = \log_2 \left| \mathbf{I}_{N_{\mathrm{BS},R}} + \mathbf{\Upsilon}^{-1}_{\mathrm{UL}} \mathbf{C}^{\star}_{\mathrm{UL}} \right| + \log_2 \left| \mathbf{I}_{N_{\mathrm{BS},R}} - \mathbf{\Psi}^{-1}_{\mathrm{UL}} \left(\mathbf{I}_{N_{\mathrm{BS},R}} + \Delta\tilde{\mathbf{C}}^{\star}_{\mathrm{UL}} \mathbf{\Upsilon}^{-1}_{\mathrm{UL}} \right)^{-1} \Delta\tilde{\mathbf{C}}^{\star}_{\mathrm{UL}} \mathbf{\Upsilon}^{-1}_{\mathrm{UL}} \mathbf{C}^{\star}_{\mathrm{UL}} \right|,$$

where $\mathbf{\Psi}_{\mathrm{UL}} = \mathbf{\Upsilon}_{\mathrm{UL}} \left(\mathbf{I}_{N_{\mathrm{BS},R}} + \mathbf{\Upsilon}^{-1}_{\mathrm{UL}} \mathbf{C}^{\star}_{\mathrm{UL}} \right)$. Therefore, the uplink estimation error term is given by:

$$\Delta R_{\mathrm{UL}} = \log_2 \left| \mathbf{I}_{N_{\mathrm{BS},R}} - \mathbf{\Psi}^{-1}_{\mathrm{UL}} \left(\mathbf{I}_{N_{\mathrm{BS},R}} + \Delta\tilde{\mathbf{C}}^{\star}_{\mathrm{UL}} \mathbf{\Upsilon}^{-1}_{\mathrm{UL}} \right)^{-1} \Delta\tilde{\mathbf{C}}^{\star}_{\mathrm{UL}} \mathbf{\Upsilon}^{-1}_{\mathrm{UL}} \mathbf{C}^{\star}_{\mathrm{UL}} \right|,$$

Following a similar derivation, the estimation error term for transmission to the k-th downlink UE ($k \in \mathcal{I}_{\mathcal{D}}$), $\Delta R_{\mathrm{DL},k}$, is given by:

$$\Delta R_{\mathrm{DL},k} = \log_2 \left| \mathbf{I}_{N_{\mathrm{UE},R}} - \mathbf{\Psi}^{-1}_{\mathrm{DL},k} \left(\mathbf{I}_{N_{\mathrm{UE},R}} + \Delta\tilde{\mathbf{C}}^{\star}_{\mathrm{DL},k} \mathbf{\Upsilon}^{-1}_{\mathrm{DL},k} \right)^{-1} \Delta\tilde{\mathbf{C}}^{\star}_{\mathrm{DL},k} \mathbf{\Upsilon}^{-1}_{\mathrm{DL},k} \mathbf{C}^{\star}_{\mathrm{DL},k} \right|,$$

where $\mathbf{\Psi}_{\mathrm{DL},k} = \mathbf{\Upsilon}_{\mathrm{DL},k} \left(\mathbf{I}_{N_{\mathrm{UE},R}} + \mathbf{\Upsilon}^{-1}_{\mathrm{DL},k} \mathbf{C}^{\star}_{\mathrm{DL},k} \right)$ and $\mathbf{\Upsilon}_{\mathrm{DL},k} = \mathbf{\Sigma}_k + \hat{\mathbf{C}}^{\star}_{\mathrm{DL},k}$. Therefore, the loss incurred due to inaccurate channel knowledge resulting in residual self-interference is given by:

$$\Delta R = \Delta R_{\mathrm{UL}} + \sum_{k \in \mathcal{I}_{\mathcal{D}}} \Delta R_{\mathrm{DL},k}.$$

References

[1] M. Duarte and A. Sabharwal, "Full-duplex wireless communications using off-the-shelf radios: feasibility and first results," in *Proc. ASILOMAR Signals, Syst., Comput.*, Nov. 2010, pp. 1558–1562.

[2] M. Jain, J. I. Choiy, T. Kim, D. Bharadia, S. Seth, K. Srinivasan, P. Levis, S. Katti, and P. Sinha, "Practical, real-time, full duplex wireless," in *Proc. Int. Conf. Mobile Comput. Netw.*, 2011, pp. 301–312.

[3] S. Huberman, C. Leung, and T. Le-Ngoc, "Dynamic spectrum management (DSM) algorithms for multi-user xDSL," *IEEE Commun. Surveys Tuts.*, vol. 14, no. 1, pp. 109–130, Feb. 2012.

[4] W. Yu, G. Ginis, and J. Cioffi, "Distributed multiuser power control for digital subscriber lines," *IEEE J. Sel. Areas Commun.*, vol. 20, no. 5, pp. 1105–1115, Jun. 2002.

[5] Y. Xu, S. Panigrahi, and T. Le-Ngoc, "Selective iterative water-filling for digital subscriber lines (DSL)," *EURASIP J. Appl. Signal Process.*, vol. 2007, pp. 1–11, May 2007.

[6] H. Bagheri, M. R. Pakravan, and B. H. Khalaj, "Iterative multi-user power allocation: performance evaluation & modification," in *Proc. IEEE Region 10 Technol., Educ. and Netw. Conf.*, vol. 3, Nov. 2004, pp. 216–219.

[7] Y. Liu and Z. Su, "Distributed dynamic spectrum management for digital subscriber lines," *IEICE Trans. Commun.*, vol. E90B, no. 3, pp. 491–498, Mar. 2007.

[8] D. Statovci, T. Nordström, and R. Nilsson, "The normalized-rate iterative algorithm: a practical dynamic spectrum management method for DSL," *EURASIP J. Appl. Signal Process.*, vol. 2006, pp. 1–17, Feb. 2006.

[9] W. Lee, Y. Kim, M. H. Brady, and J. M. Cioffi, "Band-preference dynamic spectrum management in a DSL environment," in *Proc. IEEE Global Telecommun. Conf.*, Nov. 2006, pp. 1–5.

[10] Y. Noam and A. Leshem, "Iterative power pricing for distributed spectrum coordination in DSL," *IEEE Trans. Commun.*, vol. 57, no. 4, pp. 948–953, Apr. 2009.

[11] R. Cendrillon, W. Yu, M. Moonen, J. Verlinden, and T. Bostoen, "Optimal multiuser spectrum balancing for digital subscriber lines," *IEEE Trans. Commun.*, vol. 54, no. 5, pp. 922–933, May 2006.

[12] R. Cendrillon and M. Moonen, "Iterative spectrum balancing for digital subscriber lines," in *Proc. IEEE Int. Conf. Commun.*, May 2005, pp. 1937–1941.

[13] R. Lui and W. Yu, "Low-complexity near-optimal spectrum balancing for digital subscriber lines," in *Proc. IEEE Int. Conf. Commun.*, May 2005, pp. 1947–1951.

[14] S. Wei, L. Youming, and Y. Miaoliang, "Low-complexity grouping spectrum management in multi-user DSL networks," in *Proc. Int. Conf. Commun. Mobile Comput.*, Jan. 2009, pp. 381–385.

[15] J. Huang, R. Cendrillon, M. Chiang, and M. Moonen, "Autonomous spectrum balancing (ASB) for frequency selective interference channels," in *Proc. IEEE Int. Symp. Inform. Theory*, Jul. 2006, pp. 610–614.

[16] R. Cendrillon, J. W. Huang, M. Chiang, and M. Moonen, "Autonomous spectrum balancing for digital subscriber lines," *IEEE Trans. Signal Process.*, vol. 55, no. 8, pp. 4241–4257, Aug. 2007.

[17] P. Tsiaflakis, M. Diehl, and M. Moonen, "Distributed spectrum management algorithms for multiuser DSL networks," *IEEE Trans. Signal Process.*, vol. 56, no. 10, pp. 4825–4843, Oct. 2008.

[18] R. Moraes, B. Dortschyy, A. Klautau, and J. R. i. Riuy, "Semi-blind power allocation for digital subscriber lines," in *Proc. IEEE Int. Conf. Commun.*, May 2008, pp. 1420–1425.

[19] J. Papandriopoulos and J. S. Evans, "Low-complexity distributed algorithm for spectrum balancing in multi-user DSL networks," in *Proc. IEEE Int. Conf. Commun.*, Jun. 2006.

[20] ——, "SCALE: a low-complexity distributed protocol for spectrum balancing in multiuser DSL networks," *IEEE Trans. Inf. Theory*, vol. 55, pp. 3711–3724, Aug. 2009.

[21] P. D. Tao and L.-T. H. An, "Convex analysis approach to D.C. programming: theory, algorithms and applications," *Acta Mathematica Vietnamica*, vol. 22, no. 1, pp. 289–355, 1997.

[22] S. Huberman and T. Le-Ngoc, "Dynamic spectrum management algorithms for multiuser communication systems," in *Software-defined and cognitive radio technologies for dynamic spectrum access and management*. IGI Global, to be published.

[23] B. D. Van Veen and K. M. Buckley, "Beamforming: a versatile approach to spatial filtering," *IEEE ASSP Mag.*, vol. 5, no. 2, pp. 4–24, Apr. 1988.

[24] C. Leung, S. Huberman, and T. Le-Ngoc, "Vectored DSL: its potential and its implementation issues and challenges," *IEEE Commun. Surveys Tuts.*, vol. 15, no. 4, pp. 1–17, Jan. 2013.

[25] R. Zidane, S. Huberman, C. Leung, and T. Le-Ngoc, "Vectored DSL: benefits and challenges for service providers," *IEEE Commun. Soc. Mag.*, vol. 51, no. 2, pp. 152–157, Feb. 2013.

[26] M. Tomlinson, "New automatic equaliser employing modulo arithmetic," *Electron. Lett.*, vol. 7, no. 5, pp. 138–139, Mar. 1971.

[27] H. Harashima and H. Miyakawa, "Matched-transmission technique for channels with intersymbol interference," *IEEE Trans. Commun.*, vol. 20, no. 4, pp. 774–780, Aug. 1972.

[28] G. Ginis and J. Cioffi, "Vectored transmission for digital subscriber line systems," *IEEE J. Sel. Areas Commun.*, vol. 20, no. 5, pp. 1085–1104, Jun. 2002.

[29] H. Weingarten, Y. Steinberg, and S. Shamai, "The capacity region of the gaussian multiple-input multiple-output broadcast channel," *IEEE Trans. Inf. Theory*, vol. 52, no. 9, pp. 3936–3964, Sep. 2006.

[30] D. Gesbert, M. Kountouris, R. W. Heath Jr., C.-B. Chae, and T. Salzer, "Shifting the MIMO paradigm," *IEEE Signal Process. Mag.*, vol. 24, no. 5, pp. 36–46, Sep. 2007.

[31] C. Peel, B. M. Hochwald, and A. L. Swindlehurst, "A vector-perturbation technique for near-capacity multiantenna multiuser communication - part I: channel inversion and regularization," *IEEE Trans. Commun.*, vol. 53, no. 1, pp. 195–202, Jan. 2005.

[32] R. Cendrillon, G. Ginis, E. Van den Bogaert, and M. Moonen, "A near-optimal linear crosstalk canceler for upstream VDSL," *IEEE Trans. Signal Process.*, vol. 54, no. 8, pp. 3136–3146, Aug. 2006.

[33] ——, "A near-optimal linear crosstalk precoder for downstream VDSL," *IEEE Trans. Commun.*, vol. 55, no. 5, pp. 860–863, May 2007.

[34] V. R. Cadambe and S. A. Jafar, "Interference alignment and degrees of freedom of the K-user interference channel," *IEEE Trans. Inf. Theory*, vol. 54, no. 8, pp. 3425–3441, Aug. 2008.

[35] S. W. Peters and R. W. Heath Jr., "Interference alignment via alternating minimization," in *Proc. IEEE Int. Conf. Acoust., Speech, and Signal Process.*, Mar. 2009.

[36] K. Gomadam, V. R. Cadambe, and S. A. Jafar, "A distributed numerical approach to interfernece alignment and applications to wireless interference networks," *IEEE Trans. Inf. Theory*, vol. 57, no. 6, pp. 3309–3322, Jun. 2011.

[37] I. Santamaria, O. Gonzalez, R. W. Heath Jr., and S. W. Peters, "Maximum sum-rate interference alignment algorithms for MIMO channels," in *Proc. IEEE Global Telecommun. Conf.*, Dec. 2010.

[38] H. Sung, S.-H. Park, K.-J. Lee, and I. Lee, "Linear precoder designs for K-user interference channels," *IEEE Trans. Wireless Commun.*, vol. 9, no. 1, pp. 291–301, Jan. 2010.

[39] Z. Zhi-Dong and X. Xian-Zhong, "Research on interference alignment based on dynampic power allocation in multi-cell," in *Proc. Int. Conf. Commun. Problem-Solving*, Oct. 2011, pp. 222–225.

[40] C. Suh and D. Tse, "Interference alignment for cellular networks," in *Proc. Allerton Conf. Commun. Control and Comput.*, Sep. 2008, pp. 1037–1044.

[41] B. Da and R. Zhang, "Exploiting interference alignment in multi-cell cooperative OFDMA resource allocation," in *Proc. IEEE Global Telecommun. Conf.*, Dec. 2011.

[42] D. Hwang, "Interference alignment for the multi-cell multiuser interference channel," *IEEE Commun. Lett.*, vol. 16, no. 6, pp. 831–833, Jun. 2012.

[43] M. Rezaee and S. Nader-Esfahani, "Interference alignment for downlink transmission of multiple interfering cells," *IEEE Wireless Commun. Lett.*, vol. 1, no. 5, pp. 460–463, Oct. 2012.

[44] K. Gomadam, V. R. Cadambe, and S. A. Jafar, "Approaching the capacity of wireless networks through distributed interference alignment," in *Proc. IEEE Global Telecommun. Conf.*, Dec. 2008.

[45] J. Huang, R. A. Berry, and M. L. Honig, "Distributed interference compensation for wireless networks," *IEEE J. Sel. Areas Commun.*, vol. 24, no. 5, pp. 1074–1084, May 2006.

[46] C. Shi, R. A. Berry, and M. L. Honig, "Distributed interference pricing for OFDM wireless networks with non-separable utilities," in *Proc. Conf. Inform. Sci. and Syst.*, Mar. 2008, pp. 755–760.

[47] C. Shi, D. A. Schmidt, R. A. Berry, M. L. Honig, and W. Utschick, "Distributed interference pricing for the MIMO interference channel," in *Proc. IEEE Int. Conf. Commun.*, Jun. 2009, pp. 1–5.

[48] C. Shi, R. A. Berry, and M. L. Honig, "Local interference pricing for distributed beamforming in MIMO networks," in *Proc. IEEE Military Commun. Conf.*, Oct. 2009, pp. 1–6.

[49] C. Zhang, W. Xu, Z. He, K. Niu, and B. Tian, "A beamforming algorithm based on interference pricing for the MISO interference channel," in *Proc. IEEE Veh. Technol. Conf.*, Sep. 2010, pp. 1–5.

[50] T. Riihonen, S. Werner, and R. Wichman, "Mitigation of loopback self-interference in full-duplex MIMO relays," *IEEE Trans. Signal Process.*, vol. 59, no. 12, pp. 5983–5993, Dec. 2011.

[51] P. Lioliou, M. Viberg, M. Coldrey, and F. Athley, "Self-interference suppression in full-duplex MIMO relays," in *Proc. ASILOMAR Signals, Syst., Comput.*, Nov. 2010, pp. 658–662.

[52] J.-H. Lee and O.-S. Shin, "Distributed beamforming approach to full-duplex relay in multiuser MIMO transmission," in *Proc. IEEE Wireless Commun. and Netw. Conf.*, Apr. 2012, pp. 278–282.

[53] B. Day, A. Margetts, D. Bliss, and P. Schniter, "Full-duplex MIMO relaying: achievable rates under limited dynamic range," *IEEE J. Sel. Areas Commun.*, vol. 30, no. 8, pp. 1541–1553, Sep. 2012.

[54] J. Sangiamwong, T. Asai, J. Hagiwara, Y. Okumura, and T. Ohya, "Joint multi-filter design for full-duplex MU-MIMO relaying," in *Proc. IEEE Veh. Technol. Conf.*, Apr. 2009, pp. 1–5.

[55] T. Riihonen, A. Balakrishnan, K. Haneda, S. Wyne, S. Werner, and R. Wichman, "Optimal eigenbeamforming for suppressing self-interference in full-duplex MIMO relays," in *Proc. Conf. Inform. Sci. and Syst.*, Mar. 2010, pp. 1–6.

[56] T. Riihonen, S. Werner, and R. Wichman, "Residual self-interference in full-duplex MIMO relays after null-space projection and cancellation," in *Proc. ASILOMAR Signals, Syst., Comput.*, Nov. 2010, pp. 653–657.

[57] B. Chun, E.-R. Jeong, J. Joung, Y. Oh, and Y. H. Lee, "Pre-nulling for self-interference suppression in full-duplex relays," in *Proc. Asian-Pacific Signal Inf. Process. Assoc.*, Oct. 2009, pp. 91–97.

[58] B. Chun and Y. H. Lee, "A spatial self-interference nullification method for full duplex amplify-and-forward MIMO relays," in *Proc. IEEE Wireless Commun. and Netw. Conf.*, Apr. 2010, pp. 1–6.

[59] B. Chun and H. Park, "A spatial-domain joint-nulling method of self-interference in full-duplex relays," *IEEE Commun. Lett.*, vol. 16, no. 4, pp. 436–438, Apr. 2012.

[60] H. Ju, E. Oh, and D. Hong, "Improving efficiency of resource usage in two-hop full duplex relay systems based on resource sharing and interference cancellation," *IEEE Trans. Wireless Commun.*, vol. 8, no. 8, pp. 3933–3938, Aug. 2009.

[61] T. Riihonen, S. Werner, and R. Wichman, "Spatial loop interference suppression in full-duplex MIMO relays," in *Proc. ASILOMAR Signals, Syst., Comput.*, Nov. 2009, pp. 1508–1512.

[62] Y. Hua, P. Liang, Y. Ma, A. C. Cirik, and Q. Gao, "A method for broadband full-duplex MIMO radio," *IEEE Signal Process. Lett.*, vol. 19, no. 12, pp. 793–796, Dec. 2012.

[63] J. Zhang, O. T. Motlagh, J. Luo, and M. Haardt, "Full duplex wireless communications with partial interference cancellation," in *Proc. ASILOMAR Signals, Syst., Comput.*, Nov. 2012, pp. 1295–1299.

[64] J. Zhang, O. T. Motlagh, and M. Haardt, "Robust transmit beamforming design for full-duplex point-to-point MIMO systems," in *Proc. Int. Symp. Wireless Commun. Syst.*, Aug. 2013, pp. 1–5.

[65] B. Day, A. Margetts, D. Bliss, and P. Schniter, "Full-duplex bidirectional MIMO: achievable rates under limited dynamic range," *IEEE Trans. Signal Process.*, vol. 60, no. 7, pp. 3702–3713, Jul. 2012.

[66] T. M. Kim, H. J. Yang, and A. J. Paulraj, "Distributed sum-rate optimization for full-duplex MIMO systems under limited dynamic range," *IEEE Signal Process. Lett.*, vol. 20, no. 6, pp. 555–558, Jun. 2013.

[67] D. Nguyen, L.-N. Tran, P. Pirinen, and M. Latva-aho, "Transmission strategies for full duplex multiuser MIMO systems," in *Proc. IEEE Int. Conf. Commun.*, Jun. 2012, pp. 6825–6829.

[68] ——, "Precoding for full duplex multiuser MIMO systems: spectral and energy efficiency maximization," *IEEE Trans. Signal Process.*, vol. 61, no. 16, pp. 4038–4050, Aug. 2013.

[69] B. Yin, M. Wu, C. Studer, J. R. Cavallaro, and J. Lilleberg, "Full-duplex in large-scale wireless systems," in *Proc. ASILOMAR Signals, Syst., Comput.*, Aug. 2013, pp. 1–5.

[70] Y. K. Chan, V. C. Koo, B. K. Chung, and H. Chuah, "A cancellation network for full-duplex front end circuit," *Prog. Electromagn. Res. Lett.*, vol. 7, pp. 139–148, 2009.

[71] A. Sahai, G. Patel, and A. Sabharwal, "Pushing the limits of full-duplex: design and real-time implementation," Jul. 2011, Available: http://arxiv.org/pdf/1107.0607v1.pdf.

[72] E. Everett, A. Sahai, and A. Sabharwal, "Passive self-interference suppression for full-duplex infrastructure nodes," *IEEE Trans. Wireless Commun.*, vol. 13, no. 2, pp. 680–694, Feb. 2014.

[73] E. Aryafar, M. Khojastepour, K. Sundaresan, S. Rangarajan, and M. Chiang, "MIDU: enabling MIMO full duplex," in *Proc. Int. Conf. Mobile Comput. Netw.*, 2012, pp. 257–268.

[74] B. Radunovic, D. Gunawardena, P. Key, A. Proutiere, N. Singh, V. Balan, and G. DeJean, "Rethinking indoor wireless mesh design: low power, low frequency, full-duplex," in *Workshop Wireless Mesh Netw.*, 2010, pp. 1–6.

[75] A. Sahai, G. Patel, C. Dick, and A. Sabharwal, "On the impact of phase noise on active cancelation in wireless full-duplex," *IEEE Trans. Veh. Technol.*, vol. 62, no. 9, pp. 4494–4510, Nov. 2013.

[76] D. Bharadia, E. McMilin, and S. Katti, "Full duplex radios," in *Proc. ACM SIGCOMM Conf. Data Commun.*, Oct. 2013, pp. 375–386.

[77] K. Muhammad and I. Elahi, "System and method for transmission interference cancellation in full duplex transceiver," U.S. Patent 8,306,480 B2, Nov. 6, 2012.

[78] S. Kangasmaa, S. Haapoja, and U. Parts, "Analog signal path modeling for self-interference cancellation," U.S. Patent 8,023,438 B2, Sep. 20, 2011.

[79] G. R. Kenworthy, "Self-cancellating full-duplex RF communication system," U.S. Patent 5,691,978, Nov. 25, 1997.

[80] C. Leung, S. Huberman, and T. Le-Ngoc, "Autonomous spetrum balancing using multiple reference lines for digital subscriber lines," in *Proc. IEEE Global Telecommun. Conf.*, Dec. 2010, pp. 1–6.

[81] S. Huberman, C. Leung, and T. Le-Ngoc, "A clustering approach to autonomous spectrum balancing using multiple reference lines for DSL," in *Proc. IEEE Global Telecommun. Conf.*, Dec. 2011, pp. 1–6.

[82] S. Huberman and T. Le-Ngoc, "Ergodic capacity of a DSL binder channel," in *Proc. IEEE Global Telecommun. Conf.*, Dec. 2011, pp. 1–5.

[83] S. Huberman, C. Leung, and T. Le-Ngoc, "Constant offset autonomous spectrum balancing using multiple reference lines for VDSL," *IEEE Trans. Signal Process.*, vol. 60, no. 12, pp. 6719–6723, Dec. 2012.

[84] T. Starr, J. Cioffi, and P. Silverman, *Understanding digital subscriber line technology.* Upper Saddle River, NJ: Prentice-Hall, 1999.

[85] *Single-ended line testing for digital subscriber line (DSL)*, ITU Std. G.996.2 Std., May 2009.

[86] 3GPP TS 36.214, *Evolved universal terrestrial radio accesss (E-UTRA); physical layer measurements*, Release 10 Std., Apr. 2011.

[87] American national standard for telecommunications, *Spectrum management for loop transmission systems*, ANSI Std. T1.417 Std., 2003.

[88] *Very high speed digital subscriber line transceivers 2 (VDSL2)*, ITU Std. G.993.2 Amendment 1 Std., Apr. 2007.

[89] S. Huberman and T. Le-Ngoc, "Self-interference pricing for full-duplex MIMO systems," in *Proc. IEEE Global Telecommun. Conf.*, Dec. 2013, pp. 3902–3906.

[90] ——, "Sequential convex programming for full-duplex single-user MIMO systems ," in *Proc. IEEE Int. Conf. Commun.*, Jun. 2014, pp. 5078–5082.

[91] ——, "Self-interference pricing-based MIMO full-duplex precoding," *IEEE Wireless Commun. Lett.*, to be published.

[92] ——, "Self-interference threshold-based MIMO full-duplex precoding," *IEEE Trans. Veh. Technol.*, to be published.

[93] ——, "MIMO full-duplex precoding: a joint beamforming and self-interference cancellation structure," *IEEE Trans. Wireless Commun.*, submitted for publication.

[94] T. Le-Ngoc and S. Huberman, "Multiple-input and multiple-output (MIMO) full-duplex precoding structure," U.S. Patent 61/945,507, Feb. 27, 2014.

[95] ——, "System and multiple-input and multiple-output (MIMO) full-duplex precoding," U.S. Patent in preparation.

[96] S. Huberman and T. Le-Ngoc, "Joint full-duplex precoding algorithm," U.S. Patent in preparation.

[97] C. Zillober, K. Schittkowski, and K. Moritzen, "Very large scale optimization by sequential convex programming," *Optimization Methods and Softw.*, vol. 19, no. 1, pp. 103–120, May 2004.

[98] M. Grant and S. Boyd, "Graph implementations for nonsmooth convex programs," in *Recent advances in learning and control, lecture notes in control and information sciences*, V. Blondel, S. Boyd, and H. Kimura, Ed. Springer-Verlag Limited, 2008, pp. 95–110, http://stanford.edu/~boyd/graph_dcp.html.

[99] CVX Research, Inc., "CVX: matlab software for disciplined convex programming, version 2.0," http://cvxr.com/cvx, Jun. 2013.

[100] J. R. Magnus and H. Neudecker, *Matrix differential calculus with applications in statistics and econometrics*. John Wiley & Sons, 1988.

[101] T. P. Minka, "Old and new matrix algebra useful for statistics," Tech. Rep., Dec. 2000.

[102] H. Lütkepohl, *Handbook of matrices*. John Wiley & Sons, 1996.

[103] S. Huberman and T. Le-Ngoc, "Full-duplex MIMO precoding for sum-rate maximization with sequential convex programming," *IEEE Trans. Veh. Technol.*, to be published.

[104] M. Grant, S. Boyd, and Y. Ye, "Disciplined convex programming," in *Global optimization: from theory to implementation, nonconvex optimization and its applications*. Springer, 2006, pp. 155–210.

[105] S. Boyd and L. Vandenberghe, *Convex optimization*. Cambridge University Press, 2004.

[106] H. V. Henderson and S. R. Searle, "On deriving the inverse of a sum of matrices," *SIAM Rev.*, vol. 23, no. 1, pp. 53–60, Jan. 1981.

[107] 3GPP TR 36.814, *Further advancements for E-UTRA physical layer aspects*, Release 9 Std., Mar. 2010.